Czech Technical University in Prague
Faculty of Civil Engineering
Department of steel and timber structures

Master's Thesis

The impact of the ballast and track interaction on the dynamic behaviour of a short span steel bridge

Melaku Seyoum Lemma

Supervisor: doc. Ing. Pavel Ryjáček, Ph.D.

Study Programme: Sustainable Construction under Natural Hazards and Catastrophic Events
Field of Study: Civil Engineering

January 8, 2017

CZECH TECHNICAL UNIVERSITY IN PRAGUE
Faculty of Civil Engineering
Thákurova 7, 166 29 Prague 6, Czech Republic

DIPLOMA THESIS ASSIGNMENT FORM

I. PERSONAL AND STUDY DATA

Surname: Lemma Name: Melaku Seyoum Personal number:

Assigning Department: Department of steel and timber structures

Study programme: CIVIL ENGINEERING

Branch of study: SUSCOS

II. DIPLOMA THESIS DATA

Diploma Thesis (DT) title: Vliv koleje a kolejového lože na dynamické chování ocelového mostu malého rozpětí

Diploma Thesis title in English: The impact of the ballast and track interaction on the dynamic behaviour of a short span steel bridge

Instructions for writing the thesis:
The aim of the work is to:
- analyze the results of the static and dynamic load test on the bridge in Mirošov,
- create the numerical model, including the track and the ballast, to achieve the good corellation with the load test
- create simplified model, and modify it to have a good corellation as well
- analyze the impact on the ballast and rail on the dynamic behaviour and establish the conclusions and reccomendations

List of recommended literature:
Frýba, L.: Dynamics of Railway Bridges

Name of Diploma Thesis Supervisor: doc. Ing. Pavel Ryjáček, Ph.D.

DT assignment date: 9.10.2016 DT submission date: 8.1.2017

[redacted]

DT Supervisor's signature Head of Department's signature

III. ASSIGNMENT RECEIPT

I declare that I am obliged to write the Diploma Thesis on my own, without anyone's assistance, except for provided consultations. The list of references, other sources and consultants' names must be stated in the Diploma Thesis and in referencing I must abide by the CTU methodological manual "How to Write University Final Theses" and the CTU methodological instruction "On the Observation of Ethical Principles in the Preparation of University Final Theses".

9. 10. 2016 [redacted]

Assignment receipt date Student's name

Declaration

I hereby declare that I have completed this thesis independently and that I have listed all the literature and publications used. I have no objection to usage of this work in compliance with the act §60 Zákon č.121/2000Sb. (copyright law), and with the rights connected with the copyright act including the changes in the act.

In Prague
On January 8, 2017. .....

Acknowledgements

I would first like to thank my supervisor doc. Ing. Pavel Ryjáček, Ph.D. for his valuable comments, encouragement and tolerance throughout the writing of this thesis. I would also like to thank prof. Ing. Michal Polák, PhD., Ing. Tomas Plachy, Ph.D., and their team for their unbound support and explanation of the testing procedure and equipments while carrying out the experiments on the bridge.

I make a special recognition of my brother, Endalcachew Seyoum, for his unyielding support, encouragement and patience during my study. I thank him for being there whenever I needed him.

I am thankful to all our professors who delivered the courses in this Erasmus Master's programme. All my friends and classmates have played a significant role as moral boosters and have extended all possible help and cooperation. I express my sincere gratitude to them.

My heartily gratitude is for the head of the department of international relations of the faculty, Mrs. Věra Klátová. She provided me with continuous support and cooperation in every challenge I have went through, beginning from Coimbra until graduation. I am grateful to Ms. Jana Tatcheva and Dr. Pořízek Pavel, JUDr. for their counselling and timely assistance in my stay in Prague.

Finally, I would like to take this opportunity to thank to my parents and family for always believing in my capacity. There are no words which can express my very profound gratitude to them. I express my deepest feelings of reverence to them for being the pillars of my strength by encouraging me to elevate myself academically. They gave me the opportunity to be the person I am now and they have always been supportive to all of my adventures. To them I dedicate this thesis.

Abstract

Comprehensive understanding of the behaviour of structures leads to an efficient and sound design that meets imposed safety and comfort requirements. The railway transportation sector today, where high speed railway lines are becoming more and more common, demands for a profound knowledge of the behaviour of railway bridges. A railway bridge is composed of the main load bearing structure, the track, which includes the ballast, sleepers and the rails, and the non-structural elements. The dynamic behaviour of the load bearing structure, which is usually made of steel or concrete or their composite, has been studied for long and is known to a sufficient level of details. However, the degree of influence from the track/ballast on the dynamic behaviour of railway bridges is still a research question.

A set of tests were conducted on a single tracked half-through steel railway bridge to study its static and dynamic properties. Data from the tests was processed in MATLAB to evaluate the natural frequencies and modes of the bridge. The results indicated that the structure was stiffer than originally assumed by analyzing the ‘pure steel’ structure model. A potential cause for the discrepancy between the analysis and the test results was then identified to be the impact of the interaction between the bridge and the track.

The influence of the ballast/track on the dynamic properties of the bridge was assessed in this thesis by implementing and comparing different 3D FEM models of the bridge that describe different structure and track configurations to obtain comparable results with the experiment. A model that included the ballast and Sleepers as 3D solid elements and the rails as Euler-Bernoulli beams gave good agreement with the test results. A 10.3% and 17.7% increase in the natural frequency of the first and third modes of vibration, respectively, were observed as compared to the model that accounted for the mass of the track only. In addition, different parameters influencing the natural frequencies and modes shapes of the bridge were tested and it appears that the ballast introduces considerable additional stiffness. Mass and support condition parameters as well were found to affect the dynamic properties of the bridge.

Keywords: Railway bridges, Ballast/Track, Bridge dynamics, Finite element modelling, Bridge Testing, Modal analysis

Table of contents

Declaration iii

Acknowledgements iv

Abstract v

Table of contents viii

List of figures xi

List of Tables xiv

1. Introduction 1

1.1. Half-through railway bridges 1

1.2. Railway Bridge Track Types and its Components 4

1.3. State of the art: Influence of the track on bridge dynamics 9

2. Purpose of the thesis 11

2.1. Objectives of the thesis 11

2.2. Method and outline of the thesis 12

3. Testing of the bridge 13

3.1. Brief description of the bridge under study 13

3.2. Geometry of the bridge 16

3.3. Production and Erection 19

3.4. Experiments on the bridge 20

3.4.1. Static load tests procedures 24

3.4.2. Analysis and interpretation of the static test results 26

3.4.3. Dynamic load tests procedures 31

3.4.4. Analysis and interpretation of the dynamic test results 32

4. Numerical Modelling 41

4.1. Basics of FEM 41

4.1.1. Steps in FEA Process 42

4.1.2. Types of Elements 44
4.1.3. Eigen Value Analysis 48
4.2. Material properties 50
4.3. Idealization of the bridge components 51
4.4. Interaction between Track and Bridge 54
4.5. Classical Steel Bridge Model alone (CSI-BMO) 56
4.6. ABAQUS models 60
4.6.1. Steel Bridge with the ballast only (ABQ-B3D) 60
4.6.2. Steel Bridge with the ballast and sleepers (ABQ-B&S3D) 62
4.6.3. Whole Steel Bridge – rigid rail to sleeper connection (ABQ-WTR) 64
4.6.4. Whole Steel Bridge – spring rail to sleeper connection (ABQ-WTS) 66
4.7. CSiBridge model (CSI-WTS) 68
4.7.1. Modal Analysis 69
4.7.2. Moving load - Time History Analysis 71
4.8. Simplified model using shell and beam elements 75
5. Discussion and Conclusion 76
5.1. Comparison of experimental data with numerical results 76
5.2. Impact of the ballast properties on the dynamic behaviour of the bridge 79
5.2.1. Influence of the ballast mass 79
5.2.2. Influence of the ballast stiffness 80
5.3. Influence of the support conditions 80
5.4. Conclusions 81
5.5. Recommendations and further research 82
6. Bibliography 83
7. Annexes 86
7.1. MATLAB codes used 86

List of figures

Figure 1: A Through Bridge 3
Figure 2: A Half-through Bridge [1] 3
Figure 3: Illustration of Through and Semi-through bridge configurations [3] 4
Figure 4: Rail Profile 5
Figure 5: Vosshol W14 Fastener 6
Figure 6: Rail pad 6
Figure 7: Concrete Sleeper with the rail pad and fasteners assembled 7
Figure 8: Railway track resting on ballast 8
Figure 9: Location plan of the bridge 13
Figure 10: Side views of the old bridge 14
Figure 11: Top and bottom views of the old bridge 15
Figure 12: Cross-section of the bridge at mid-span 17
Figure 13: Cross-section of the bridge at the supports 17
Figure 14: Longitudinal section of the bridge 18
Figure 15: Bearing fixities and releases 18
Figure 16: Production stage of the bridge 19
Figure 17: Erection of the bridge (On-site placement) 19
Figure 18: Inductive deflection sensors at the abutments 20
Figure 19: Potentiometric deflection sensor at quarter span 21
Figure 20: Inductive displacement sensor at mid-span 21
Figure 21: Acceleration sensor (A31) and Strain gauges (T2X & T3Y) 22
Figure 22: Acceleration sensor (A33) and Strain gauges (T6Y & T7X) 22
Figure 23: Location and designation of sensors 23
Figure 24: Wagon placed on the bridge for LC1 24
Figure 25: View of the wagon with uneven distribution of the additional mass 25
Figure 26: Static Test - Loading Condition 1 25
Figure 27: Static Test - Loading Condition 2 25
Figure 28: Static deflection versus time plot for mid-span sensors in loading condition 1 27
Figure 29: Static deflection versus time plot for mid-span sensors in loading condition 2 28
Figure 30: Strain versus time plot for the static load test 1 29
Figure 31: Strain versus time plot for the static load test 2 30
Figure 32: HV730 Test locomotive making a pass on the bridge 31

Figure 33: Time versus acceleration plots for a train passing at a speed of 50km/hr.....32
Figure 34: Time versus filtered acceleration plots for a train passing at a speed of 50km/hr .35
Figure 35: FFT plot of A33 for a train passing at 50km/hr 37
Figure 36: Original versus filtered signal for the 1st mode of vibration 38
Figure 37: Isolated filtered signal and its FFT for the range 12s – 13s. 38
Figure 38: Isolated filtered signal and its FFT for the range 32s – 40s. 39
Figure 39: Comparison between the oscillation patterns of A32 and A22 for DZS081-50 39
Figure 40: Comparison between the oscillation patterns of A32 and A22 for DZS081-50 40
Figure 41: Commonly used element types (Source: [9]).....44
Figure 42: 2D bar/truss element.....45
Figure 43: 2D beam element.....45
Figure 44: Shell elements.....47
Figure 45: 3D Solid elements 47
Figure 46: Main steel structure as modelled in CSI Bridge and Abaqus (left to right) 51
Figure 47: The ballast as modelled in CSiBridge and Abaqus (left to right) 52
Figure 48: 3D Solid Sleeper model in Abaqus 52
Figure 49: An equivalent section of the rails used for analysis 53
Figure 50: Longitudinal resistance of the track as a function of longitudinal displacement ...54
Figure 51: Resistance (k) of the track per unit length vs. longitudinal displacement (u) 55
Figure 52: Longitudinal resistance of Vossloh W14 Clamp Slk 14 fastner node [13].....55
Figure 53: First mode of vibration - Frequency 9.295Hz 57
Figure 54: Second mode of vibration - Frequency 16.27Hz.....57
Figure 55: Third mode of vibration - Frequency 17.68Hz.....58
Figure 56: Fourth mode of vibration - Frequency 26.68Hz.....58
Figure 57: Fifth mode of vibration - Frequency 27.96Hz.....59
Figure 58: Steel Bridge modelled with the ballast only.....60
Figure 59: First and second mode shapes - Frequencies 9.23Hz and 15.77Hz, resp.....61
Figure 60: Third and fourth mode shapes - Frequencies 18.73Hz and 25.95Hz, resp.....61
Figure 61: Fifth mode shape - Frequency 26.46Hz 61
Figure 62: Steel Bridge with the ballast and sleepers 62
Figure 63: First and second mode shapes - Frequencies 10.24Hz and 16.58Hz, resp.....62
Figure 64: Third and fourth mode shapes - Frequencies 21.07 and 28.58Hz, resp. 63
Figure 65: Fifth mode shape - Frequency 32.18Hz 63
Figure 66: The whole bridge model including all elements of the track 64

Figure 67: First and second mode shapes - Frequencies 10.663Hz and 16.54Hz, resp. 64
Figure 68: Third and fourth mode shapes - Frequencies 22.7Hz and 26.48Hz, resp. 65
Figure 69: Fifth mode shape - Frequencies 31.49Hz 65
Figure 70: First and second mode shapes - Frequencies 10.435Hz and 16.626Hz, resp. 66
Figure 71: Third and fourth mode shapes - Frequencies 21.668Hz and 29.705Hz, resp. 67
Figure 72: Fifth mode shape - Frequency 32.498Hz 67
Figure 73: CSiBridge models 68
Figure 74: First and second mode shapes - Frequencies 10.79Hz and 16.98Hz, resp. 69
Figure 75: Third and fourth mode shapes - Frequencies 22.03Hz and 30.74Hz, resp. 70
Figure 76: Fifth mode shape - Frequency 34.56Hz 70
Figure 77: HV 730 dimensions 71
Figure 78: Definition of the test locomotive 71
Figure 79: Moving load definition for the locomotive at a speed of 40km/hr. 72
Figure 80: Values of damping to be assumed for design purposes 72
Figure 81: Definition of the time history load case 74
Figure 82: Mid-span acceleration in the direction of U_z 74
Figure 83: Simplified model for quick analysis 75

List of Tables

Table 1: Steel bridge plate dimensions 16
Table 2: Summary of static load test results for loading condition 1 26
Table 3: Summary of static load test results for loading condition 2 27
Table 4: Strains measured in static load test 1 28
Table 5: Strains measured during static load test 2 29
Table 6: Extreme vertical accelerations of the bridge at the quarter-span 33
Table 7: Extreme vertical accelerations of the bridge at mid-span 34
Table 8: Extreme vertical accelerations of the bridge from sensors at the third quarter-span 34
Table 9: Summary of the first five natural frequencies and their associated mode shapes 40
Table 10: Material properties used in the models 50
Table 11: Dimension details for B03 type concrete sleepers 56
Table 12: Summary of modes for model CSI-BMO 59
Table 13: Summary of modes for model ABQ-B3D 61
Table 14: Summary of modes for model ABQ-B&S3D 63
Table 15: Summary of modes for model ABQ-WTR 65
Table 16: Summary of modes for model ABQ-WTS 67
Table 17: Summary of modes for model CSI-WTS 70
Table 18: Summary of modes for the simplified model 75
Table 19: Brief description of the models' parameters 76
Table 20: Summary of frequencies and modes of vibration from the numerical models 78
Table 21: Comparison of FEM results with the experiment 79
Table 22: Influence of ballast mass on vibration frequencies 79
Table 23: Influence of ballast elastic modulus on vibration frequencies 80
Table 24: Influence of boundary condition on vibration frequencies 81

1. Introduction

1.1. Half-through railway bridges

A railway bridge will have two basic functional requirements: provision of support to the railway traffic and provision of adequate clearances between the structure and the traffic on and underneath it. The former is to be fulfilled by designing and constructing a robust structure with satisfactory strength that is durable and which undergoes limited deformation under the action of loads. The later however is achieved by ensuring adequate clearance gauges according to railway and highway authorities.

A bridge provides a running surface for the traffic that crosses it. Therefore, to ensure minimum interface issues, it is best to arrange all the structural elements below that surface – i.e. the traffic runs on top of the bridge structure. But the depth of structure, including the thickness of surfacing or ballast, that is needed may in some cases be too great to be accommodated between the level of the trafficked surface (as dictated by levels adjacent to the bridge and by maximum gradients) and the level of minimum clearance above the ground, river, road or railway below. [1]

For bridges on new alignments there's greater freedom with the design, both depth and structure typology may undergo substantial changes due to the wide range of possibilities in the choosing of track formation, clearances etc. Replacement bridges are more likely to be constrained to a shallow construction depth, due to the need to maintain a clearance below and to avoid the lifting of the track.

The 'construction depth' of a railway bridge is the vertical dimension between the tops of the rails and the bridge soffit. Because the lowest acceptable soffit level is usually constrained by the existing roadway and its required headroom, and the level of the railway is very tightly constrained by track geometry, the available construction depth is a very important design parameter. It has a strong influence on the form of construction that can be adopted.

There are three components that add up to the construction depth of the bridge: the track depth (top of rail to underside of sleeper), the ballast depth beneath the sleepers and the structure depth (top of the deck or ballast tray to the underside of the structure and including the thickness of the waterproofing). Of these components, the track depth is fixed by the choice of track and the ballast depth is usually 300 mm. The structure depth is therefore

usually constrained by the difference between the available construction depth and the sum of track depth and ballast depth.

For short spans, a deck-type structure, where the deck acts mainly as a beam spanning between abutments, can be entirely arranged within a shallow construction depth. Two common forms of such construction using steel as the main structural material are: solid steel slabs and orthotropic decks. Solid steel slabs comprise simply supported slabs spanning longitudinally between abutments. These solid steel slabs can be used to form such decks for railway bridges approximately up to 3m. The slab simply sits on the abutments on elastomeric strip bearings, it is approximately 200 or 250 mm thick and no fabrication is involved (other than cutting to size). Their advantage is very low structure depth. Orthotropic decks, on the other hand, are used for spans up to 9m. A very shallow structure depth of approximately 300 to 400mm can be achieved using an all-steel units spanning longitudinally between abutments. This deck unit comprise a steel deck plate (20 or 25 mm thick) with T sections welded to its lower face (usually 600mm of spacing). The deck unit is relatively flexible transversally, so robust kerbs of containment can be achieved using independent parapet walkway units located clear of the tracks; alternatively , parapets and robust kerbs can be provided by bolt-down steel units at either side of the deck (to resist the horizontal loads, transverse bracing must be provided between the T sections). [2]

For longer spans, a different structural arrangement can be adopted, in which the traffic runs through the structural envelope. There then are two basic options – a ‘through’ configuration and a ‘half-through’ configuration. In a ‘through bridge’ the traffic is completely inside the structural envelope – typically the traffic runs inside a truss, with the trusses either side of the carriageway, top bracing above the carriageway and the deck that directly supports the traffic below. (See Figure 1)

In a half-through bridge, the traffic is only partially inside the structural envelope – there are girders (or trusses) either side and a deck below but the girders are not as high as the traffic envelope and thus there cannot be any bracing to the top flanges (or chords). This means that a half-through bridge is in the form of a ‘trough’, i.e. it has a square U-shaped form. (See Figure 2)

A ‘half-through’ bridge configuration provides a solution for small and medium span bridges where the depth available between the trafficked surface (top of rails for a railway bridge)

and the clearance level beneath the bridge is too shallow to accommodate the structural elements spanning across the bridge supports. This form of construction is more commonly seen in railway bridges and footbridges, but is sometimes used for highway bridges.

Figure 1: A Through Bridge

Figure 2: A Half-through Bridge [1]

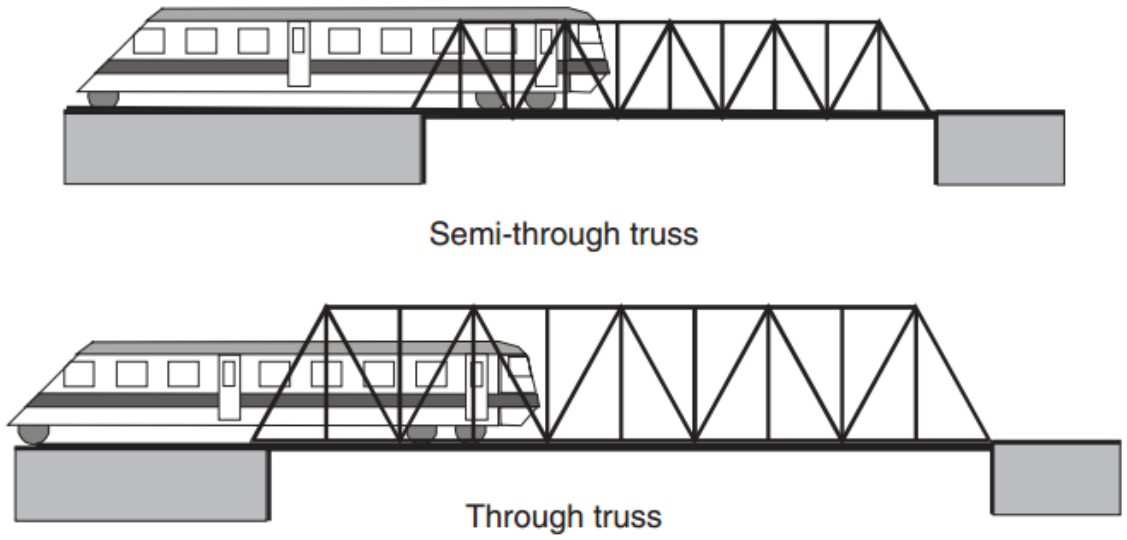

Figure 3: Illustration of Through and Semi-through bridge configurations [3]

1.2. Railway Bridge Track Types and its Components

Railway bridges are mainly constituted by the load bearing bridge structure and the track. The track can be defined as comprising the rails, sleepers and ballast that provide support and guidance to rail traffic. The great majority of tracks these days are of the conventional ballasted, cross-sleepered type. The rails are fixed to transverse sleepers (of either timber, steel or pre-stressed concrete), which are set in a bed of crushed stone ballast.

New or replacement bridges are usually designed to accommodate this type of track, and the weight of the ballast usually adds substantially to the superimposed dead load. However, in order to achieve the minimum possible construction depth, or to minimise dead weight of a bridge, it may be necessary in extreme cases to omit the sleepers and ballast and to fasten the rails directly to the bridge deck. This is known as “direct fastening”.

Direct fastening comes at the cost of difficulties in maintaining satisfactory transition from the directly fastened track to the ballasted track at the ends of the bridge. Such fastening requires high degree of care and precision during maintenance. The reduced dead load, compared to a ballasted bridge, may have an adverse effect on the dynamic response of the bridge, particularly for short spans, and a check should be made that the natural frequency is within the prescribed limits. Very light bridges can also be prone to hammering of the bearings under load, and are less resistant to accidental vehicle impact where they span over

highways. In general, a reduced ballast depth is often preferable to direct fastening from the point of view of track maintenance.

On many older steel bridges, the rails are fixed to longitudinal timber sleepers, which are fixed directly to the bridge structure without any ballast. However, such construction details are now rarely used for new bridges on main line railways because of track maintenance problems, especially the run-on/run-off effects and the lack of flexibility in track location. [2]

Rails are the longitudinal steel members that directly guide the train wheels evenly and continuously. They provide smooth running surfaces for the train wheels and guide the wheel sets in the direction of the track. The rails also accommodate the wheel loads and distribute these loads over the sleepers or supports. Lateral forces from the wheel sets and longitudinal forces due to traction and braking of the train are also transmitted to the sleepers and further down into the track bed. They must have sufficient stiffness to serve as beams that transfer the concentrated wheel loads to the spaced sleeper supports without excessive deflection between supports. A modern steel rail has a flat bottom and its cross section looks to be derived from an I-profile. The upper flanges of the I-profile have been converted to form the rail head, as shown in Figure 4.

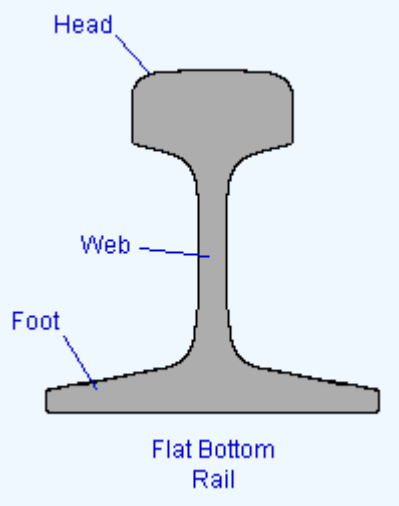

Figure 4: Rail Profile

Fasteners are typically required to retain the rails on the sleepers and to resist vertical, lateral, longitudinal and overturning moments of the rails. The force systems causing these movements are from the wheels and from temperature change in the rails. The choice of fastening greatly depends on the type of sleeper and geometry of the rail.

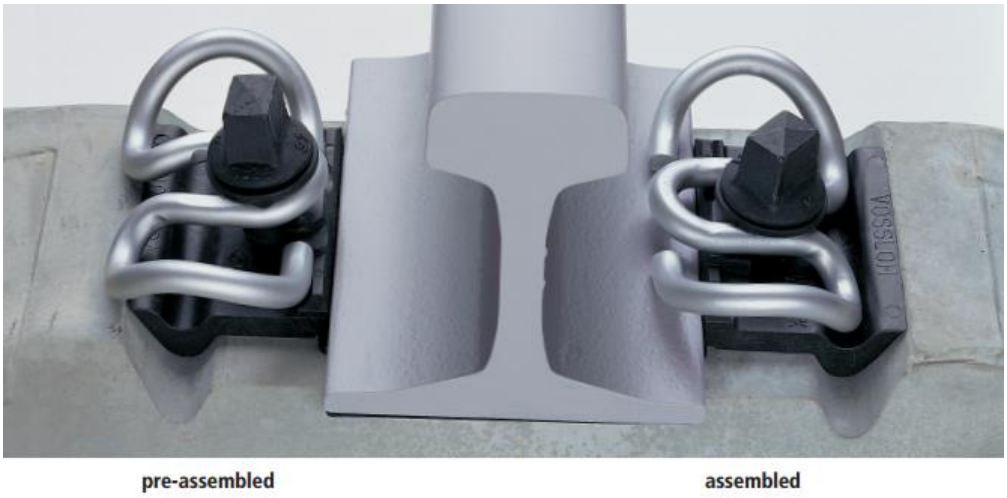

Figure 5: Vosshol W14 Fastener

Rail Pads or **Plates** are required between the rail seat and the sleeper surface to fulfil various functions. These include providing resilience for the rail-sleeper system, damping of wheel induced vibrations, and reduction of rail-sleeper contact attrition.[4] Rail-pads are inserted between the sleepers and the rails. The rail pads provide electrical insulation of the rails and they protect the sleepers from wear. The rail pads also affect the dynamic behaviour of the track. The rail pad stiffness should be as low as possible to a certain limit. Rail-pads with a dynamic stiffness between 100 and 200 MN/m and static pad stiffness between 50 and 100 MN/m are commonly used in Europe.

Figure 6: Rail pad

Sleepers are essentially beams that span across and tie together the two rails. They have several important functions including receiving the load from the rail and distributing it over the supporting ballast at an acceptable ballast pressure level, holding the fastening system to maintain proper track gauge, and restraining the lateral, longitudinal and vertical rail movement by anchorage of the superstructure in the ballast. In addition, sleepers provide a cant to the rails to help develop proper rail-wheel contact by matching the inclination of the conical wheel shape. They also provide electrical insulation between the two rails. Most sleepers today are of pre-stressed concrete, which is preferred for heavily used high-speed routes, but some timber sleepers are in use, together with increasing numbers of steel sleepers. The choice usually depends on the speed of the train and economic reasons. For standard gauge tracks, the optimum spacing between sleepers is 0.60m.

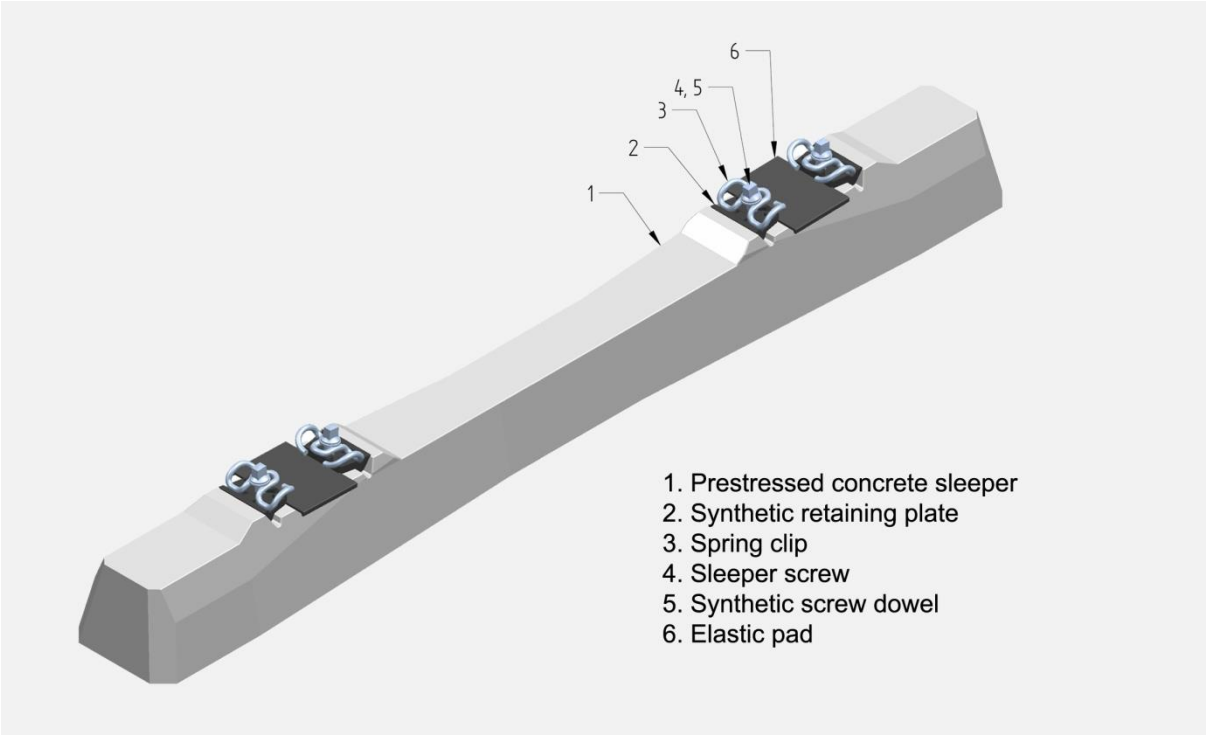

Figure 7: Concrete Sleeper with the rail pad and fasteners assembled

Ballast is the layer of crushed stone on which the sleepers rest. It usually consists of hard angular pieces of crushed stone of about 50 – 65 mm size. The ballast assists in track stability by distributing load from the sleepers uniformly over the bridge. It anchors the track in place against lateral, vertical and longitudinal movement by way of irregular shaped ballast particles that interlock with each other. Any moisture introduced into the system can easily drain through the ballast away from the rails and sleepers. The coarse grained nature of

ballast assists in track maintenance operations due to its easy manipulation. The rough interlocking particles also assist in absorbing shock from dynamic loads by having only a limited spring-like action. The British normal practice, for instance, is to provide at least 300 mm of ballast under the sleeper, but it is sometimes necessary to provide less than this where construction depth is limited. A minimum of 200 mm depth of ballast is necessary to prevent damage to the bridge waterproofing by track maintenance machines and to ensure the satisfactory distribution of wheel loads. However, where construction depth is severely restricted, ballast depths of 150 mm (minimum) may be preferable to direct fastening, provided that the effect on load distribution is considered and appropriate precautions are taken to protect the waterproofing. During normal track maintenance, the ballast is mechanically compacted under the sleeper. The compaction is not uniform under the length of the sleeper but is concentrated in the areas under the rails. [2]

Figure 8: Railway track resting on ballast

1.3. State of the art: Influence of the track on bridge dynamics

The behaviour of the main load bearing elements of a railway bridge have been studied for a long time now and as a result, numerous well defined idealizations and methods of modelling are available for the majority of today's bridge construction materials. However, the properties of the ballast/track, that are hard to model, were not given as equal focus in the past as their bridge construction material counterparts (timber/steel/concrete/composite).

Due to modernization of the railway transportation sector, as high speed railway lines are becoming more and more common, researches are nowadays being carried out to assess the material properties of the track and its influence on the overall bridge dynamics. This section presents a brief summary of pertinent researches on this topic of interest.

In the dynamic analysis of railway bridges discrepancies between calculation results and test results are frequently observed. In many cases, the dynamic response of bridges under moving loads is overestimated and the predictions made are too conservative.[5][6] This problem especially applies to relatively short railway bridges (spans below 30m) with ballast superstructure.

Most idealizations of the interaction between the track and the bridge try to simplify the generalized problem in to a 2D system. As such, a 2D model consisting two layers of Euler-Bernoulli beams, one placed on top of the other and connected to each other by a spring – dashpot system has been studied in [5],[7]. The springs and dashpots are set to represent the vertical and longitudinal stiffness and damping characteristics at the interface between the two entities. Apart from bridges, this method had gained popularity among researchers focusing on the track dynamics and sub grade interaction.

Efforts have been made to prepare both 2D and 3D models with springs that resulted in close agreement between experimental observations and analytical model results. In [8] the track was first approximated as a rail (beam) on discrete supports. Later, the same was modelled using 3D elements including the sub grade.

In recent developments, 3D FEM models that represent the ballast as a solid element were proposed by [9] and [10]. Such systems of modelling take good advantage of the capacity of modern FEM software, such as Abaqus and Ansys, in modelling the continuity of the track beyond the bridge by imposing appropriate boundary conditions along the railway. Liu [9] used Shell elements to model the steel boxes, Solid elements for the ballast and concrete slab

and Beam elements for the rail while representing the sleepers only with their mass in the numerical analysis of a composite bridge in Ansys. The track had significant effect on the dynamic properties of the bridge and the analysis presented remarkable agreement with the experiment.

In [10] , again, Bornet achieved good conformity between measured and analyzed dynamic properties by using solid elements to model the ballast, 3D Thick (Timoshenko) Beam elements for the main beams, sleepers and rails and Thin (Kirchhoff) shell elements for the steel deck plates of a truss railway bridge in LUSAS. This method of modelling is used in this thesis as it is suitable for 3D FE analysis and delivers good results.

2. Purpose of the thesis

As the needs for better means of transportation are rising as a result of globalization and a more connected world, maintaining and revitalizing older transportation infrastructure plays a significant role. The railway route from Rokycany – Nezvěstice was studied by the appropriate authorities and the need for revitalization and upgrading was believed necessary. This revitalization included the replacement of an old single track railway bridge at station 9,296km in Mirošov, a small town in Czech Republic. A road way passes underneath this bridge and thus limitations on the depth of the were put by concerned authorities. As a result, a steel half through bridge of small depth that is first of its kind in the Czech Republic was proposed and designed by doc. Ing. Pavel Ryjáček. The construction of this ballasted and cross-sleepered steel railway bridge of half through type was close to completion by the end of July 2016. Since not much was known about the degree of influence the track will have on the dynamic properties of the such a bridge, a set of tests were conducted on it before commencing service in August.

It was found from the tests that the structure is stiffer than originally assumed from the 'pure steel' structure model. A potential cause for the discrepancy between the analysis and test results was then identified to be the impact of the interaction between the bridge and the track and ballast. The need to analyze the degree of impact of this interaction is the reason for this Master's thesis. The purpose of this thesis is to estimate the influence of the ballast and the track on the dynamic properties of the bridge by analyzing the results from the tests conducted and creating FEM models of the bridge that best describe the structure and track configuration to obtain comparable numerical natural frequencies and modes with experimental ones.

The thesis also aims at assessing the influence of the ballast and track components on the static properties of the bridge by examining the degree of influence of the mentioned components in providing additional stiffness to the bridge.

2.1. Objectives of the thesis

The aim of the work is to:

- analyze the results of the static and dynamic load test on the bridge in Mirošov

- create the numerical model, including the track and the ballast, to achieve the good correlation with the load test
- create simplified model, and modify it to have a good correlation as well
- analyze the impact on the ballast and track on the dynamic behaviour and establish conclusions and recommendations

2.2. Method and outline of the thesis

The first chapter gives some general introduction about railway bridges in general and half through bridges in particular. Common track types and their components are discussed; followed by a review of relevant researches in assessing the impact of track on the dynamic properties of railway bridges. The purpose of this thesis and its objectives are briefly outlined in chapter two.

Chapter three presents the testing of the bridge. A brief description of the bridge is given along with its geometric properties and production. The static and dynamic load test procedures are discussed in detail and results are presented and analyzed.

Chapter four describes the numerical modelling portion of the thesis. An introduction about FEM and Eigenvalue analysis is presented in short. The idealization of the bridge components in the numerical models is discussed and material properties used in the models are tabulated. Six different models are then presented and discussed along with the results obtained for each model.

The results obtained for the different models in chapter four are summarized, analyzed and compared in chapter five. The influence of crucial track and bridge parameters are evaluated compared and discussed. A conclusion is finally drawn from this analysis followed by recommendations for future research.

3. Testing of the bridge

3.1. Brief description of the bridge under study

The bridge under study is a half-through steel railway bridge located in Mirošov town on the track from Rokycany to Nezvěstice, Czech Republic. Its physical coordinates are at 49°41'13.1"N 13°39'48.5"E and is stationed at km9296. It serves as a replacement to an old bridge underneath which passes a road way. The free height under the bridge is just 3.5m. This brought about the need to limit the structural depth, which in turn lead to the choice of a steel half-through type structural configuration.

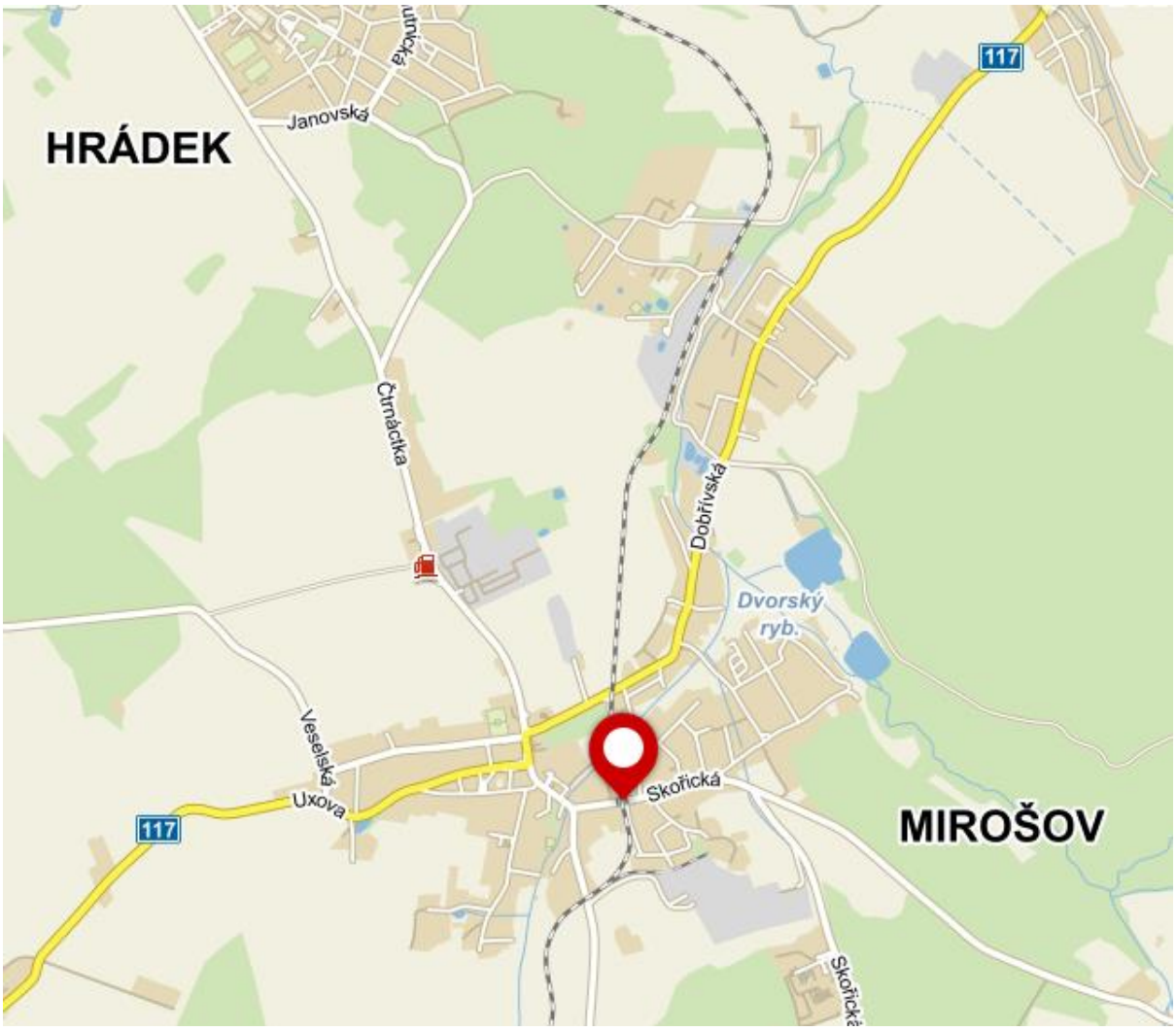

Figure 9: Location plan of the bridge

Figure 10: Side views of the old bridge

Figure 11: Top and bottom views of the old bridge

3.2. Geometry of the bridge

The new half-through bridge is simply supported over a span of 10.6m as it supports a single-track railway line. The superstructure is composed of two main load bearing elements:

1. The steel plate that acts as the deck of the bridge providing direct support for the ballast and track. And,
2. The steel boxes at the two edges longitudinal to the track direction that give support and strength to the steel plate.

It has a transverse structural width of 4400mm and measures 5950mm when accounting for the non structural elements such as the guard rails. S355 grade steel is used in all the structural elements of this bridge and class II construction was implemented.

The bridge has an overall depth of just 665mm with the deck plate having a thickness of 80mm. ČSN 736201 requires a minimum ballast depth of 300mm below the sleeper's bottom. Accordingly, a total ballast depth of 450mm and a net depth of at least 300mm have been provided. The bridge carries a single track positioned/situated in the middle of the transverse width of the bridge. This track is supported by B03 type concrete sleepers that are placed at a spacing of 600mm. Two S49 (49E1) type rails are fastened on to these sleepers by Vossloh W14 fasteners.

	Material	**Thickness**	**Width/Height**
		[mm.]	**[mm.]**
Deck at span	S355	80	4440
Deck at support	S355	160	4440
Box webs	S355	25	505
Box flanges	S355	80	420

Table 1: Steel bridge plate dimensions

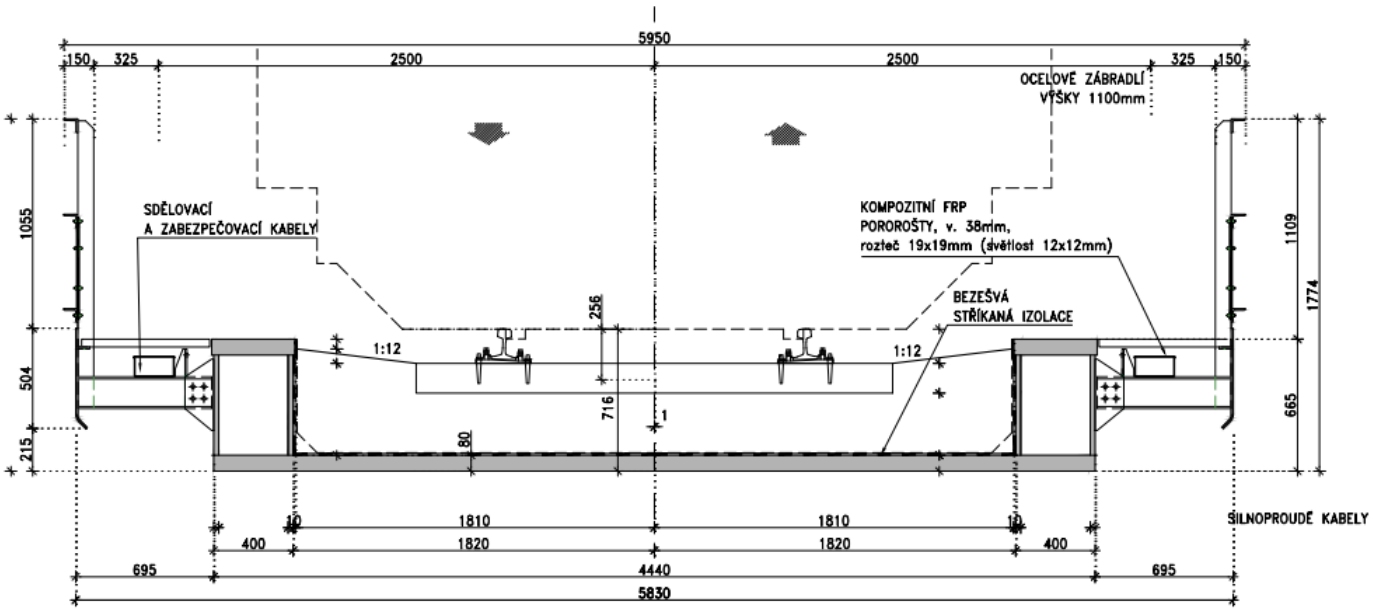

Figure 12: Cross-section of the bridge at mid-span

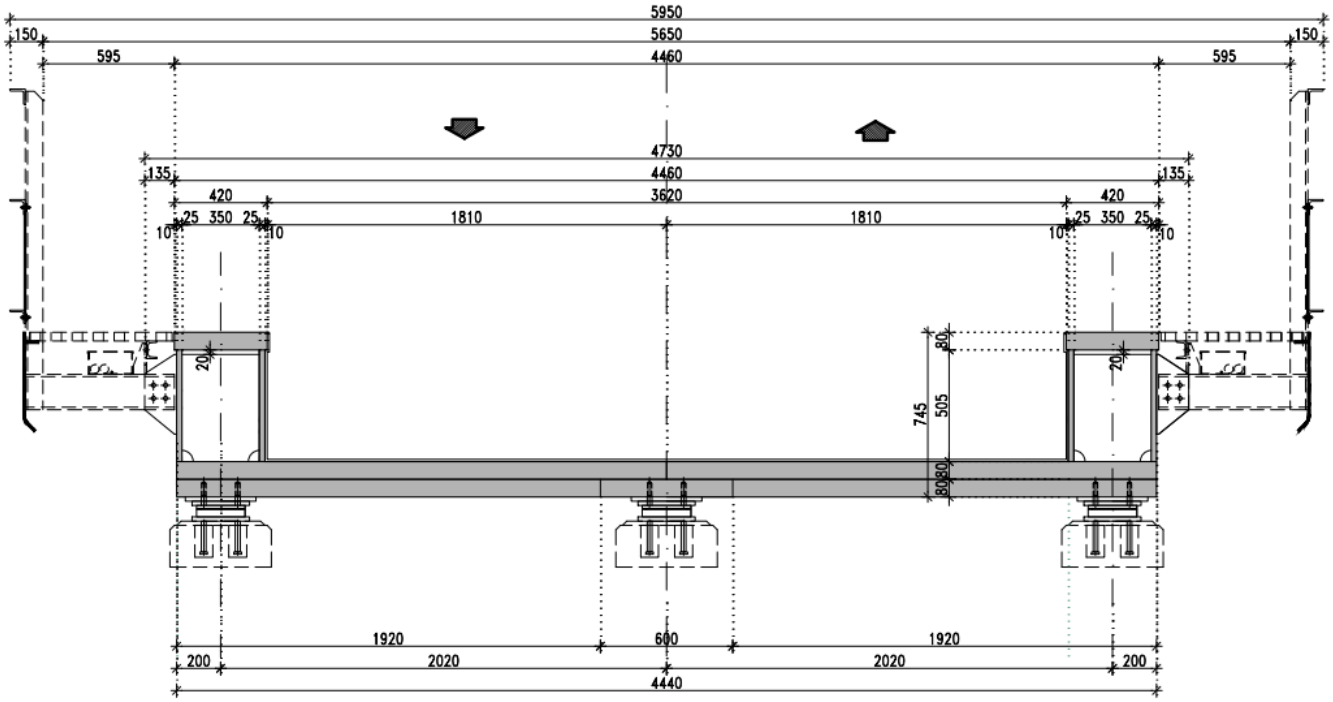

Figure 13: Cross-section of the bridge at the supports

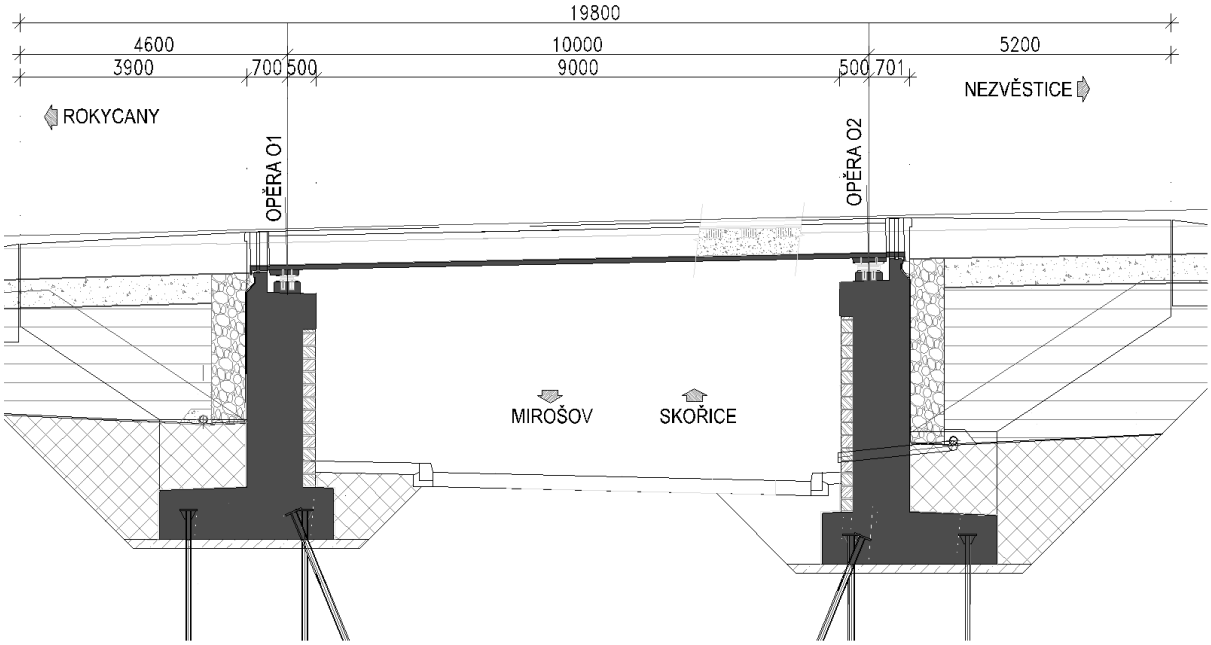

Figure 14: Longitudinal section of the bridge

The bridge bearing support mechanism is illustrated in Figure 15 below. The left centre bearing is fully fixed against all translations, the right centre bearing allows for longitudinal translation and the remaining four bearings allow translations in both the longitudinal and transverse directions. All bearings allow for rotation.

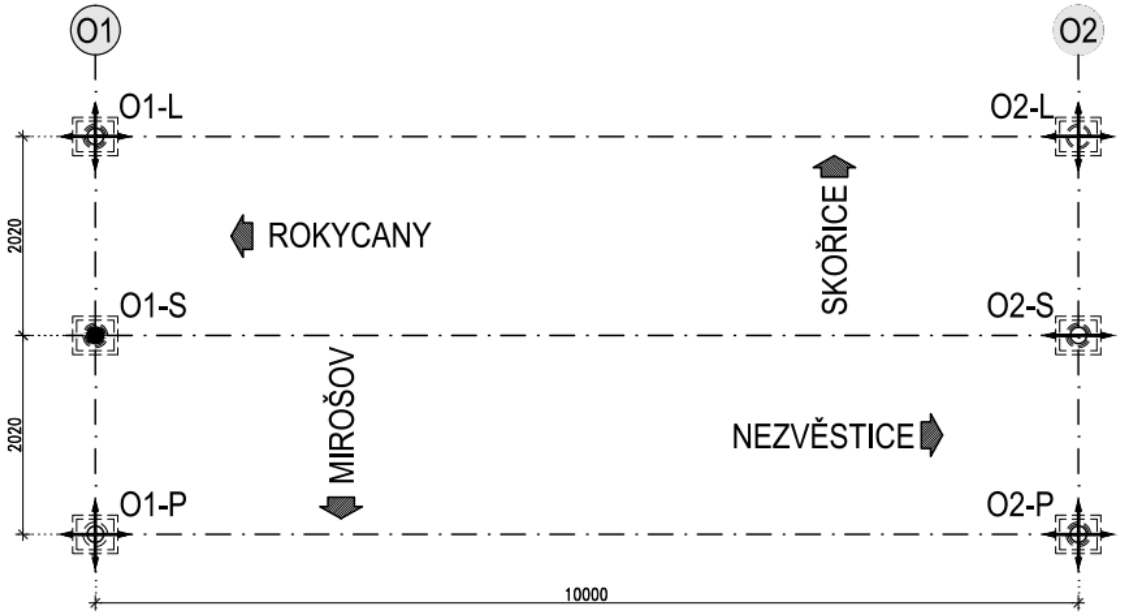

Figure 15: Bearing fixities and releases

3.3. Production and Erection

The new bridge was produced and assembled in a factory and brought over to the site where it was put to its current coordinates by a crane. The deck is formed from four thick steel plates that are welded in such a way that the weld lines in the transverse direction close to the mid-span of the bridge are not aligned. The box sections at the two edges, too, are formed by welding three individual steel plates (two serving as the web and one as the top flange of the box) on the deck. A thicker flange steel plate is welded on top of the two webs and this forms the box. Figure 16 and Figure 17 demonstrate the production stage and the erection/placement after the construction of the supporting abutments have been completed.

Figure 16: Production stage of the bridge

Figure 17: Erection of the bridge (On-site placement)

3.4. Experiments on the bridge

A set of tests were conducted on the bridge on August 3, 2016 to determine the actual structural behavior and basic properties of the bridge. These include deflections, stresses and accelerations at particular points of interest on the bridge under static load and dynamic loads. Sensors were placed at three points in the transverse direction: one at the middle of the plate, one each at the edges just below the box sections on the left and right. Five spots of interest were assessed in the longitudinal direction: one each at the abutments/supports, one at quarter span, one at mid span and one at three quarter of the span. The scheme is illustrated in Figure 23.

Three types of relative deflection sensors were used: induction deflection sensors at the abutments where the deflections are small and potentiometric deflection sensors at the span. Details of the equipments used are discussed below.

Inductive displacement sensors (Figure 18) of measuring range ± 1 mm and accuracy class 0.5 were employed near the abutments where deflections are considerably small. These sensors are used at points ISD11, ISD12, ISD13, ISD51, ISD52 and ISD53.

Figure 18: Inductive deflection sensors at the abutments

Potentiometric deflection sensors (Figure 19) allow measuring static deflections of structures in the range of ± 50 mm since a smaller radius pulley sensor was used. These sensors were used to measure the vertical static deflections of the supporting structure of the bridge at points P21, P22, P23, P41, P42 and P43.

Figure 19: Potentiometric deflection sensor at quarter span

Inductive displacement sensors (Figure 20) with frequency range of 0 to 400 Hz and measuring range of ± 25 mm at a corresponding accuracy class 0.2 were used in both the static load test and also during the dynamic load test to measure vertical deflections of the supporting structure of the bridge in points P31, P32 and P33.

Figure 20: Inductive displacement sensor at mid-span

Acceleration sensors measuring vibrations in the range of 0.2kHz to 8kHz were employed at 9 locations along with eight LY11-10 / 120 resistive foil strain gauges. A thermometer and an anemometer were used to check the temperature and wind speed variation all along the tests. Data from these sensors and measuring instruments was stored in two data loggers. The test procedures and their outcome for each case are discussed in the following sections.

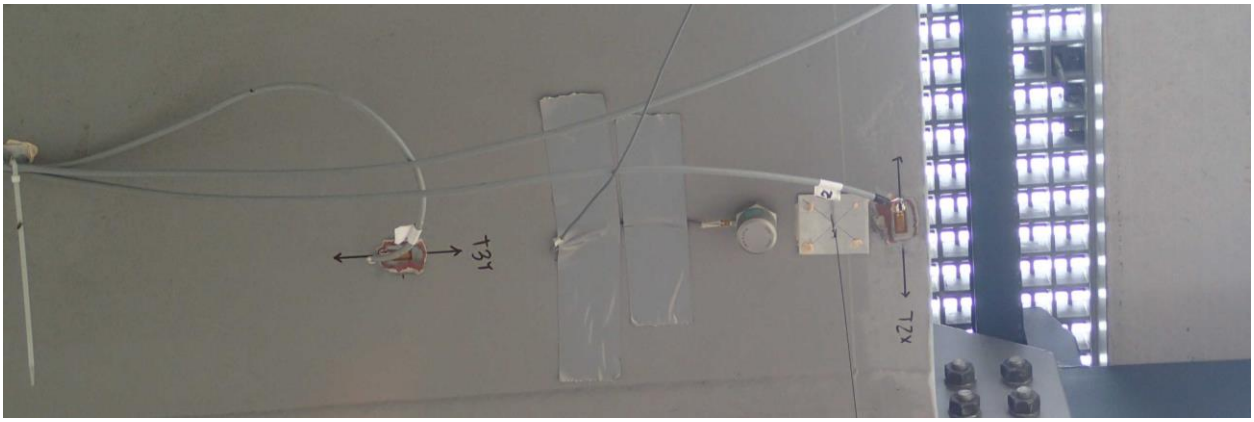

Figure 21: Acceleration sensor (A31) and Strain gauges (T2X & T3Y)

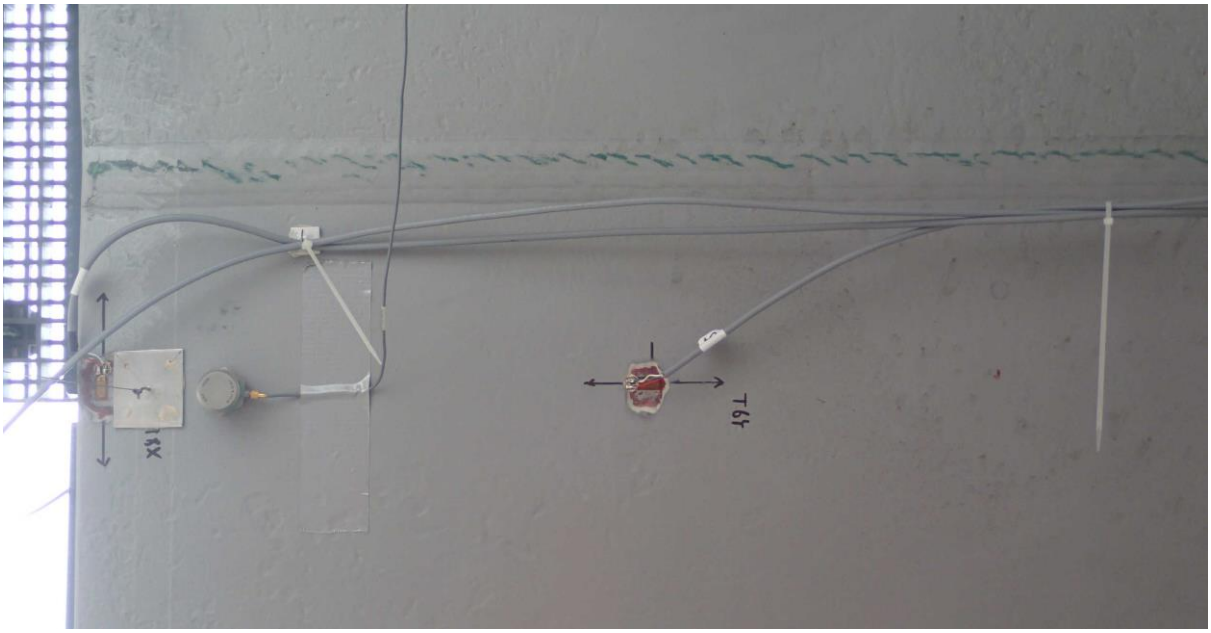

Figure 22: Acceleration sensor (A33) and Strain gauges (T6Y & T7X)

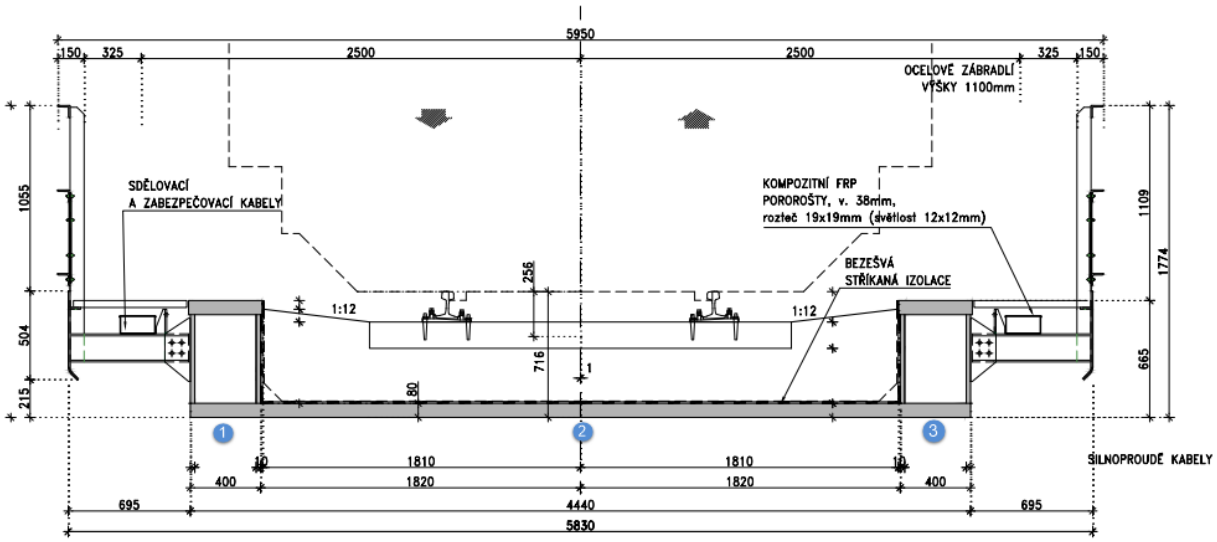

Abutment 01:

UZ1		UZ2
ISD11	ISD12	ISD13

Quarter span:

P21	P22	P23
A21	A22	A23

Mid-span:

P31	P32	P33
A31	A32	A33
T1X, T2X, T3Y	T4X, T5Y	T6Y, T7X, T8X

Three quarters span:

P41	P42	P43
A41	A42	A43

Abutment 02:

ISD51	ISD52	ISD53
UZ3		UZ4

Figure 23: Location and designation of sensors

3.4.1. Static load tests procedures

The goal of this test was to determine the actual deflections and stresses on the bridge due to a standard load according to the Czech national code for testing bridges. With the aim of extracting the mentioned parameters, a special four axle coach/wagon with tare mass of 72.5tonnes carrying an additional mass of 20tonnes was placed on the bridge (see Figure 24) in such a way that it would cause maximum stresses and deflections on the structure. Although the test was previously designed assuming equal distribution of this load to the four axles (23.125tonnes), it was later found out that the additional mass was not evenly distributed in the vehicle. (See Figure 25) Therefore, the axle loads were recalculated considering the mass distribution to suit for the analysis. Two loading conditions were thus evaluated to see the resulting deformation from each case. The final axle load and the sensors locations are shown in Figure 26 & Figure 27.

Figure 24: Wagon placed on the bridge for LC1

Figure 25: View of the wagon with uneven distribution of the additional mass

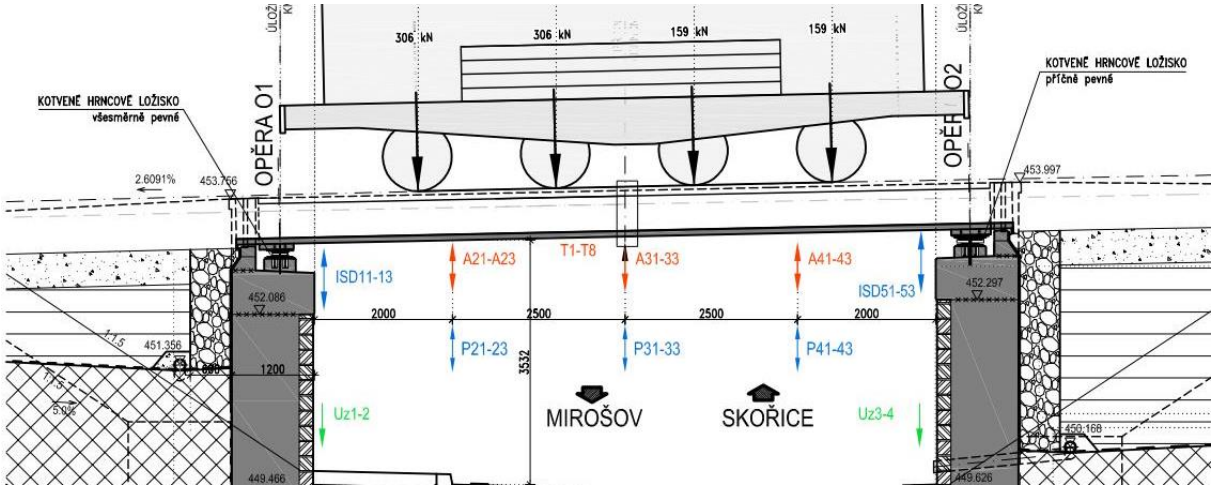

Figure 26: Static Test - Loading Condition 1

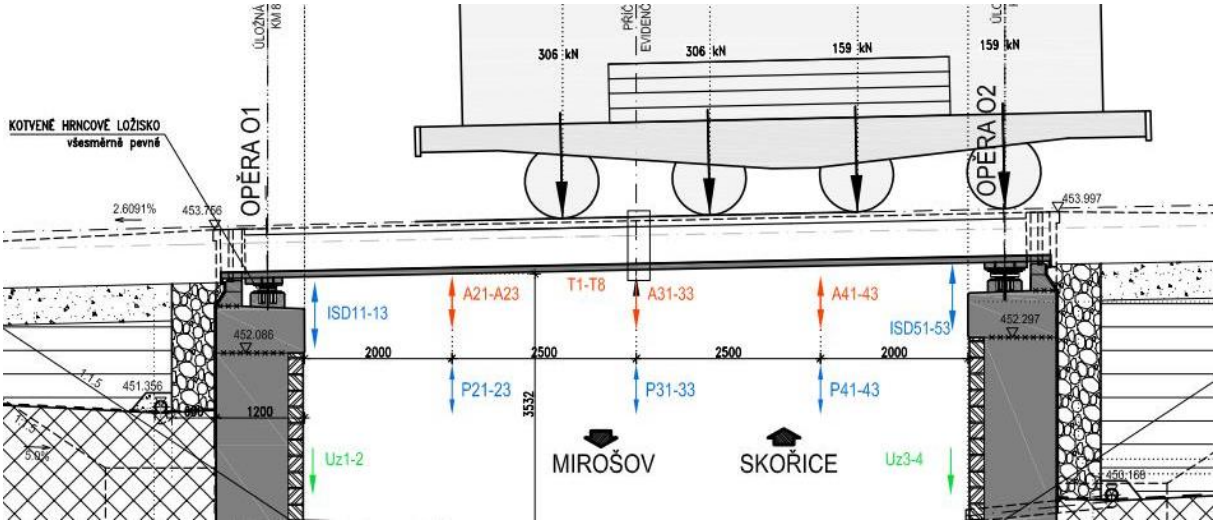

Figure 27: Static Test - Loading Condition 2

3.4.2. Analysis and interpretation of the static test results

Structural behaviour has always been monitored until the effect of the load can be regarded as stable within as stated in Article A.5 of ČSN 736209 [11]. According to the standard, static load tests should be carried out with a static load that stays on the structure for at least 5 minutes for steel structures. Both static load tests have been assessed with the loading vehicle standing still in the span of the bridge for at least 15 minutes which fulfils the requirements stated in the above mentioned standard. The test results are affected by inaccurate measurements. Expanded uncertainty $U_k = 2$ interval determines the assessed values that represents the probability of coverage approximately 95%. These values are calculated and defined to every sensor up on calibration and are shown in the following tables.

Sensor designation	Measured static deflections			
	at full load		after unloading	
	value	Extended uncertainty	value	Extended uncertainty
	[mm.]	[mm.]	[mm.]	[mm.]
P21	2.19	± 0.68	0.22	± 0.68
P22	6.40	± 0.62	0.25	± 0.62
P23	2.27	± 0.47	0.25	± 0.47
P31	3.10	± 0.03	0.07	± 0.03
P32	7.49	± 0.07	0.08	± 0.07
P33	3.12	± 0.02	0.05	± 0.02
P41	2.10	± 0.44	0.22	± 0.44
P42	5.01	± 0.33	0.26	± 0.33
P43	2.23	± 0.50	0.25	± 0.50
ISD11	0.47	± .004	0.03	± .004
ISD12	0.48	± .004	0.05	± .004
ISD13	0.42	± .006	0.03	± .006
ISD51	0.40	± .005	0.01	± .005
ISD52	0.58	± .004	0.03	± .004
ISD53	0.49	± .004	0.04	± .004

Table 2: Summary of static load test results for loading condition 1

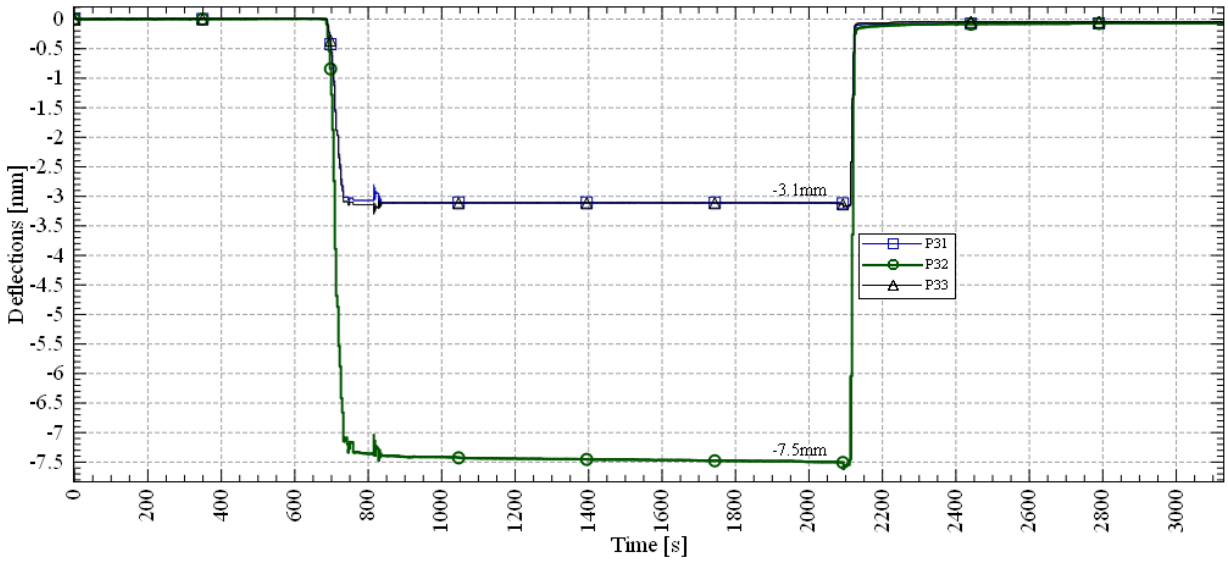

Figure 28: Static deflection versus time plot for mid-span sensors in loading condition 1

Sensor designation	Measured static deflections			
	at full load		after unloading	
	value	Extended uncertainty	value	Extended uncertainty
	[mm.]	[mm.]	[mm.]	[mm.]
P21	2.00	± 0.68	0.16	± 0.68
P22	4.75	± 0.62	0.04	± 0.62
P23	1.94	± 0.47	0.02	± 0.47
P31	2.91	± 0.03	0.04	± 0.03
P32	7.72	± 0.07	0.06	± 0.07
P33	3.00	± 0.02	0.02	± 0.02
P41	1.88	± 0.44	0.00	± 0.44
P42	5.23	± 0.33	0.06	± 0.33
P43	2.06	± 0.50	0.01	± 0.50
ISD11	0.32	± 0.004	0.00	± 0.004
ISD12	0.30	± 0.005	0.01	± 0.005
ISD13	0.28	± 0.006	0.01	± 0.006
ISD51	0.51	± 0.005	0.02	± 0.005
ISD52	0.82	± 0.004	0.05	± 0.004
ISD53	0.59	± 0.004	0.03	± 0.004

Table 3: Summary of static load test results for loading condition 2

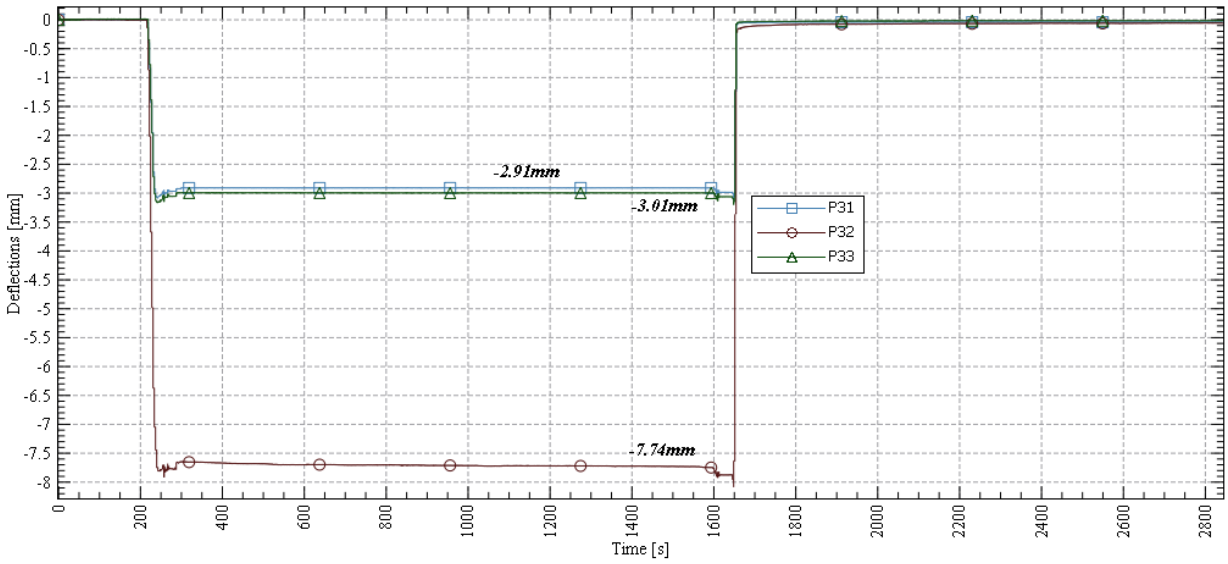

Figure 29: Static deflection versus time plot for mid-span sensors in loading condition 2

The strain gauges also recorded relative strains at nine selected locations. Six of which were placed along the direction of the bridge and three in the transverse direction. Equivalent stresses were calculated from these values by multiplying with the elastic modulus value of steel E_s = 210GPa. Table xxx shows the results obtained and tensile stresses are indicated positive.

Designation	At full load		After unloading	
	Relative strain	Equivalent stress	Relative strain	Equivalent stress
	[µm/m]	MPa	[µm/m]	MPa
T1X	-149	-31.3	-2	-0.4
T2X	45	9.5	1	0.2
T4X	39	8.2	0	0
T7X	-149	-31.3	-2	-0.4
T8X	46	9.7	3	0.6
T3Y	-87	-18.3	0	0
T5Y	110	23.1	3	0.6
T6Y	-82	-17.2	0	0

Table 4: Strains measured in static load test 1

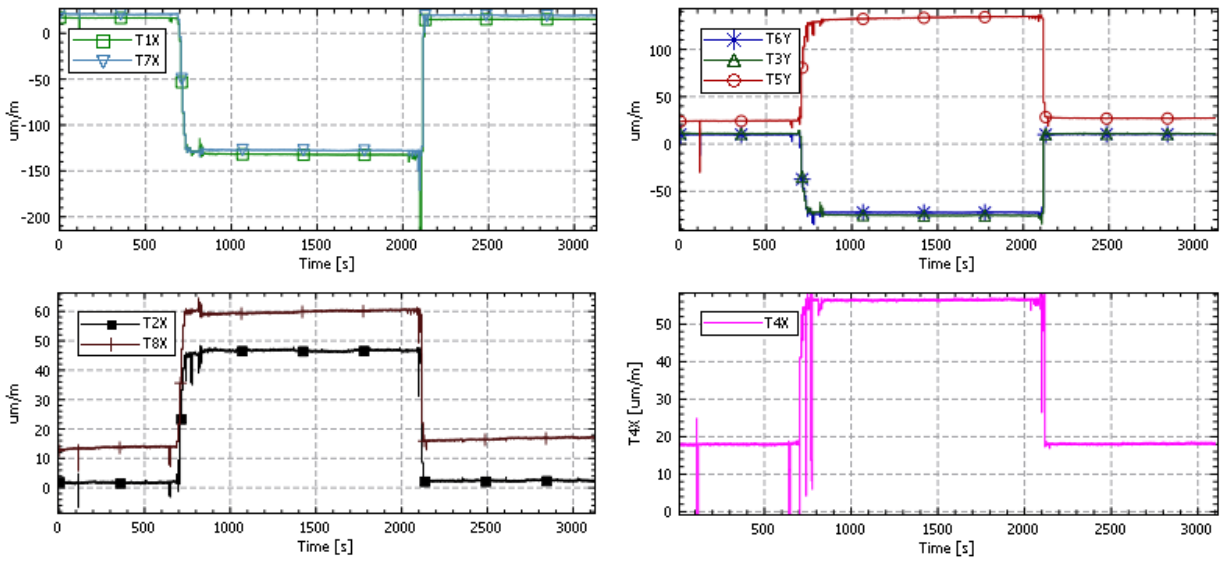

Figure 30: Strain versus time plot for the static load test 1

Designation	At full load		After unloading	
	Relative strain	Equivalent stress	Relative strain	Equivalent stress
	[μm/m]	MPa	[μm/m]	MPa
T1X	-147	-30.9	0	0
T2X	44	9.2	3	0.6
T4X	47	9.9	-1	-0.2
T7X	-149	-31.3	0	0
T8X	46	9.7	2	0.4
T3Y	-112	-23.5	0	0
T5Y	125	26.3	2	0.4
T6Y	-111	-23.3	1	0.2

Table 5: Strains measured during static load test 2

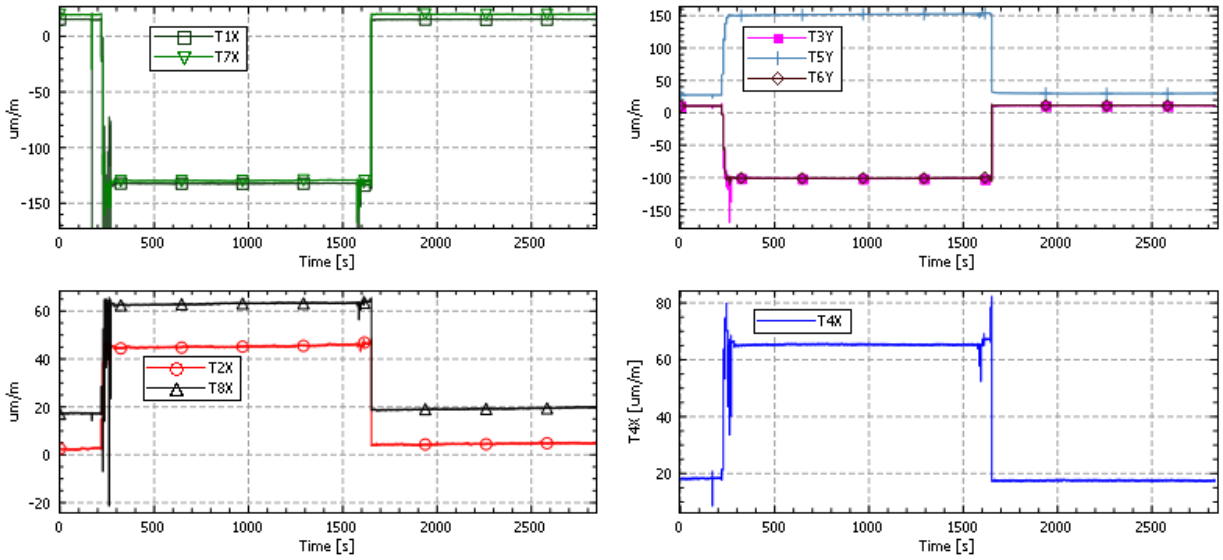

Figure 31: Strain versus time plot for the static load test 2

3.4.3. Dynamic load tests procedures

The dynamic load test examines the response of the structure to a free vibration due to the passage of a standard diesel locomotive HV 730. The locomotive's whole weight is transferred to the bridge via its four axles and each axle weighs 171kN. It was planned to run the locomotive at 10 different speeds beginning from 10km/hr till 100km/hr. However due to the physical location of the bridge and the existence of a horizontal curve close to the bridge, speeds more than 50km/hr were not achieved. The vehicle made passes on the bridge in the two different directions at speeds of 5, 10, 15, 20, 30 & 40km/hr. Driving speeds of 45 & 50km/hr were achieved only in the direction where the vehicle is free from the influence of the curve. A total of 20 crossings were made including four re-runs that are marked by letter A in the following tables.

Figure 32: HV730 Test locomotive making a pass on the bridge

3.4.4. Analysis and interpretation of the dynamic test results

The nine sensors measured accelerations at the selected points of interest at a frequency of 512Hz. The 'raw' acceleration data obtained from these sensors is presented in Figure 33 for a vehicle speed of 50km/hr. However, Article A2.4.4.2.1 paragraph 4 of EN1990 Annex A2:2005 states that the maximum peak values of bridge deck vertical acceleration calculated along each track shall not exceed a recommended value of 3.5m/s² for ballasted track considering frequencies (including consideration of associated mode shapes) up to the greater of:

i. 30 Hz;
ii. 1,5 times the frequency of the fundamental mode of vibration of the member being considered;
iii. The frequency of the third mode of vibration of the member.

Accordingly the raw values of acceleration obtained from the test were filtered in the frequency range of 0.5 Hz to 30 Hz. This is done in MATLAB by applying a Butterworth band pass filter of third order in the mentioned frequency ranges to eliminate the effect of high frequency vibrations that are not of interest from a practical structural design point of view. [12]

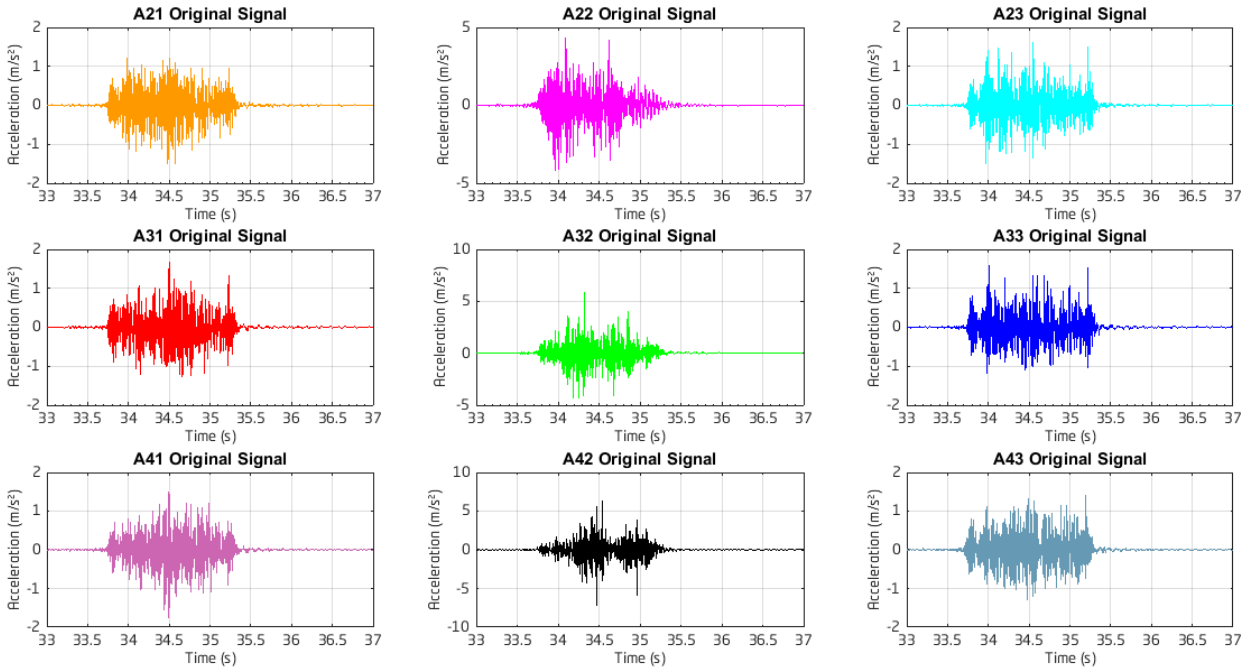

Figure 33: Time versus acceleration plots for a train passing at a speed of 50km/hr

A summary of the extreme vertical accelerations registered while the locomotive crossed the bridge at different speeds in the two distinct directions are presented in

Table 6, Table 7 and Table 8. It is evident from these tables that the maximum registered acceleration on the bridge was 1.1m/s². This value is well below the limit acceleration of 3.5m/s² for ballasted track bridges. The filtered version of the acceleration record for a crossing speed of 50km/hr is plotted against time in Figure 34.

Test Designation	Locomotive Speed	A21		A22		A23	
		min	max	min	max	min	max
	[km/hr]	[m/s²]	[m/s²]	[m/s²]	[m/s²]	[m/s²]	[m/s²]
DZS011-05	5	-0.16	0.16	-0.31	0.29	-0.16	0.19
DZS011A-05	5	-0.15	0.18	-0.30	0.29	-0.14	0.14
DZS012-05	5	-0.13	0.15	-0.41	0.31	-0.17	0.14
DZS012A-05	5	-0.13	0.14	-0.32	0.35	-0.17	0.18
DZS021-10	10	-0.17	0.18	-0.28	0.31	-0.18	0.17
DZS022-10	10	-0.14	0.14	-0.33	0.45	-0.14	0.15
DZS031-15	15	-0.15	0.15	-0.29	0.39	-0.16	0.16
DZS032-15	15	-0.16	0.14	-0.32	0.29	-0.16	0.16
DZS041-20	20	-0.21	0.14	-0.44	0.31	-0.16	0.19
DZS042-20	20	-0.15	0.15	-0.32	0.35	-0.15	0.16
DZS051-30	30	-0.17	0.16	-0.32	0.26	-0.15	0.20
DZS052-30	30	-0.19	0.16	-0.31	0.34	-0.15	0.20
DZS061-40	40	-0.19	0.16	-0.54	0.57	-0.22	0.19
DZS061A-40	40	-0.14	0.13	-0.64	0.62	-0.14	0.18
DZS062-40	40	-0.20	0.21	-0.67	0.61	-0.23	0.21
DZS062A-40	40	-0.22	0.26	-0.65	0.65	-0.23	0.26
DZS071-45	45	-0.22	0.20	**-1.11**	**0.98**	-0.22	0.21
DZS072-40	40	-0.17	0.20	-0.61	0.70	**-0.26**	0.23
DZS081-50	50	**-0.38**	**0.27**	-0.80	0.85	-0.25	**0.32**
DZS082-40	40	-0.19	0.18	-0.84	0.79	-0.25	0.26

Table 6: Extreme vertical accelerations of the bridge at the quarter-span

Test Designation	Locomotive Speed	A31		A32		A33	
		min	max	min	max	min	max
	[km/hr]	[m/s²]	[m/s²]	[m/s²]	[m/s²]	[m/s²]	[m/s²]
DZS011-05	5	-0.19	0.17	-0.44	0.44	-0.18	0.23
DZS011A-05	5	-0.15	0.18	-0.38	0.40	-0.18	0.14
DZS012-05	5	-0.18	0.23	-0.33	0.35	-0.18	0.17
DZS012A-05	5	-0.20	0.17	-0.35	0.29	-0.17	0.20
DZS021-10	10	-0.21	0.19	-0.35	0.40	-0.23	0.17
DZS022-10	10	-0.16	0.15	-0.41	0.39	-0.16	0.17
DZS031-15	15	-0.14	0.16	-0.39	0.37	-0.15	0.18
DZS032-15	15	-0.18	0.16	-0.33	0.38	-0.20	0.16
DZS041-20	20	-0.21	0.18	-0.38	0.38	-0.22	0.26
DZS042-20	20	-0.17	0.17	-0.32	0.39	-0.20	0.18
DZS051-30	30	-0.26	0.21	-0.38	0.41	-0.19	0.21
DZS052-30	30	-0.26	0.22	-0.52	0.38	-0.20	0.29
DZS061-40	40	-0.22	0.19	-0.45	0.54	-0.25	0.20
DZS061A-40	40	-0.19	0.18	-0.45	0.46	-0.23	0.26
DZS062-40	40	-0.27	0.24	-0.44	0.37	-0.27	0.28
DZS062A-40	40	-0.24	0.26	-0.53	0.35	-0.31	0.33
DZS071-45	45	-0.29	0.25	-0.45	0.41	-0.33	0.31
DZS072-40	40	-0.21	0.23	-0.40	0.42	-0.28	0.29
DZS081-50	50	**-0.41**	**0.44**	**-0.63**	**0.78**	**-0.35**	**0.44**
DZS082-40	40	-0.21	0.20	-0.42	0.52	-0.28	0.28

Table 7: Extreme vertical accelerations of the bridge at mid-span

Test Designation	Locomotive Speed	A41		A42		A43	
		min	max	min	max	min	max
	[km/hr]	[m/s²]	[m/s²]	[m/s²]	[m/s²]	[m/s²]	[m/s²]
DZS011-05	5	-0.16	0.14	-0.38	0.38	-0.17	0.17
DZS011A-05	5	-0.15	0.19	-0.35	0.31	-0.17	0.13
DZS012-05	5	-0.17	0.21	-0.37	0.31	-0.15	0.16
DZS012A-05	5	-0.18	0.18	-0.36	0.40	-0.17	0.20
DZS021-10	10	-0.18	0.16	-0.38	0.43	-0.17	0.16
DZS022-10	10	-0.15	0.15	-0.39	0.46	-0.16	0.19
DZS031-15	15	-0.15	0.15	-0.31	0.38	-0.15	0.14
DZS032-15	15	-0.15	0.13	-0.34	0.38	-0.17	0.13
DZS041-20	20	-0.17	0.18	-0.31	0.41	-0.18	0.23
DZS042-20	20	-0.15	0.17	-0.33	0.46	-0.18	0.15
DZS051-30	30	-0.22	0.15	-0.31	0.44	-0.18	0.18
DZS052-30	30	-0.21	0.19	-0.41	0.35	-0.16	0.19
DZS061-40	40	-0.17	0.18	-0.81	0.70	-0.22	0.20
DZS061A-40	40	-0.19	0.16	-0.62	0.71	-0.21	0.21
DZS062-40	40	-0.18	0.23	-0.61	0.58	-0.25	0.23
DZS062A-40	40	-0.16	0.20	-0.53	0.53	-0.29	0.24
DZS071-45	45	-0.24	0.26	**-0.90**	0.98	-0.29	0.32
DZS072-40	40	-0.15	0.19	-0.62	0.58	-0.22	0.23
DZS081-50	50	**-0.30**	**0.36**	-0.79	**1.02**	**-0.31**	**0.33**
DZS082-40	40	-0.20	0.22	-0.75	0.73	-0.22	0.22

Table 8: Extreme vertical accelerations of the bridge from sensors at the third quarter-span

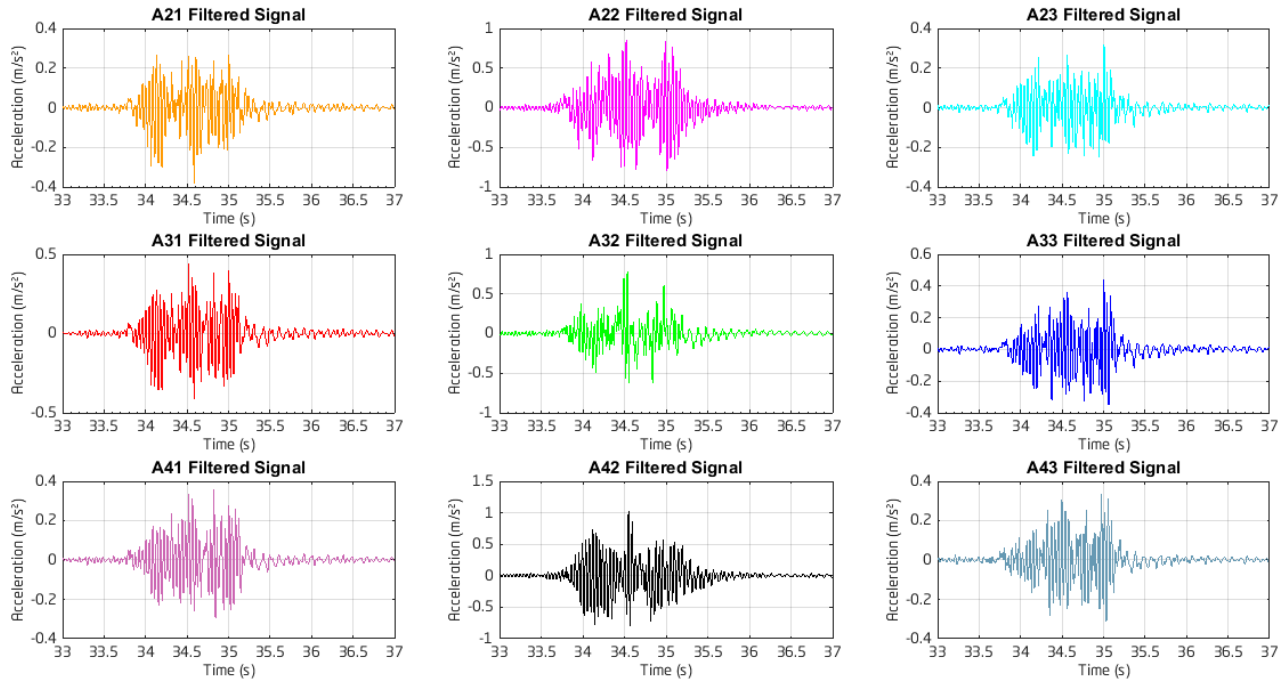

Figure 34: Time versus filtered acceleration plots for a train passing at a speed of 50km/hr

3.4.4.1. Evaluation of the natural frequencies and mode shapes

Evaluation of the natural frequencies and shapes involves a series of data manipulation. The vertical oscillation signals are not described by mathematical functions but come from measurement acquired with a selected sampling interval Δt (its inverse is the sampling frequency or rate F_s). Thus the signal is not continuous but discrete. The accelerograms recorded acceleration at a frequency of 512Hz implying that data for the vertical oscillation was captured approximately every 0.00195s. This 'raw' record is extracted from the data loggers and these can be plotted on a time versus acceleration graph. However, it is not easy to identify the natural frequencies from looking at this graph as it includes vibrations at high frequency as well. In order to simplify the process of obtaining these frequencies, the record needs to be converted from the time-domain to the frequency domain.

The purpose of frequency analysis is to devise a method to extract an estimate of frequency components which are not known a priori. The Fast Fourier Transform (FFT) method/algorithm becomes handy in such a situation. As was stated earlier, the frequency range that is relevant to our studies is in the range of 0.5Hz – 30Hz. For this reason, an initial transformation of the whole acceleration signal for a given measurement point is made from the time domain to the frequency domain in the mentioned range by using the FFT command

in MATLAB. This allows for a general overview of the important frequencies that are depicted by spikes in the FFT plot.

Once these resonant peak frequencies of interest are identified, the whole original signal is filtered in such a way that oscillations that are in the range of the frequency of interest are the only ones present in the acceleration record. Now that a filtered acceleration plot is obtained, a number of windows that cover particular time intervals in the time vs. acceleration plot are made in an attempt to isolate and extract the natural frequency of the structure. The isolation of the signal of interest can be achieved by setting all accelerations that precede and follow the range of interest to zero in a process called zero-padding. For longer recordings, averaging of several windows was used. The number of windows was selected depending on the length of each recording. Data relevant to the windows chosen is further refined by applying a hamming function. This isolated and filtered signal is finally Fast Fourier transform converted from time domain to frequency domain to compute the natural frequency.

The mode shapes associated with these frequencies are identified by studying the characteristics of the acceleration from the 9 measurement points A21 to A43. All measurements have the same time stamp since the logging starts at the same time for every sensor. This allows for comparison of two signals on the same time frame. Subsequently, Time vs. acceleration diagrams of two selected signals are plotted on the same graph to see if the two accelerations are in phase or not. If the two accelerations are in phase, irrespective of their amplitudes, it could be considered as a sign that the two accelerations are following the same direction at a given time step. On the contrary, when two signals are out of phase with each other, it implies that the bridge at those two measuring points is accelerating in different directions. By carefully selecting pertinent measurement points and carrying out such comparisons, one can make deductions about the modal shapes relevant to the frequency. An illustration of the procedure is provided in the following chapters for the first two modes.

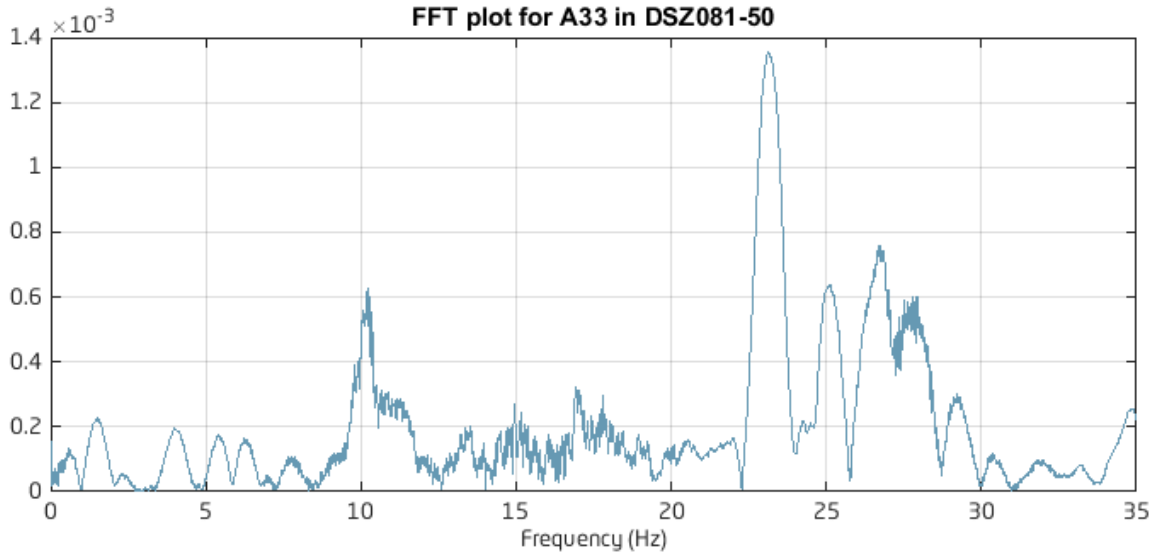

Figure 35: FFT plot of A33 for a train passing at 50km/hr

As it is evident from Figure 35, a peak exists between 9.5 and 10.5Hz. Therefore the original acceleration record is filtered between these two frequencies in order to extract and display vibrations/oscillations particularly related to this range. The difference between the original signal and the one that is filtered can be seen from Figure 36. It is now possible to see and select windows or time frames from the filtered signal plot where the vibration for the required frequency was significant. For this frequency for instance, the following windows can be chosen: [11.5s – 13.5s] and [32s – 40s]. Isolation of the signal in the windows chosen is achieved by applying the zero-padding function and the signal is further optimized by applying a hamming function to it. Figure 37 and Figure 38 show the isolated filtered signals for the windows stated above along with the FFT plot for their respective isolated filtered signals from which the natural frequencies are extracted.

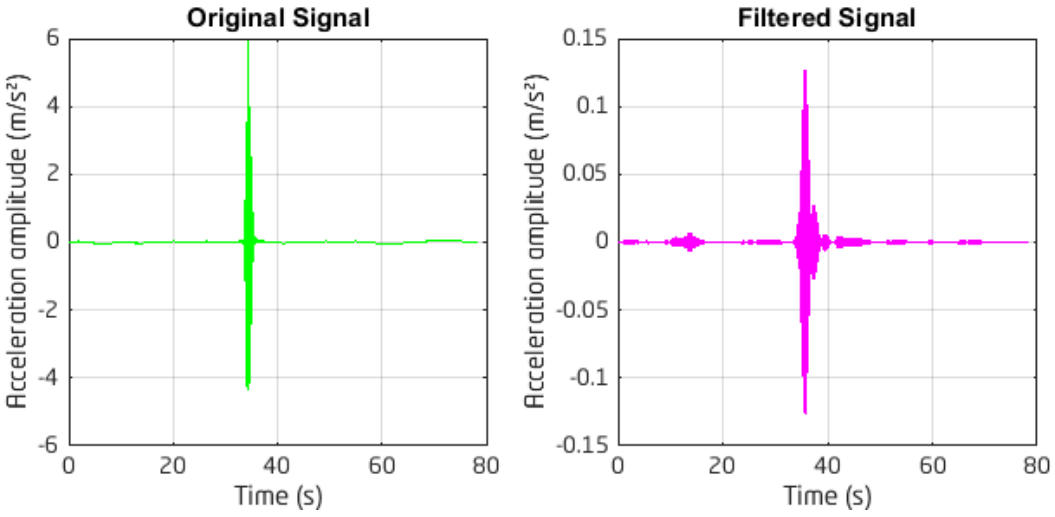

Figure 36: Original versus filtered signal for the 1st mode of vibration

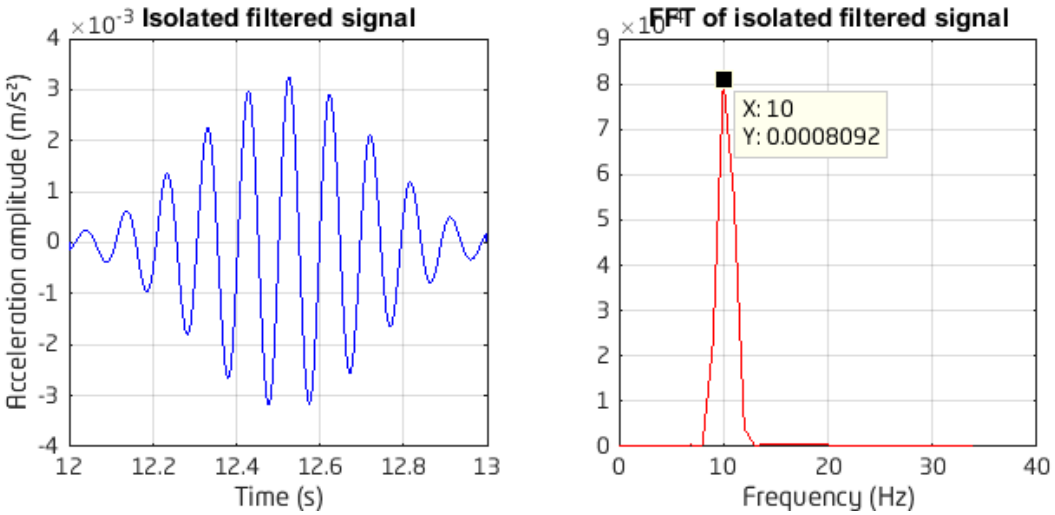

Figure 37: Isolated filtered signal and its FFT for the range 12s – 13s.

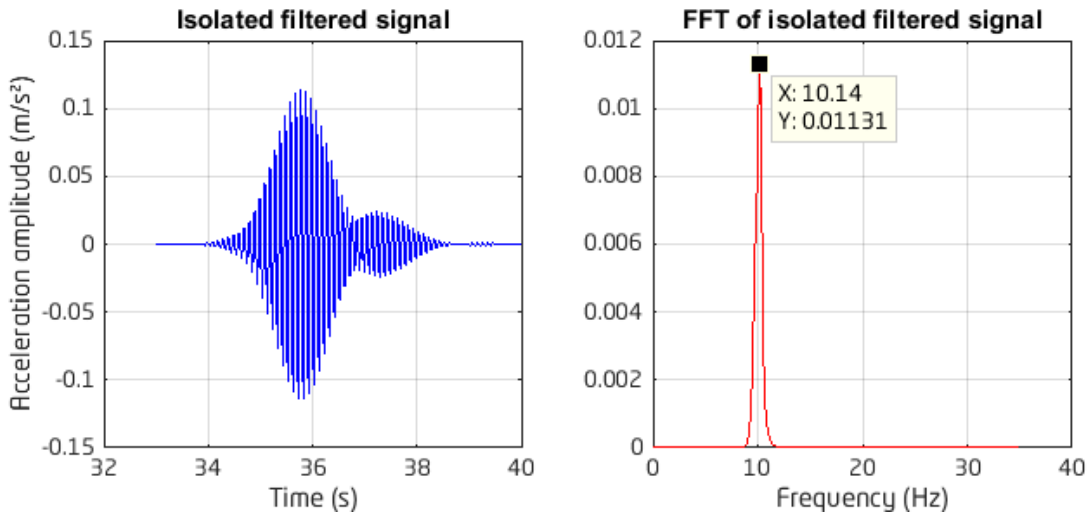

Figure 38: Isolated filtered signal and its FFT for the range 32s – 40s.

Frequencies were calculated in a similar fashion for the other signals from the rest of the measurement points and averaged to give the first natural frequency of 10.4 ± 0.3Hz. The modal shape of this frequency is then investigated by studying the oscillation pattern at the different measurement points. Figure 39 and Figure 40 demonstrate that A32 is in-phase with the signal from A22 and A42 respectively. The same is true for the signal sets [A21, A31, and A41] and [A23, A33, A43]. Based on this, it can be deduced that this is the modal shape of a first degree longitudinal bending.

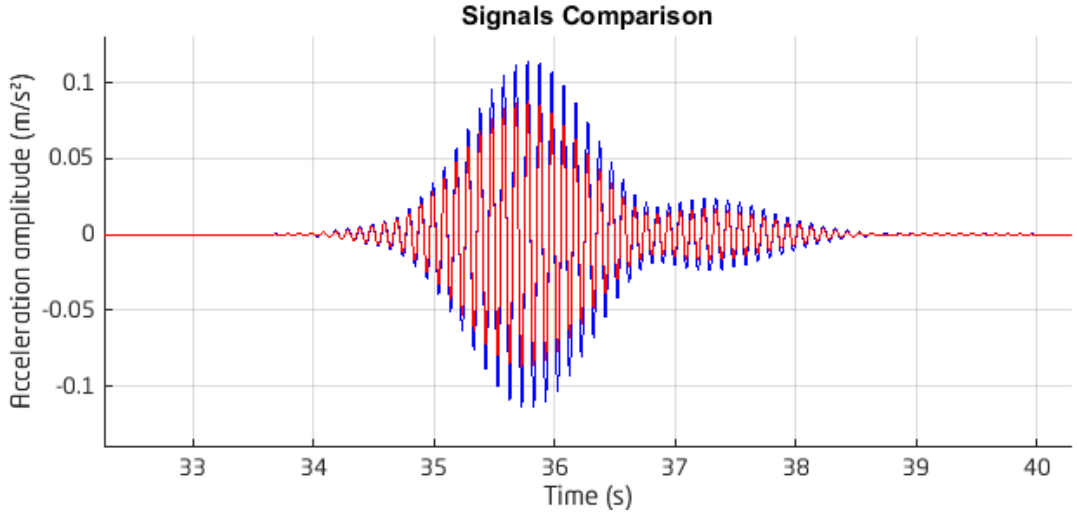

Figure 39: Comparison between the oscillation patterns of A32 and A22 for DZS081-50

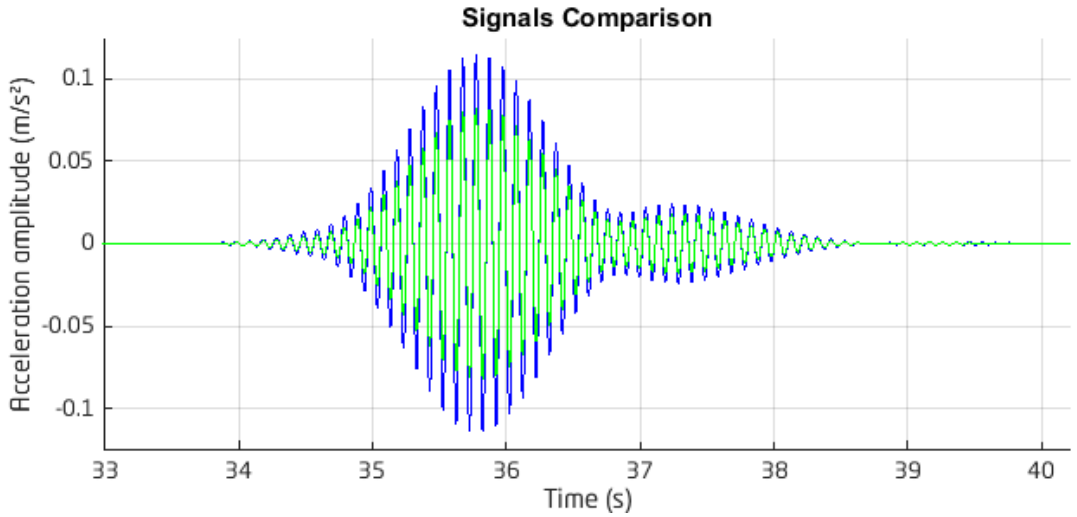

Figure 40: Comparison between the oscillation patterns of A32 and A22 for DZS081-50

A summary of the remaining natural frequencies and their mode shapes are presented in Table 9 along with the major measurement points used to identify the mode shapes.[13]

Mode	Averaged natural frequency [Hz.]	Expanded uncertainty [Hz.]	Main Comparison			Second Comparison			Mode shape
1	10.4	± 0.3	A32	A22	In-phase	A32	A42	In-phase	Longitudinal bending vibration of first degree
2	15.9	± 0.3	A31	A33	Out of phase	A21	A23	Out of phase	Torsional vibration
3	22.5	± 0.3	A22	A42	Out of phase				Longitudinal bending vibration of second degree
4†	27.8	± 1.1	A33	A31	In-phase	A32	A31	Out of phase	Transverse bending vibration of first degree
5	31.5	± 0.3	A32	A42	Out of phase	A22	A42	In-phase	Longitudinal bending vibration of third degree

Table 9: Summary of the first five natural frequencies and their associated mode shapes

† Natural frequency decreased gradually from 28.9 Hz to 27.0 Hz during the dynamic load test. Therefore, the expanded measurement uncertainty at this frequency is higher than the remaining frequencies.

4. Numerical Modelling

Modelling has been a useful tool for engineering design and analysis. The definition of modelling may vary depending on the application, but the basic concept remains the same: the process of solving physical problems by appropriate simplification of reality. In engineering, modelling is divided into two major parts: physical/empirical modelling and theoretical/analytical modelling. Laboratory and in situ model tests are examples of physical modelling, from which engineers and scientists obtain useful information to develop empirical or semi-empirical algorithms for tangible application. Theoretical modelling usually consists of four steps. The first step is construction of a mathematical model for corresponding physical problems with appropriate assumptions. This model may take the form of differential or algebraic equations. In most engineering cases, these mathematical models cannot be solved analytically, requiring a numerical solution. The second step is development of an appropriate numerical model or approximation to the mathematical model. The numerical model usually needs to be carefully calibrated and validated against pre-existing data and analytical results. Error analysis of the numerical model is also required in this step. The third step of theoretical modelling is actual implementation of the numerical model to obtain solutions. The fourth step is interpretation of the numerical results in graphics, charts, tables, or other convenient forms, to support engineering design and operation. [14]

A model is an appropriate simplification of reality. The skill in modelling is to spot the appropriate level of simplification, distinguish important features from those that are unimportant in a particular application, and use engineering judgment.

4.1. Basics of FEM

The finite element method (FEM) is the dominant discretization technique in structural mechanics. The basic concept in the physical interpretation of the FEM is the subdivision of the mathematical model into disjoint (non-overlapping) components of simple geometry called finite elements or elements for short. The response of each element is expressed in terms of a finite number of degrees of freedom characterized as the value of an unknown function, or functions, at a set of nodal points.

The response of the mathematical model is then considered to be approximated by that of the discrete model obtained by connecting or assembling the collection of all elements. The disconnection-assembly concept occurs naturally when examining many artificial and natural systems. For example, it is easy to visualize a building or a bridge as an assembly of simpler components.

4.1.1. Steps in FEA Process

Finite element modelling is divided into three phases: pre-processing, computation, and post processing.

Pre-processing phase: In the pre-processing phase the following decisions and actions are taken:

- The geometry of the part is imported from the CAD model. Because solid models contain great detail, they often must be simplified by deleting small non-structural features and taking advantage of symmetry to reduce computation time.
- Make decisions concerning the division of the geometry into elements, often called meshing. The issue is knowing which types of elements to use, linear, quadratic, or cubic interpolation functions, and building a mesh that will provide a solution with the needed accuracy and efficiency. Most FEA software provides a means for automatically meshing the geometry. The finite element mesh is applied in one of two ways: structured (mapped) mesh or unstructured (free) mesh. Structured meshes have a clear structure of triangles or quadrilateral elements (for 2-D) or tetrahedral or hexes (for 3-D) that are produced by rule-based mapping techniques. Grid points can be distributed along lines with effective spacing, and well-graded grids can be constructed. This approach is effective when the geometry is relatively simple. With complex geometries a multi-block approach is used, in which the geometry is filled with an assemblage of meshed cubes. This requires the additional step of setting up the connections between the blocks. Unstructured meshing does not show structure in the placement of the elements.
- Determine how the structure is loaded and supported, or in a thermal problem determine the initial conditions of temperature. Make sure you understand the

boundary conditions. It is important to incorporate sufficient restraints to displacement so that rigid body motion of the structure is prevented.

- Select the constitutive equation for describing the material (linear, nonlinear, etc.) that relates displacement to strain and then to stress.

Computation: The operations in this phase are performed by the FEA software.

- The FEA program renumbers the nodes in the mesh to minimize computational resources by minimizing the size of the global stiffness matrix K.
- It generates a stiffness matrix K for each element and assembles the elements together so that continuity is maintained to form the global or structural matrix K. Based on the load vector the software generates the external loads and applies displacement boundary conditions.
- Then the computer solves the massive matrix equation for the displacement vector or whatever is the dependent variable in the problem. The constraint forces P are also determined.

Post processing: These operations are also performed by the FEA software.

- In a stress analysis problem, post processing takes the displacement vector and converts into strains, element by element, and then, with the appropriate constitutive equation, into a field of stress values.
- A finite element solution could easily contain thousands of field values. Therefore, post processing operations are needed to interpret the numbers efficiently.
- Typically the geometry of the part is shown on which contours of constant stress are plotted. Mathematical operations may have to be performed on the data by the FEA software before it is displayed, such as determining the Von Misses effective stress.

Increasingly, FEA software is being combined with an optimization package and used in iterative calculations to optimize a critical dimension or shape.

4.1.2. Types of Elements

Elements fall into four major categories: 2D line elements, 2D planar elements, and 3D solid elements which are all used to define geometry; and special elements used to apply boundary conditions. For example special elements might include gap elements to specify a gap between two pieces of geometry. Spring elements are used to apply a specific spring constant at a specified node or set of nodes. Rigid elements are used to define a rigid connection to or in a model. The figures below show nodes in red and the element in translucent blue except for the beam element which is bright blue. The most common geometry elements are show below. Most FEA tools support additional element types as well as somewhat different implementations of even these common elements.

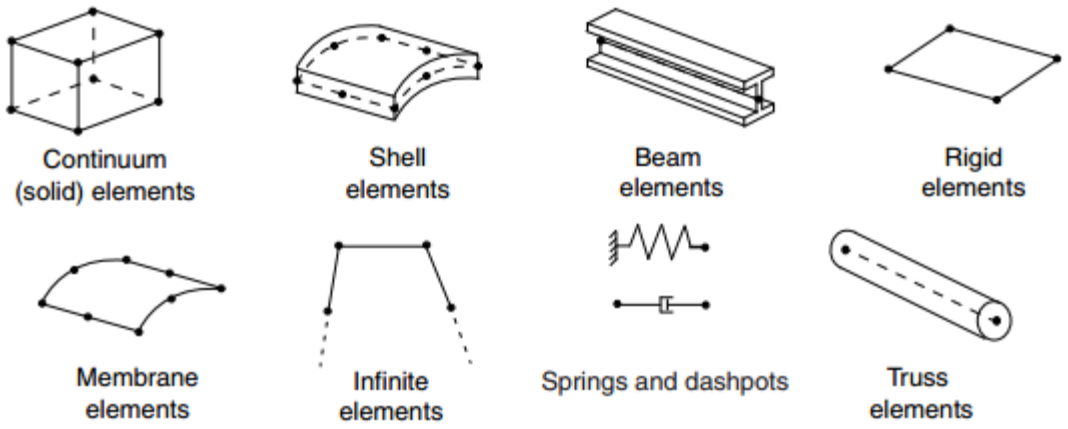

Figure 41: Commonly used element types (Source: [15])

Truss/Bar Element (2D Line)

Truss elements are long and slender, have 2 nodes, and can be oriented anywhere in 3D space. Truss elements transmit force axially only and are 3 DOF elements which allow translation only and not rotation. Trusses are normally used to model towers, bridges, and buildings. A constant cross section area is assumed and they are used for linear elastic structural analysis.

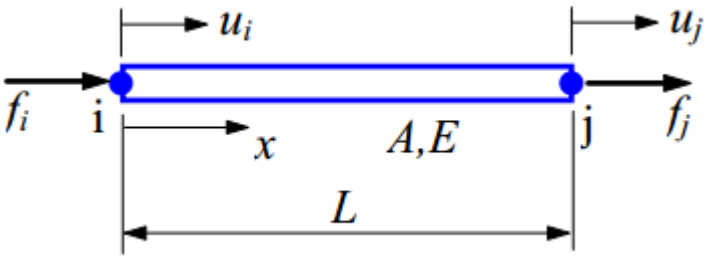

Figure 42: 2D bar/truss element

Beam Element (2D Line)

Beam elements are long and slender, have three nodes, and can be oriented anywhere in 3D space. Beam elements are 6 DOF elements allowing both translation and rotation at each end node. That is the primary difference between beam and truss elements. The I J nodes define element geometry, the K node defines the cross sectional orientation. This is how you differentiate between the strong and weak axis of bending for a beam. A constant cross section area is assumed.

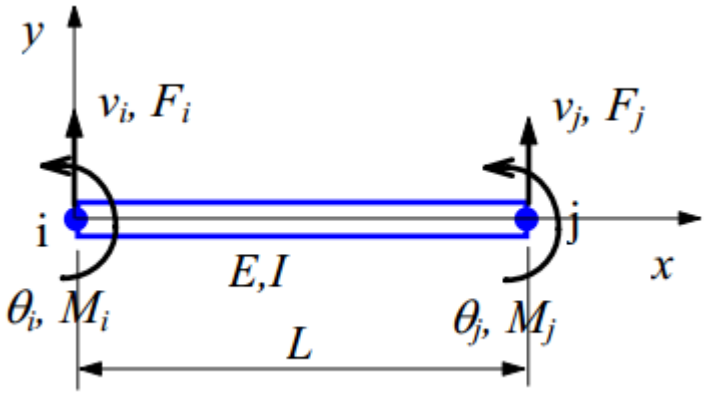

Figure 43: 2D beam element

The most commonly used beam theories are Euler-Bernoulli, often denoted classical beam theory, and Timoshenko beam theory. The latter has been developed from Euler-Bernoulli with the addition that shear deformations are taken into account and is therefore preferable in design and analysis of deep beams. The Euler-Bernoulli beam theory is valid for slender beams with high aspect ratio, i.e. L/H > 5-10, where L is the span and H represents the height of the beam cross-section.

2D Element (2D Planar)

2D Elements are 3 or 4 node elements with only 2 DOF, Y and Z translation, and are normally created in a single plane. They are used for Plane Stress or Plane Strain analyses. Plane Stress implies no stress normal to the cross section defined - strain is allowed - suitable to model the 2D cross section of a body of revolution. Plane Strain implies no strain normal to the cross section defined - stress is allowed.

Membrane Element (2D Planar)

Membrane Elements are 3 or 4 node 2D elements that can be oriented anywhere in 3D space. They can be used to model thin membrane like materials like thin metal sheets. These elements will not support or transmit a moment load or stress normal to the surface. They support only translational DOF not rotational and in-plane loading. The thickness of the membrane must be small relative to its length or width. Membrane thickness is defined as a fixed parameter which can be varied. The geometry is drawn at the mid-plane with zero thickness shown.

Plate Element (2D Planar)

Plate elements are 3 or 4 node 2D planar elements that can be oriented anywhere in 3D space. They are typically used to model structures bending mainly out of plane. All translational DOF are supported as well as rotational DOF that are not out of plane. That is rotation about the normal to the element surface is not allowed. Plate thickness is defined as a fixed parameter which can be varied. The geometry is drawn at the mid-plane.

Shell Element (3D Curved)

Shell elements are developed from plate elements, based on plate theory, and plane stress elements that take membrane action into account. Shell elements are defined as mid-plane surfaces assigned a certain thickness. A plate is defined by its small height in comparison with the in-plane dimensions and that loading is applied perpendicular to the plane. The out-of-plane loading results in bending moments about in-plane axes and shear force in the out-of-plane direction. The combined effect of the plate element and the plane stress element is achieved in shell elements with generally 5 degrees of freedom in each node. In some cases, however, a sixth degree of freedom should be assigned to a node, for example if shell elements are coupled to other types of structural elements or to rigid links, or if there are imposed rotational moments or boundary conditions at the node.

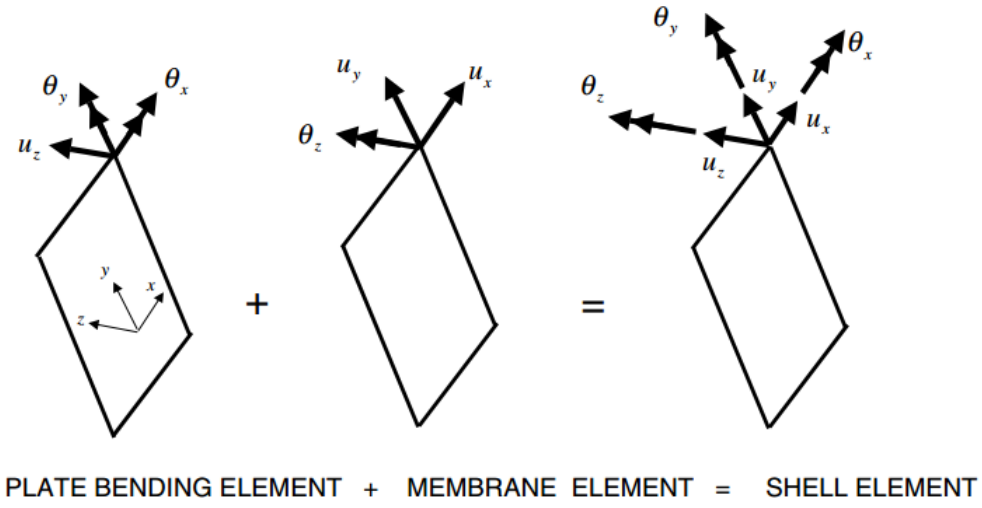

Figure 44: Shell elements

3D Brick or Tetrahedral Elements (3D Solid)

Brick or tetrahedral elements may have 8, 10 or 20 nodes and support only translational DOF. They are normally used to model solid objects for which plate elements are not appropriate. You can usually specify all tetrahedral, all bricks, or a mixture of both with some automatic mesh generators. This is the most common, and frequently the only element type supported by automatic mesh generators. Bricks work quite well for any "blocky" structures. [16]

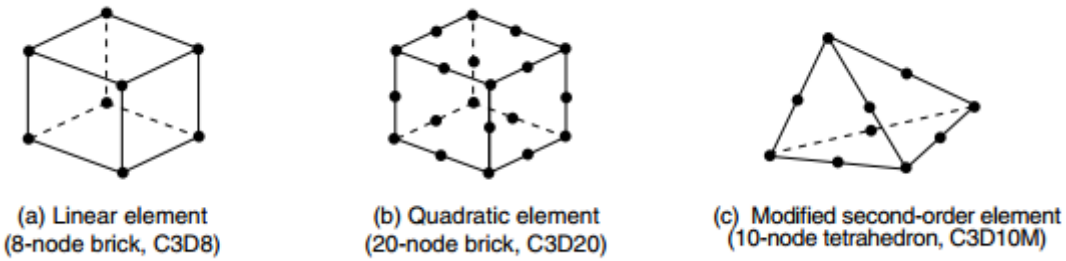

Figure 45: 3D Solid elements

4.1.3. Eigen Value Analysis

The most important dynamic characteristics of railway bridges are their natural frequencies. Natural frequencies characterize the extent to which the bridge is sensitive to dynamic loads and are measured by the number of vibrations per unit of time. The unit of frequency is Hertz (Hz) which is the number of cycles executed per second. The notation for natural frequencies is f_i, where the subscript i = 1, 2, 3… indicates their sequence. Natural frequency is related to the natural circular frequency ω_i and the period of vibration T_i, as expressed in the equation below. The period expresses the duration of one cycle.

$$\omega_i = \sqrt{\frac{K}{M}} = 2\pi f_i \qquad\qquad T_i = \frac{1}{f_i}$$

There are an infinite number of natural frequencies of mechanical system with continuously disturbed mass. Only the lowest frequencies have any practical application when studying the dynamic response of a bridge. The bridge structure selects and reacts to only the frequencies near its own natural frequencies, when excitation forces are applied to a system over a wide spectrum of frequencies. Because of that, natural frequencies have a great importance in dynamic analysis. [17]

Mass of Bridge

The maximum acceleration of a structure is inversely proportional to the mass of the bridge structure at resonance. The maximum dynamic load effects are likely to occur at resonance peaks, where a multiple of the frequency of loading coincide with a natural frequency of the structure. Any underestimation of the mass will overestimate the natural frequency of the structure, and therefore overestimate the traffic speed at resonance occurs.

There are two special cases to be considered for the mass of the bridge structure, including ballast and track. A lower bound estimate of mass shall be considered, predicting maximum deck accelerations, by using the minimum likely dry clean density and minimum thickness of ballast. An upper bound estimate of mass shall also be considered, predicting the lowest speed at which resonant effects are likely to occur, by using the maximum saturated density of dirty ballast, with allowance for future track lifts.

Stiffness of Bridge

Just as the damping and the mass, the stiffness of the bridge structure has an influence of the dynamic effects. The maximum dynamic load effects are likely to occur at resonance peaks. Any overestimation of the bridge stiffness will overestimate the natural frequency of the structure and the traffic speed, at which resonance occurs. Throughout the structure, a lower bound estimate of the stiffness shall be used. The value of the bridge stiffness may be determined in accordance with EN 1992 – EN 1994. [18]

4.2. Material properties

The following material properties are used in the CSiBridge and Abaqus models discussed in the following sections. The influence of variation of these physical parameters has been tested for the ballast as discussed in section 5.2.

Variables	Unit	Value
Steel Bridge		
Modulus of Elasticity, E	N/mm²	210×10³
Poisson's ratio, ν	-	0.3
Mass density, ρ	kg/m³	7850
Deck Thickness (Span)	mm	80
Deck Thickness (Supports)	mm	160
Box Flange Thickness	mm	80
Box Web Thickness	mm	25
Ballast		
Modulus of Elasticity, E	N/mm²	80
Poisson's ratio, ν	-	0.16
Mass density, ρ	kg/m³	1850
Layer depth	mm	450
Sleepers (B03)		
Modulus of Elasticity, E	N/mm²	36×10³
Poisson's ratio, ν	-	0.2
Mass density, ρ	kg/m³	2550
Spacing	mm	600
Width	mm	2400
Breadth	mm	240
Height	mm	195
Rails (S49)		
Modulus of Elasticity, E	N/mm²	210×10³
Poisson's ratio, ν	-	0.3
Mass density, ρ	kg/m³	49.5

Table 10: Material properties used in the models

4.3. Idealization of the bridge components

The Bridge superstructure itself is composed of a series of steel plates whose thickness is so small relative to their length. For that reason, a simple shell model that can sufficiently model both plate and membrane type properties of the bridge was used. As the shell element represents the mid-surface of a plate, the thicker plates at the support have been defined as an independent section of thickness 160mm and an eccentricity was applied to the centrelines to dictate the natural position.

Figure 46 shows the schematic representation of the steel bridge superstructure as modelled in both CSiBridge and Abaqus from left to right respectively.

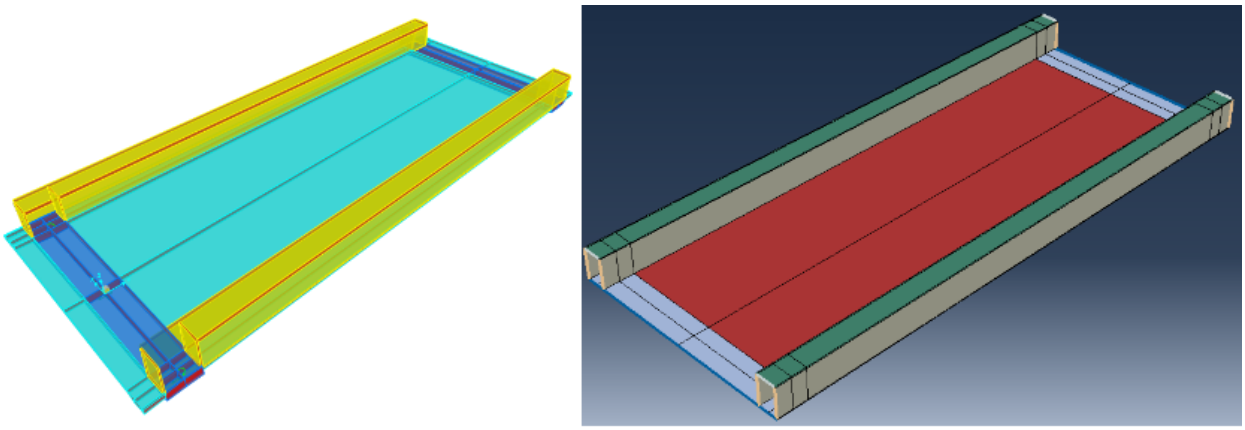

Figure 46: Main steel structure as modelled in CSI Bridge and Abaqus (left to right)

However, modelling the track is the challenging task and the assumptions made in the models are discussed below.

Ballast material in particular deflects in a highly non-linear manner under load due to voids within the material itself and also at the sleepers/ballast interface. Despite this, ballast beds are often modelled by discrete or distributed linear springs and viscous dampers in the vertical direction. In this thesis, the ballast has been modelled as a linear-elastic element with a 3D solid element of specified Elastic modulus, thus, stiffness. The mass properties of a ballast bed are also included from the mass density definitions in the material properties.

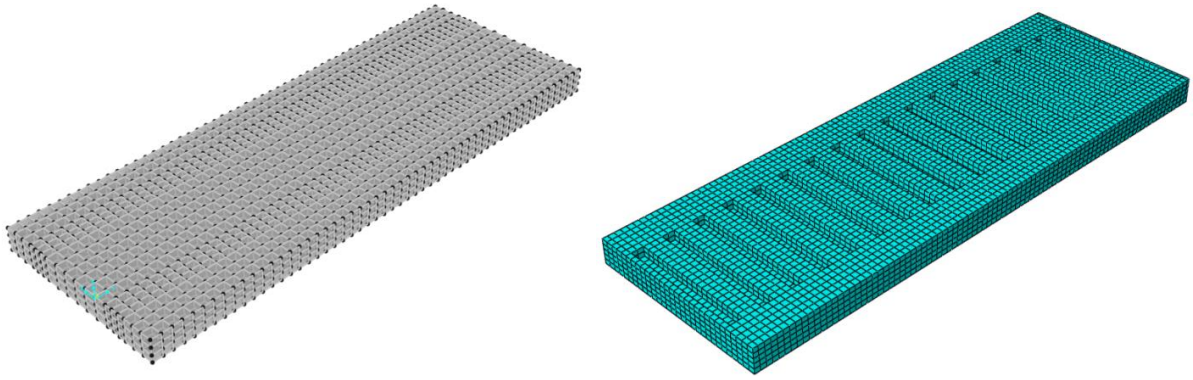

Figure 47: The ballast as modelled in CSiBridge and Abaqus (left to right)

Sleepers are also modelled as linear elements, positioned in the horizontal plane just below the rails. Literature suggests that sleepers may be modelled as rigid beams or beams with flexural and shear stiffness or as rigid solids. Considering the computation time required to analyse the models, first a Euler-Bernoulli beam element were used and in the more refined model a solid element with elastic properties has been used. An approximation of the cross-section to a solid box has been made in order to simplify the modelling and analysis time required by giving due consideration to the total mass and stiffness of each element.

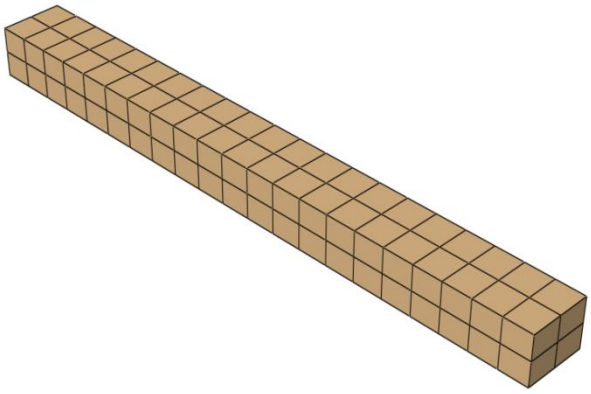

Figure 48: 3D Solid Sleeper model in Abaqus

Rails are linear elements characterised typically by an infinite length. This allows modelling the rail as beams. Rails have flexural stiffness in vertical and lateral directions and compression stiffness in the longitudinal direction. Rails also have a shear stiffness which is often neglected. Rails can be modelled using either the Euler-Bernoulli or the Timoshenko beam theories. Literatures [4] comment that several studies have shown that when the frequency of the vertical excitation force on the rail is less than 500Hz, the Euler-Bernoulli beam model leads to satisfactory results. However, in the case of higher frequencies, the shear deformation effect becomes increasingly important and Timoshenko beam models lead

to accurate results. In this study all rails have been modelled as simple Euler-Bernoulli beams.

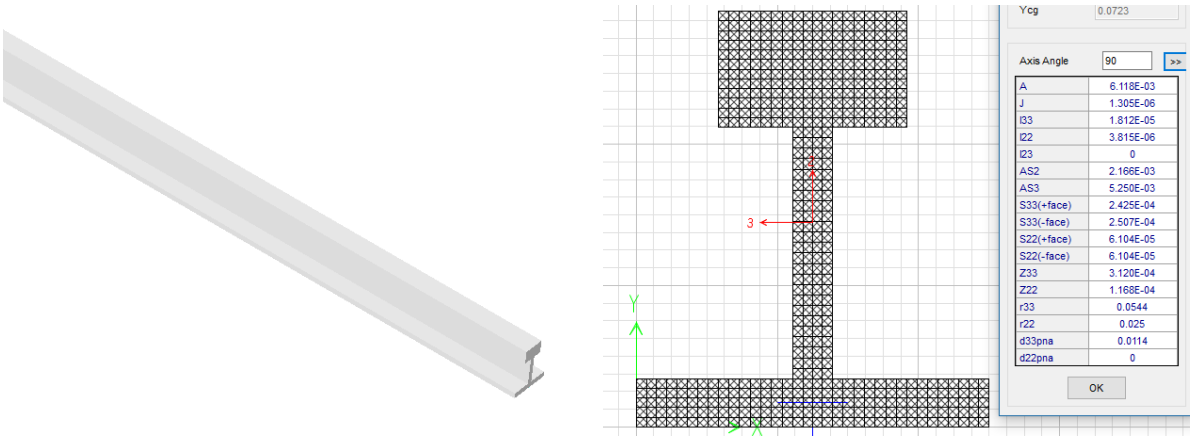

Figure 49: An equivalent section of the rails used for analysis

The rail **Fastening System** commonly used on concrete sleepers comprises a resilient spring **Fastener**, acting essentially in parallel with a much stiffer **Rail-pad**. For vertical vibration a pad is usually modelled as a spring and viscous damper in parallel. The pad is represented similarly in models of the lateral dynamic behaviour of track. Rail pads are mainly loaded in compression, permanently by the fastening system and/or repetitively by the rail traffic. [4] The spring can be assumed to be linear, and the damping is assumed to be proportional to the deformation rate of the rail-pad. [8]

4.4. Interaction between Track and Bridge

In the vertical direction, and for the purposes of the interaction analysis, a rigid union between rail and deck is considered. Therefore, in the model the connecting nodes of the rail and the connecting nodes of the deck cannot have relative vertical displacement. In the longitudinal direction, the connection between the track and the deck is characterized by the track resistance to relative displacements with respect to the base. This resistance has two components: the resistance to rail displacement with respect to the sleeper and the resistance of the sleeper to displacement with respect to the ballast.

The resistance of the track to longitudinal displacement is a function of the displacement of the rail relative to its supporting structure. The longitudinal resistance of the ballast track develops gradually. Following a displacement of some millimetres, the longitudinal resistance reaches its maximum and that value does not change any more during further displacement. Aiming to facilitate practical calculations, the initial section with changing resistance is traditionally neglected, i.e. only a constant value is taken into account.

The resistance increases rapidly while the displacement is too low, but remains virtually constant as the displacement reaches a certain magnitude. The resistance of longitudinal displacement is higher on loaded track than on unloaded. In order to simplify calculations, the curves in Figure 50 can be replaced by bilinear functions as shown where the magnitude of resistance (k) is expressed as a function of longitudinal displacement (u) of the track relative to the supporting structure.

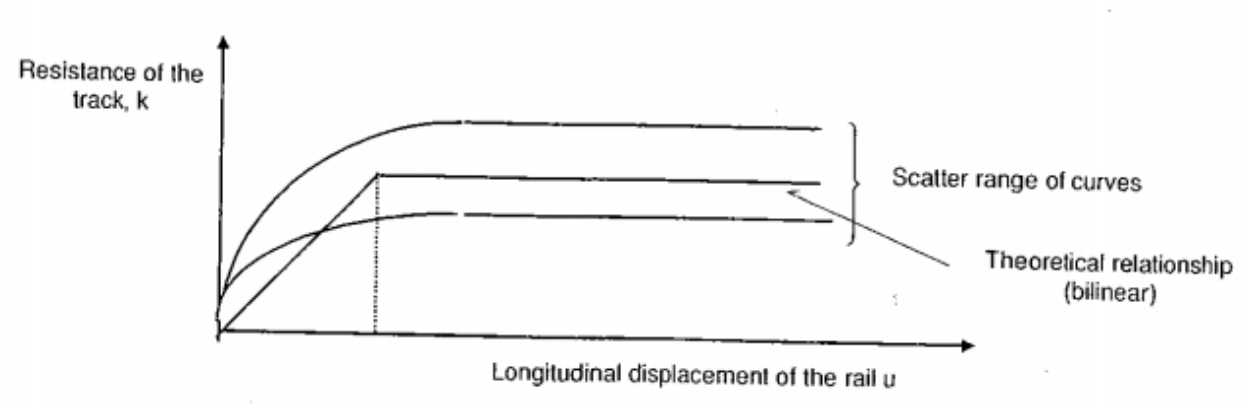

Figure 50: Longitudinal resistance of the track as a function of longitudinal displacement

The following characteristics are adopted for ballasted track. [19]

k = 12 kN per unit length of track, for unloaded track with fair maintenance level;

k = 20 kN per unit length of track, for unloaded track with good maintenance level;

k = 60 kN unit length of track, for loaded track;

u_o = 2 mm in all cases

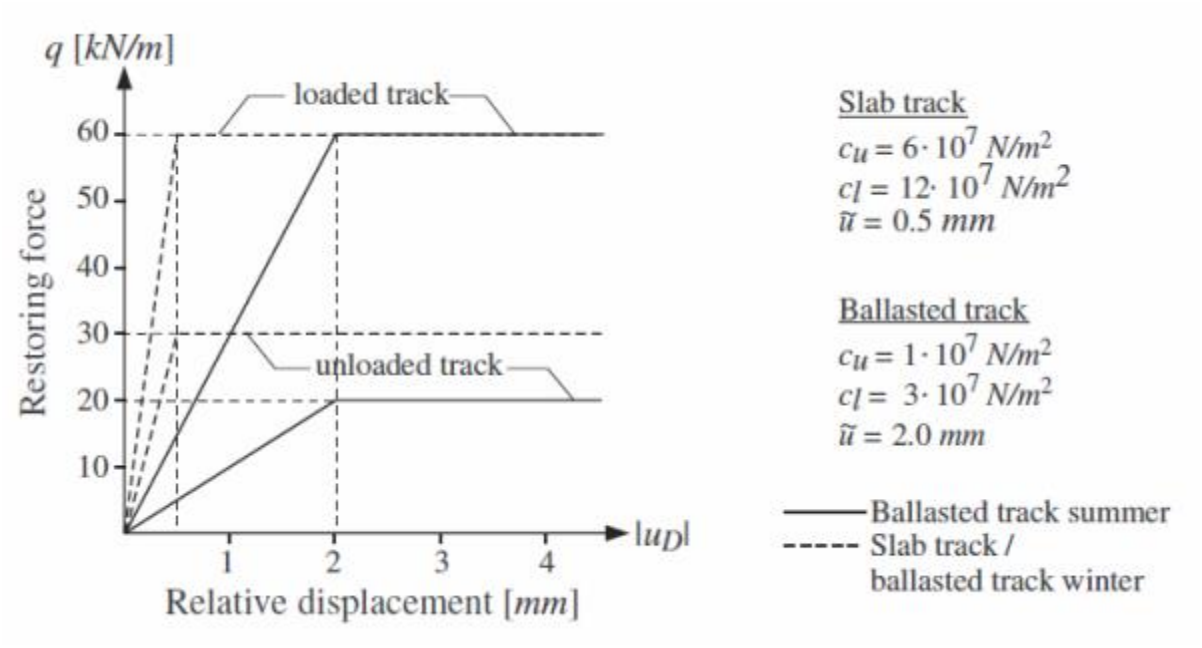

Figure 51: Resistance (k) of the track per unit length vs. longitudinal displacement (u)

For the rail-pad and fasteners alone, the property shown in Figure 52was used.

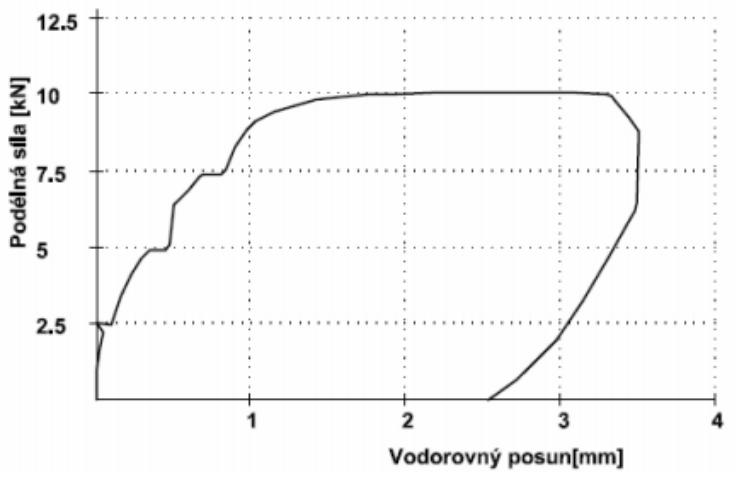

Figure 52: Longitudinal resistance of Vossloh W14 Clamp Slk 14 fastner node [20]

4.5. Classical Steel Bridge Model alone (CSI-BMO)

For the sake of comparison, a simple model of the bridge neglecting the stiffness contribution of the track was prepared in CSiBridge. The webs of the boxes at the left and right edges of the bridge have 25mm thickness while the deck plate is 80mm in thickness. The flanges of the boxes are 80mm thick as well. Near the abutments on the location where the bridge is placed on the bearings the thickness of the steel deck is 160mm. The mass of the ballast and track has been considered as follows.

Ballast:

Overall thickness of the ballast: 0.45m

Area mass of the ballast = 0.45m × 20kN/m³ = 9kN/m²

According to article 5.2.3(2) of EN 1991-1 Table A-6, nominal depth ± 30% deviation should be taken in to account. Since the depth is nearly constant on site except for an inclined addition near the edges, this has been considered to be taken in to account by using a conservative unit weight for normal ballast of 20kN/m³.

Sleepers:

Considering the B03- var. 1 type pre-stressed concrete sleepers used (See Table 11 below), a single sleeper weighs 252kg. For a centre to centre spacing of 600mm, a total of 19 sleepers rest on the bridge, therefore, 19 × 252kg = 4788kg.

Technické údaje:

	Obchodní značka	Rozměry v mm				Třída betonu	Objem (m³)	Hmotnost (kg)
		L	B	H	H´			
Pražce řady B03-DP	Var.1	2415	240	205	175	C45/55 XF1	0,097	252
	Var. 2	2415	234	190	160	C45/55 XF1	0,088	208

Table 11: Dimension details for B03 type concrete sleepers

Rails:

Each S49 (49E1) rail on the track weighs 49.39kg/m. For the whole span:

= 10.6m × 2 ×49.39kg/m = 1047kg.

This total mass is to be applied on a contact area of 10.6m × (4.4m – 0.8m) = 38.16m². This results in a weight per unit area of 1.5kN/m² (for the sleepers + rails) + 9kN/m² for the ballast

= 10.5kN/m² of area load which is equivalent to $1.07\frac{kNs^2}{m^3}$. This mass was applied on the portion of the bridge deck confined between the edge boxes. The first five modes of vibration obtained after analysis of the model are presented in Figure 53 through Figure 57.

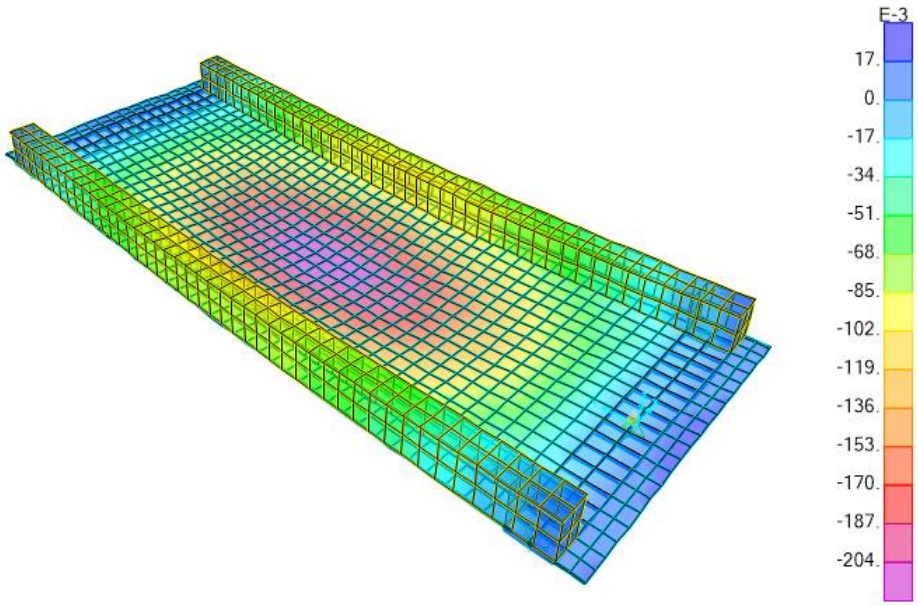

Figure 53: First mode of vibration - Frequency 9.295Hz

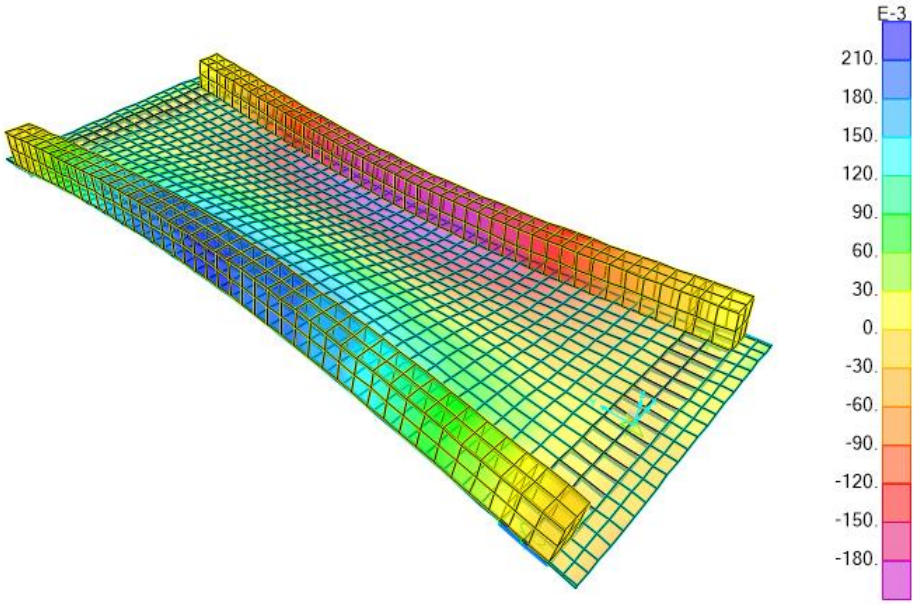

Figure 54: Second mode of vibration - Frequency 16.27Hz

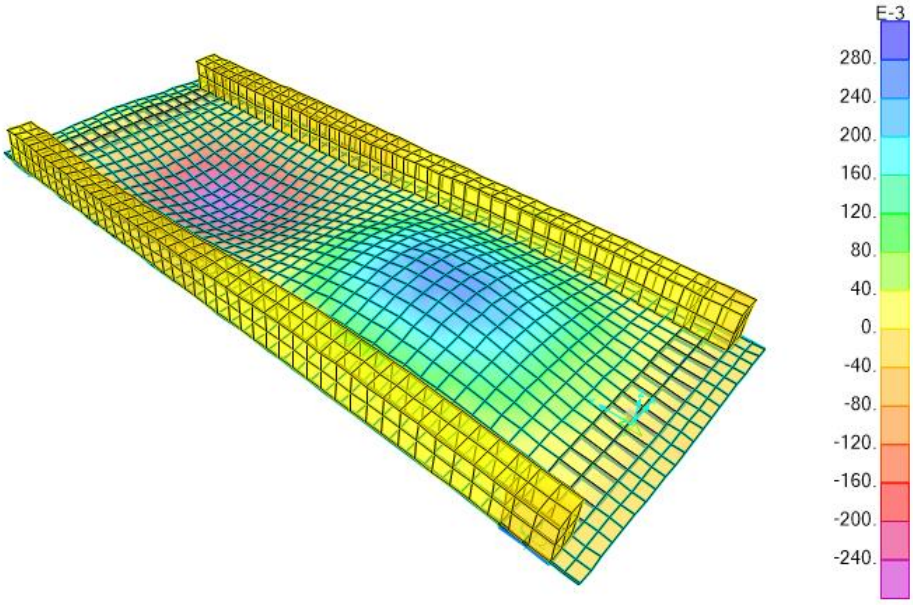

Figure 55: Third mode of vibration - Frequency 17.68Hz

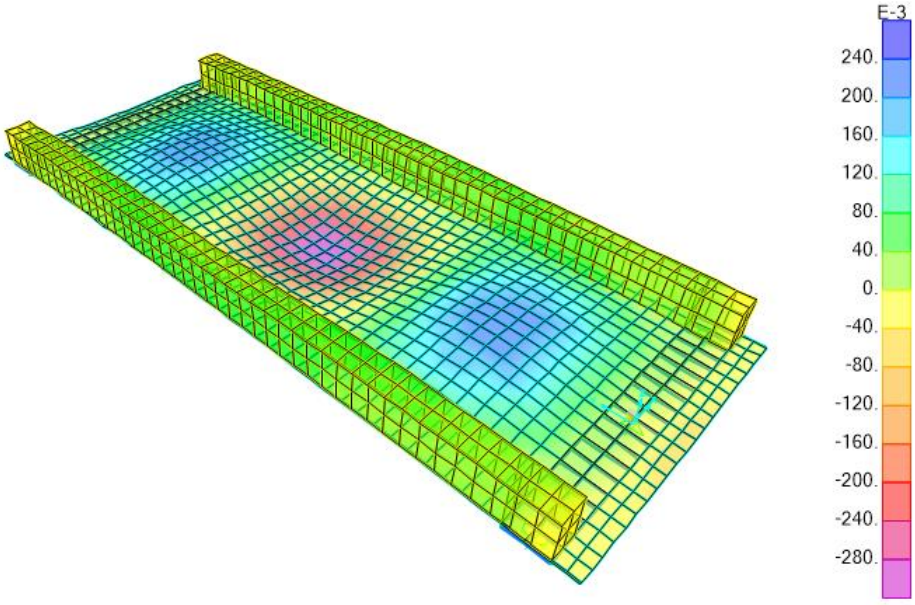

Figure 56: Fourth mode of vibration - Frequency 26.68Hz

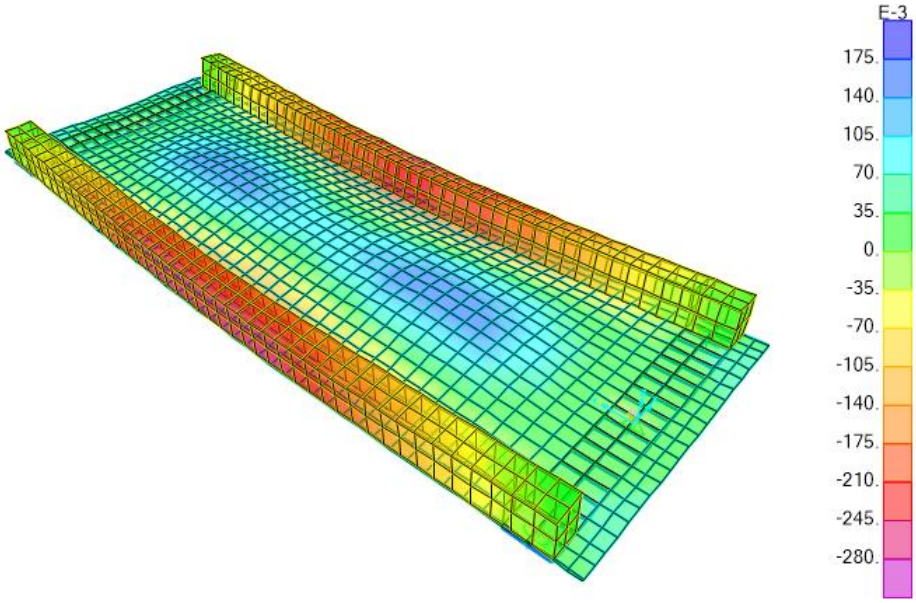

Figure 57: Fifth mode of vibration - Frequency 27.96Hz

Mode	Frequency [Hz.]	Mode shape
1	9.295	First degree longitudinal bending
2	16.27	Torsional
3	17.68	Second degree longitudinal bending
4	26.68	Third degree longitudinal bending
5	27.69	First degree Transverse bending

Table 12: Summary of modes for model CSI-BMO

4.6. ABAQUS models

The working procedure of Abaqus was followed to arrive at the models presented in this subtopic. Each part, i.e., the steel bridge, the ballast, the sleepers and the rails were modelled independently in the Parts module first. Material properties were then defined and assigned to the parts in the properties module. These parts were then assembled by creating instances of the parts defined earlier in the assembly module. The interaction between these instances was defined in the interactions module in an effort to portray the mechanism how these individual parts enact as an assemblage. The evaluation of the natural frequencies and mode shapes was possible by defining and executing a linear perturbation step in the steps module. The first 10 modes that do not exceed a frequency of 40Hz were requested from the Lanczos Eigen solver in this step. Boundary conditions that define how the structure is supported were defined in the Load module. The actual bridge bearing support mechanism as demonstrated in Figure 15 were implemented in all models. The assumptions stated in section 4.3 are kept valid in all the following models.

4.6.1. Steel Bridge with the ballast only (ABQ-B3D)

In this model, both the stiffness and mass effects of the ballast have been considered. However, the influence of the sleepers and the rails are an accounted for comparison purposes. The material properties used for this model are the default ones provided in section 4.2 of this report. Figure 58 demonstrates the undeformed shape of the meshed model. The first six natural frequencies were evaluated by running a linear perturbation analysis. The results are summarized in Table 13 and their shapes are presented in the figures below for better illustration.

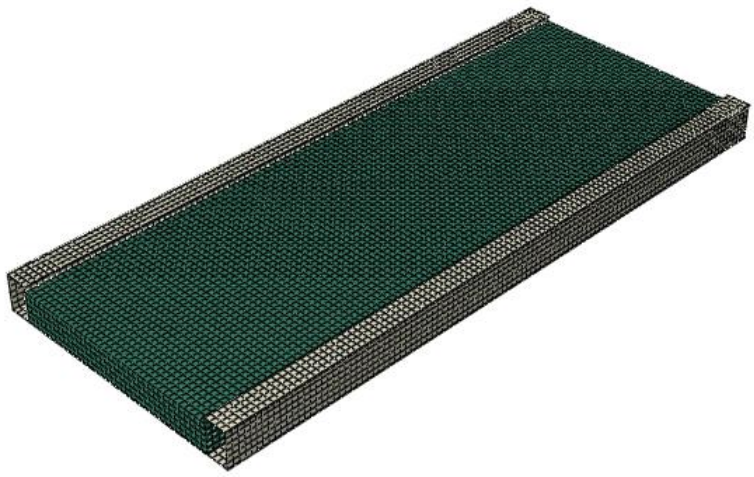

Figure 58: Steel Bridge modelled with the ballast only

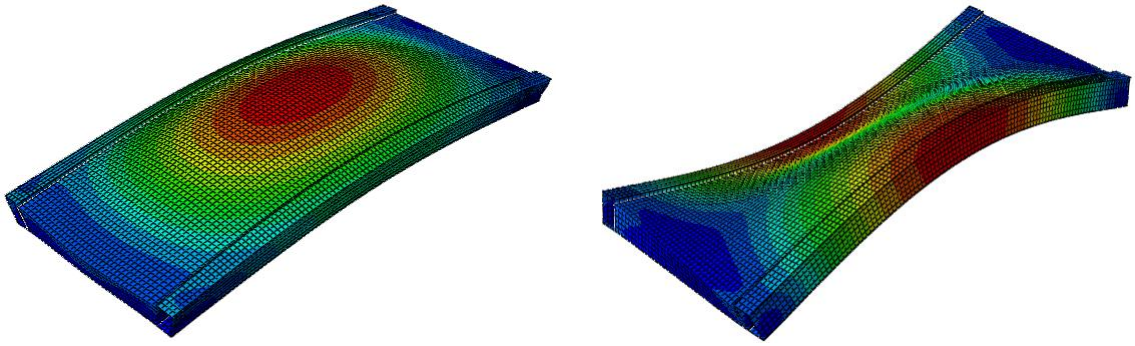

Figure 59: First and second mode shapes - Frequencies 9.23Hz and 15.77Hz, resp.

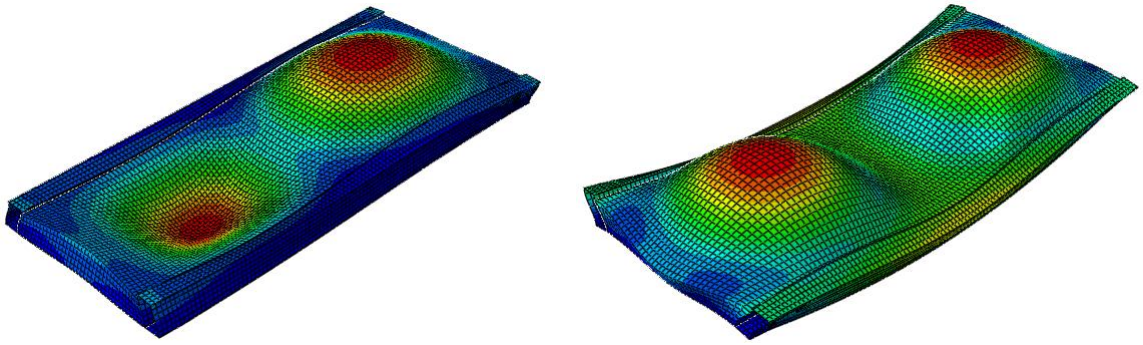

Figure 60: Third and fourth mode shapes - Frequencies 18.73Hz and 25.95Hz, resp.

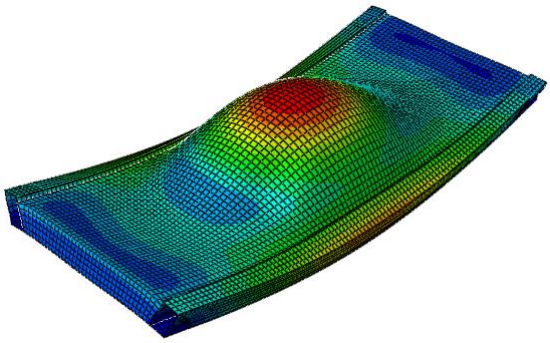

Figure 61: Fifth mode shape - Frequency 26.46Hz

Mode	Frequency [Hz.]	Mode shape
1	9.23	First degree longitudinal bending
2	15.77	Torsional
3	18.73	Second degree longitudinal bending
4	25.95	Third degree longitudinal bending
5	26.46	First degree Transverse bending

Table 13: Summary of modes for model ABQ-B3D

4.6.2. Steel Bridge with the ballast and sleepers (ABQ-B&S3D)

In this model, both the stiffness and mass effects of the ballast and the sleepers have been considered. However, the influence of the rails is neglected. The material properties used for this model are the default ones provided in section 4.2 of this report. Figure 62 demonstrates the undeformed shape of the meshed model. The first five natural frequencies were evaluated by running a linear perturbation analysis. The results are summarized in Table 14 and their shapes are presented in the figures below for better illustration.

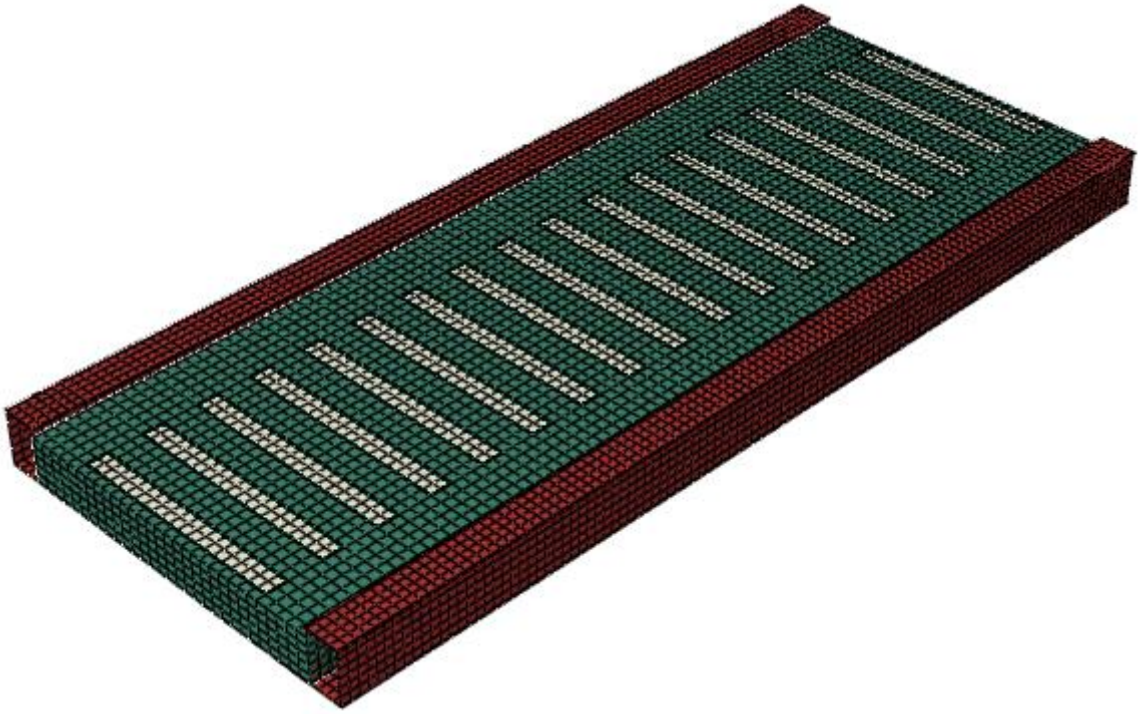

Figure 62: Steel Bridge with the ballast and sleepers

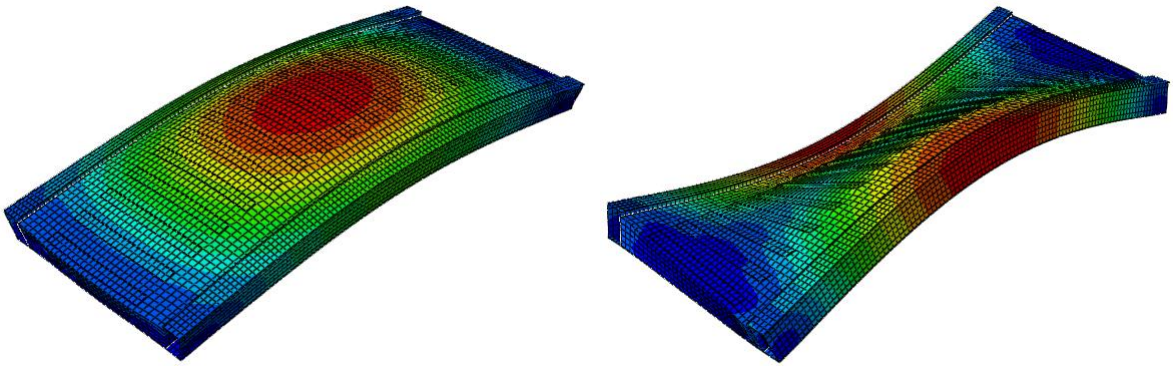

Figure 63: First and second mode shapes - Frequencies 10.24Hz and 16.58Hz, resp.

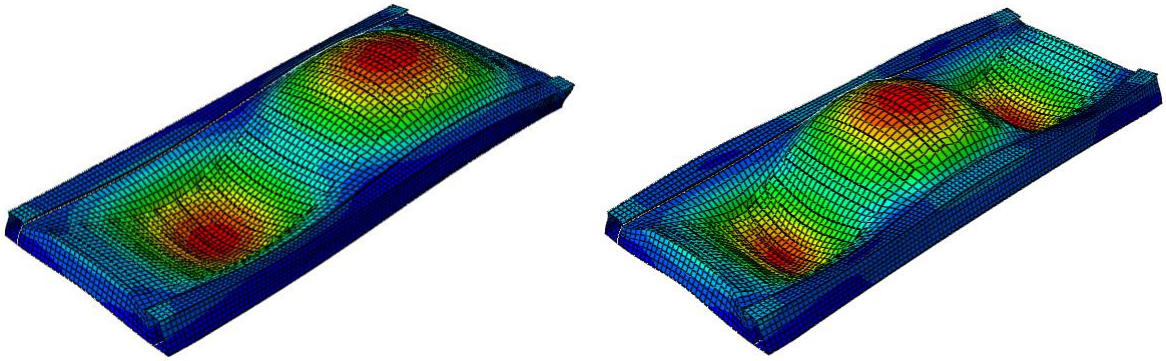

Figure 64: Third and fourth mode shapes - Frequencies 21.07 and 28.58Hz, resp.

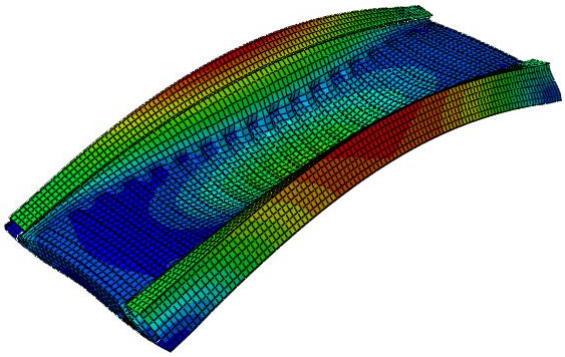

Figure 65: Fifth mode shape - Frequency 32.18Hz

Mode	Frequency [Hz.]	Mode shape
1	10.24	First degree longitudinal bending
2	16.58	Torsional
3	21.01	Second degree longitudinal bending
4	25.58	Third degree longitudinal bending
5	32.18	First degree Transverse bending

Table 14: Summary of modes for model ABQ-B&S3D

4.6.3. Whole Steel Bridge – rigid rail to sleeper connection (ABQ-WTR)

In this model, both the stiffness and mass effects of the ballast, the sleepers and the rails have been considered. The rails have been modelled projecting out of the bridge span at least 15m on each side. This is assumed to simulate the continuity of the rails to the track on either side. These rails have been assigned a tie constraint with the sleepers ensures a full connection. The material properties used for this model are the default ones provided in section 4.2 of this report. Figure 66 demonstrates the undeformed shape of the meshed model and the rail support mechanism outside the bridge. The first five natural frequencies were evaluated by running a linear perturbation analysis. The results are summarized in Table 15 and their shapes are presented in the figures below for better illustration.

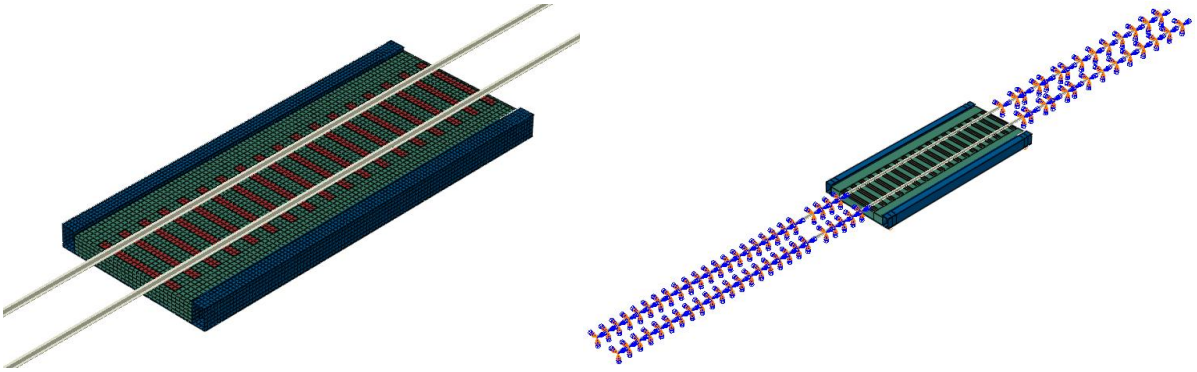

Figure 66: The whole bridge model including all elements of the track

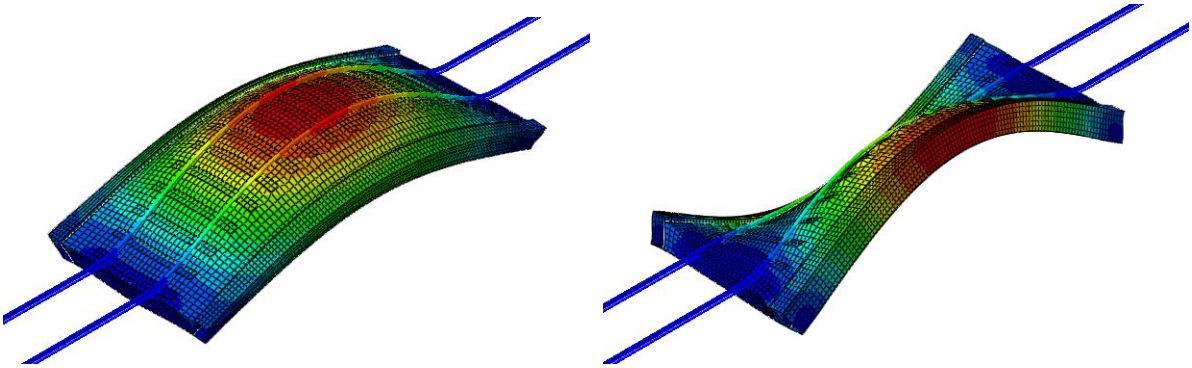

Figure 67: First and second mode shapes - Frequencies 10.663Hz and 16.54Hz, resp.

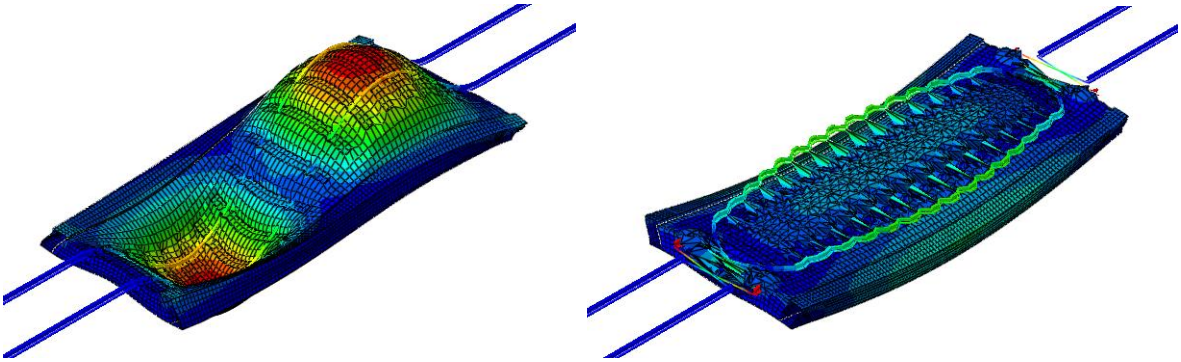

Figure 68: Third and fourth mode shapes - Frequencies 22.7Hz and 26.48Hz, resp.

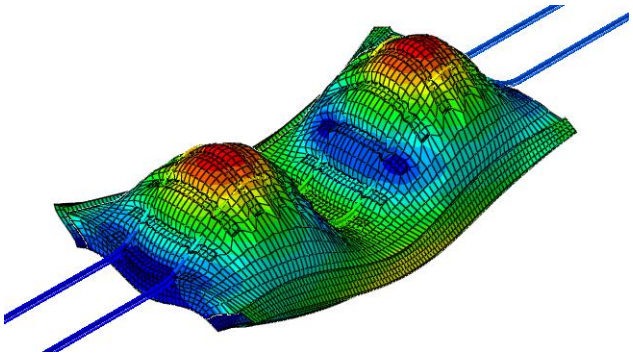

Figure 69: Fifth mode shape - Frequencies 31.49Hz

Mode	Frequency [Hz.]	Mode shape
1	10.663	First degree longitudinal bending
2	16.54	Torsional
3	22.7	Second degree longitudinal bending
4	26.48	First degree Transverse bending
5	31.49	Third degree longitudinal bending

Table 15: Summary of modes for model ABQ-WTR

4.6.4. Whole Steel Bridge – spring rail to sleeper connection (ABQ-WTS)

In this model, both the stiffness and mass effects of the ballast, the sleepers and the rails have been considered. The rails have been modelled projecting out of the bridge span at least 15m on each side. This is assumed to simulate the continuity of the rails to the track on either side. The rail – sleeper interface has been assigned a spring constant representing the relative resistances both in the vertical and longitudinal directions. The vertical stiffness accounts for the resistance of the rail-pads and fasteners in vertical actions and a value of 40MN/m² was used considering a unit length of the track for a unit deflection. Accordingly, a spring constant of 12kN/mm was used at each node. Similarly for the longitudinal stiffness, the UIC recommended value of 20KN/m was used outside the bridge to represent the whole track. Whereas, inside the bridge, since the ballast and sleepers have been modelled, the only stiffness modelled was that coming from the rail-pads and fasteners. A value of 7.5kN/mm has been used, see Figure 52.

The material properties used for this model are the default ones provided in section 4.2 of this report. Figure 66 demonstrates the undeformed shape of the meshed model and the rail support mechanism outside the bridge. The first six natural frequencies were evaluated by running a linear perturbation analysis. The results are summarized in Table 16 and their shapes are presented in the figures below for better illustration.

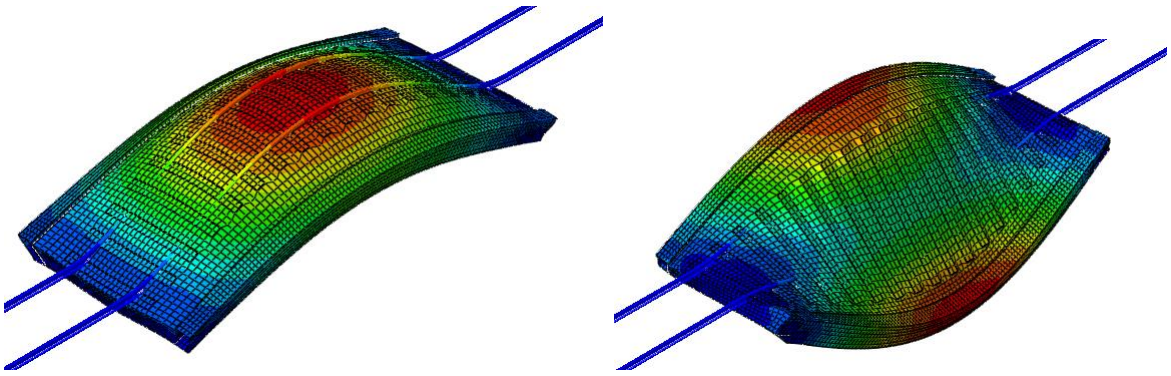

Figure 70: First and second mode shapes - Frequencies 10.435Hz and 16.626Hz, resp.

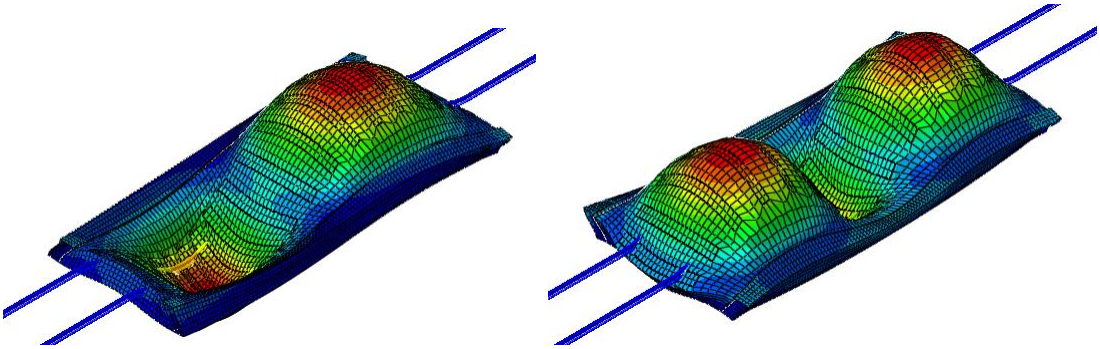

Figure 71: Third and fourth mode shapes - Frequencies 21.668Hz and 29.705Hz, resp.

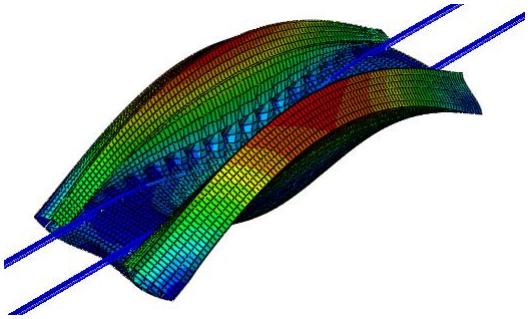

Figure 72: Fifth mode shape - Frequency 32.498Hz

Mode	Frequency [Hz.]	Mode shape
1	10.435	First degree longitudinal bending
2	16.626	Torsional
3	21.668	Second degree longitudinal bending
4	29.705	First degree Transverse bending
5	32.498	Third degree longitudinal bending

Table 16: Summary of modes for model ABQ-WTS

4.7. CSiBridge model (CSI-WTS)

The same bridge was also modelled in CSiBridge, a simple but feature rich software used by ordinary engineers on a day to day basis in design offices. The possibilities to model the whole bridge, including the ballast, sleepers and rails were checked. Accordingly, the author of this thesis tried to exploit the options in the advanced modelling module of the program. The steel structure components were idealized by shell elements of their own respective thicknesses. A 3D solid element was used to model the ballast. This element was manually meshed with approximately the same mesh size as that of the shell elements surrounding it in order to ensure node compatibility. However, this comes at the expense of larger model size and longer analysis time. Compared to a model that is assigned an automatic (program based) mesh, the model size was approximately four folds. The rails and the sleepers are modelled as classical beams with the rails assigned the approximate cross-section size presented in section 4.3. The connection between the sleepers and the rails was ensured by creating nodes on both elements at particular points of intersection.

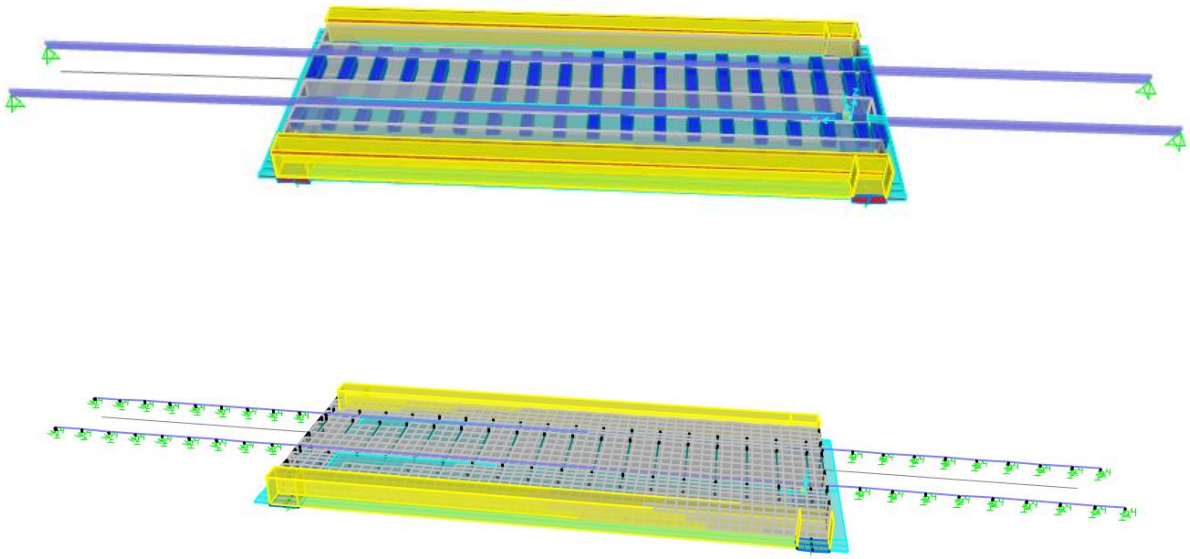

Figure 73: CSiBridge models

The main function of the rails here is not to model the continuity of the track outside of the bridge. Instead the beams are modelled here to allow a more or less similar load transfer pattern as the real bridge when applying moving loads in the model.

Property modifiers are applied to the approximate rail section to obtain exact similar stiffness value in both directions. In addition, appropriate eccentricities were introduced to the sleepers and the rail beams to best fit the actual geometric configurations on site.

Verification of this model was made by applying different set of forces to the model and examining the response of the structure. A check on the mass and load distribution was made by applying area mass and a set of point loads. The boundary conditions as well as the deck behaviour were studied by imposing a temperature load.

Five set of load cases were defined to represent the different loading scenarios implemented in both the static and dynamic loading procedure of the test.

- Dead load with self weight included
- Static test loading condition 1
- Static test loading condition 2
- Bridge live load [Dynamic moving load case]
- Bridge Time History [Dynamic moving load case]

The static load cases were used to verify the results from the static loading test by comparing the static deflections and stresses whilst the acceleration time history was extracted from the time history load case for comparison with the measured acceleration histories. The stiffness of the structure is checked against the xxxxxxxxxxxxxxxxxxxxxxx.

4.7.1. Modal Analysis

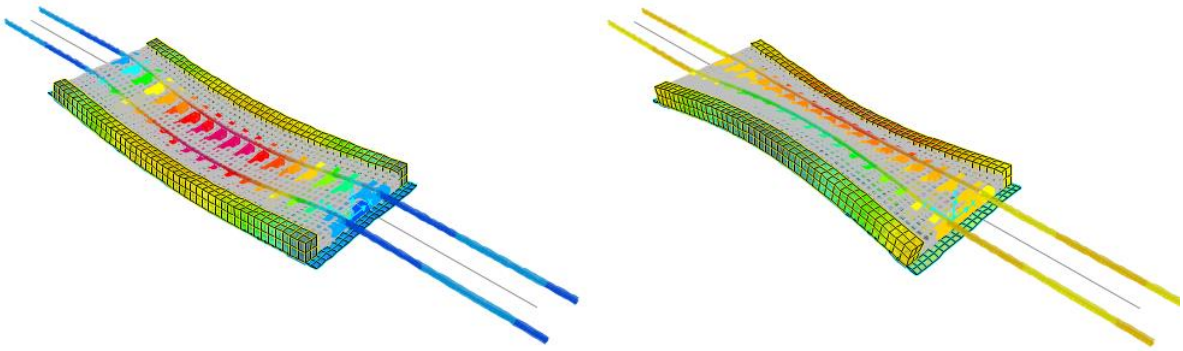

Figure 74: First and second mode shapes - Frequencies 10.79Hz and 16.98Hz, resp.

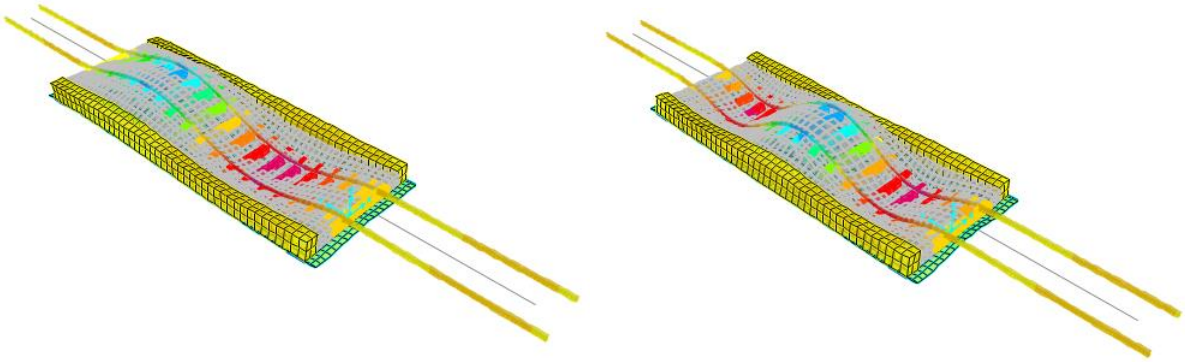

Figure 75: Third and fourth mode shapes - Frequencies 22.03Hz and 30.74Hz, resp.

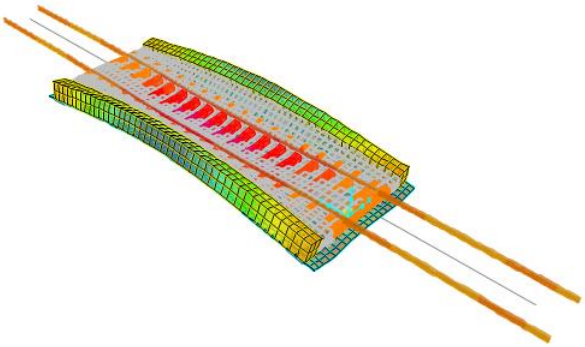

Figure 76: Fifth mode shape - Frequency 34.56Hz

Mode	Frequency [Hz.]	Mode shape
1	10.79	First degree longitudinal bending
2	16.98	Torsional
3	22.03	Second degree longitudinal bending
4	30.74	Third degree longitudinal bending
5	34.56	First degree Transverse bending

Table 17: Summary of modes for model CSI-WTS

4.7.2. Moving load - Time History Analysis

CSiBridge is a suitable application for such analysis as its platform allows for easy modelling of the vehicle data and lanes. The purpose of this analysis was to obtain the calculated acceleration time-history at quarter and mid-spans of the bridge for comparison with the measured values. Figure 77 shows the schematics of the locomotive with the dimensions between the wheels.

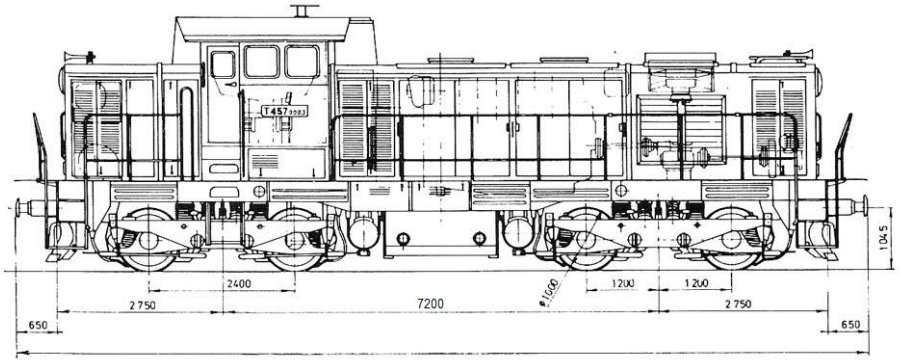

Figure 77: HV 730 dimensions

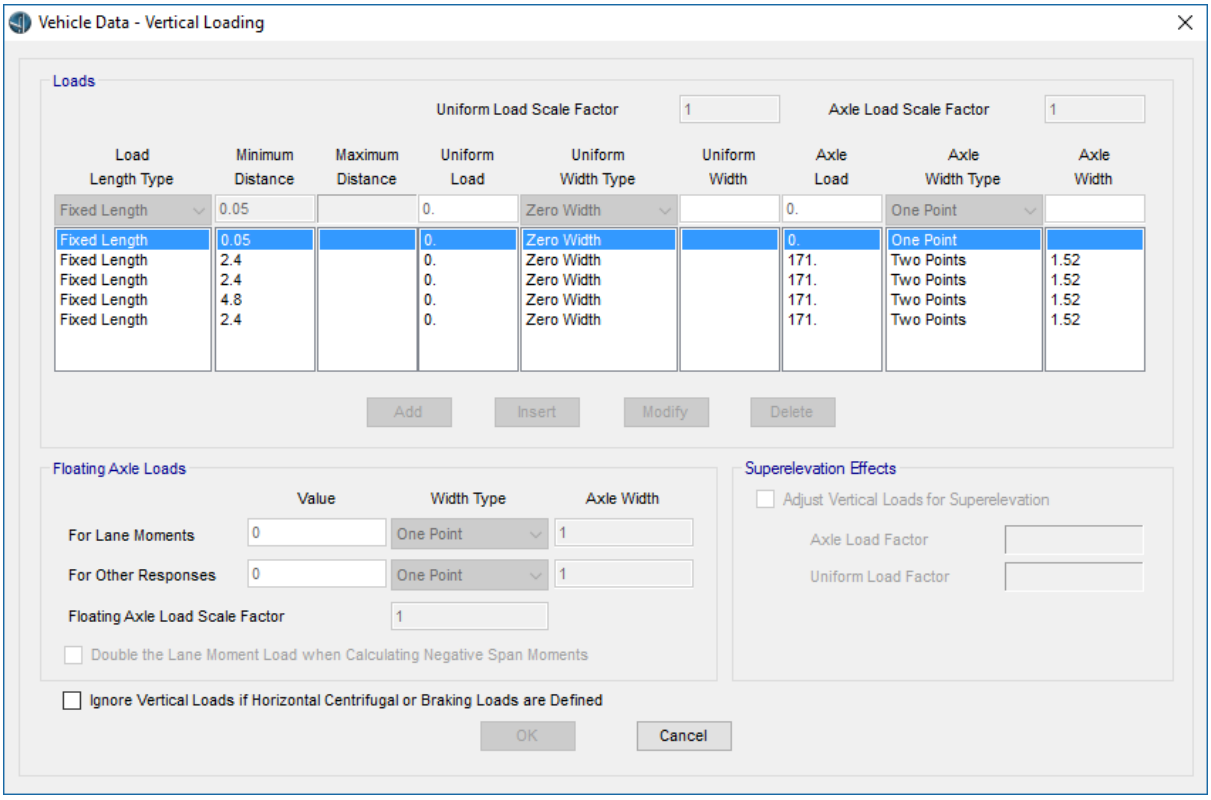

Figure 78: Definition of the test locomotive

A lane is defined at the height of the rails where the simulated vehicle that was input for the program as shown in Figure 78 makes the pass at different speeds. The definition of the specific case in which the locomotive makes a pass speed of 40km/hr (12.5m/s) is shown in Figure 79.

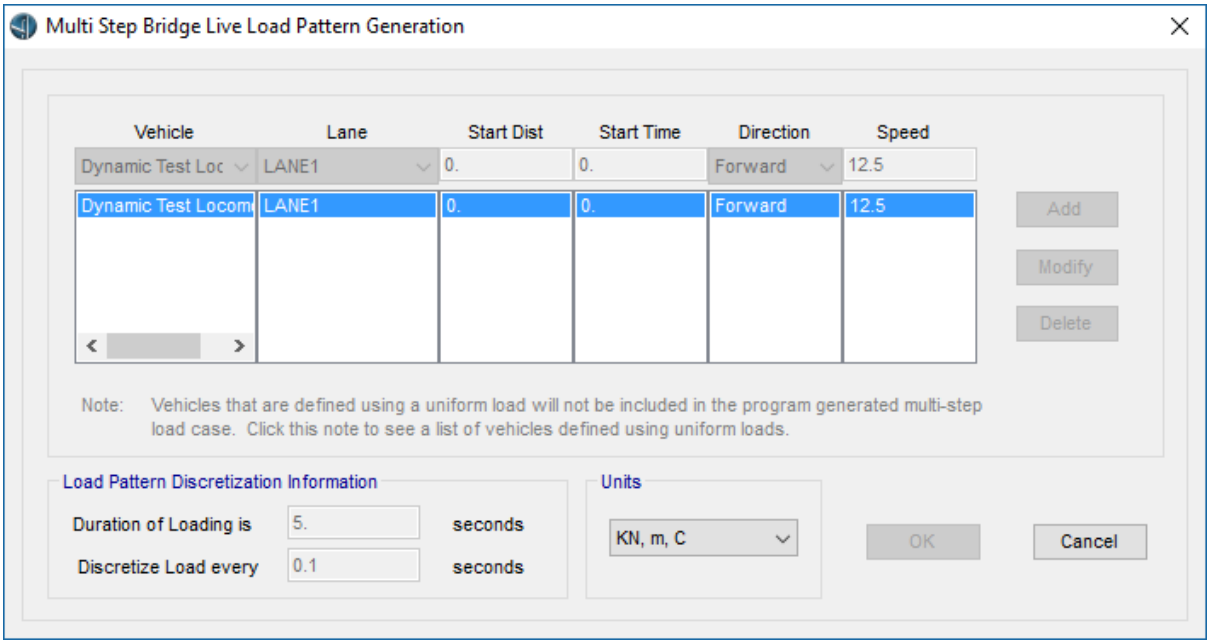

Figure 79: Moving load definition for the locomotive at a speed of 40km/hr.

Structural Damping

The peak response of bridge structures due to traffic speeds corresponding to resonant excitation is highly dependent upon the damping. Recommended characteristic values of damping to be used in dynamic analysis are based on the bridge type and the span length of the bridge given in Table 6.6 of EN1991-2 [18] are presented below.

Bridge Type	ζ Lower limit of percentage of critical damping [%]	
	Span L < 20m	Span $L \geq$ 20m
Steel and composite	$\zeta = 0{,}5 + 0{,}125\ (20 - L)$	$\zeta = 0{,}5$
Prestressed concrete	$\zeta = 1{,}0 + 0{,}07\ (20 - L)$	$\zeta = 1{,}0$
Filler beam and reinforced concrete	$\zeta = 1{,}5 + 0{,}07\ (20 - L)$	$\zeta = 1{,}5$

Figure 80: Values of damping to be assumed for design purposes

Accordingly, for the steel bridge in this case:

$$\xi = 0.5 + 0.125(20 - L) = 0.5 + 0.125(20 - 10) = 1.75\%$$

However result from the test indicated a damping ratio of 1.07% for the whole bridge with an uncertainty margin of ±0.11%. Base on this, Rayleigh damping coefficients (mass and stiffness proportional damping coefficients) were determined and applied in the following procedure.

$$C = \eta M + \delta K$$

Where: $\delta = \frac{2\xi}{\omega_i + \omega_j}$ and $\eta = \omega_i \omega_j \delta$

η is the mass-proportional damping coefficient

M is the mass matrix,

δ is the stiffness-proportional damping coefficient

K is the stiffness matrix

ξ is the damping value = 1.07% between the frequencies 0.5Hz – 30Hz

ω_i is the first circular frequency of vibration = 64.34 = 2π ×10.4Hz

ω_j is another circular frequency of vibration = 197.92 = 2π × 31.5Hz.

Substituting the above values, $\delta = 8.43 \times 10^{-5}$ and $\eta = 1.0384$

A modal linear time history load case was created with the a 0.01s step size for a duration of 5 seconds for the case of a locomotive passing at a speed of 40km/hr (12.5m/s). The definition of this load case is shown in Figure 81.

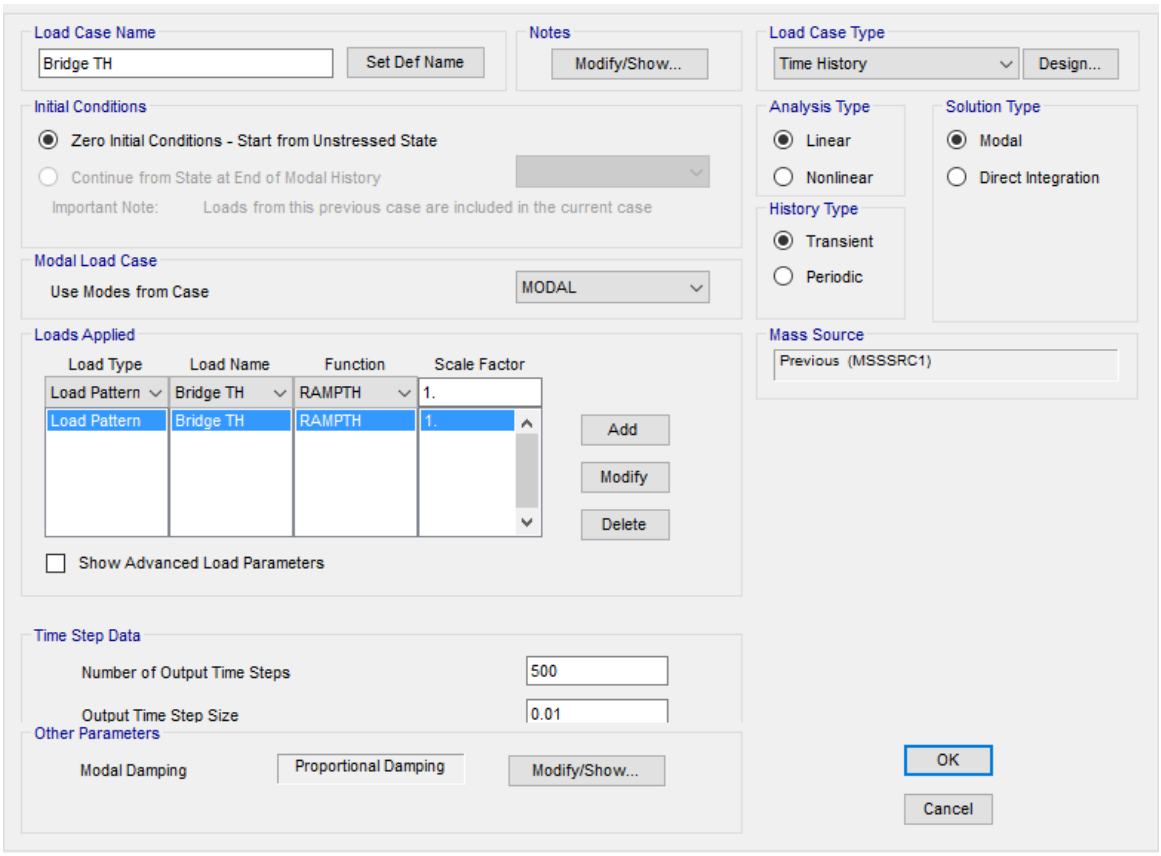

Figure 81: Definition of the time history load case

Figure 82 shows the acceleration history plot for a point at the mid-span obtained from the analysis.

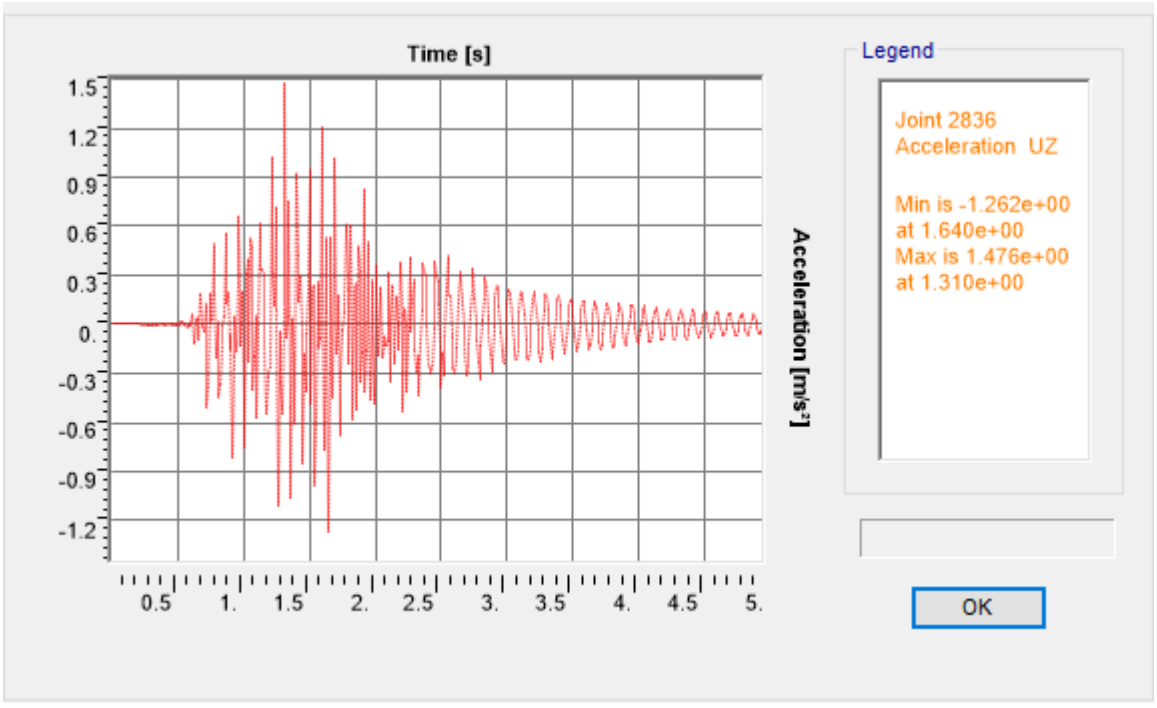

Figure 82: Mid-span acceleration in the direction of U_z

4.8. Simplified model using shell and beam elements

As evident from the test results, the natural frequencies of the supporting structure of the bridge are greater than those calculated from the ‘steel only’ model. This shows that the actual bridge structure is substantially stiffer than the theoretical model used for dynamic calculation. Based on this fact, the bridge designer included non-load bearing parts of the bridge (eg. the rails, guard rails and ballast) in to the original computational model. [13] These parts were modelled using beam elements with specified eccentricity. Further, the ballast was defined as a new material and assigned to the ‘ballast beams’ to approximately represent the ballast. These ‘beams’ were placed both in the longitudinal and transverse direction. The modified calculation model is shown in Figure 83. The newly calculated Eigen frequencies are presented in Table 18.

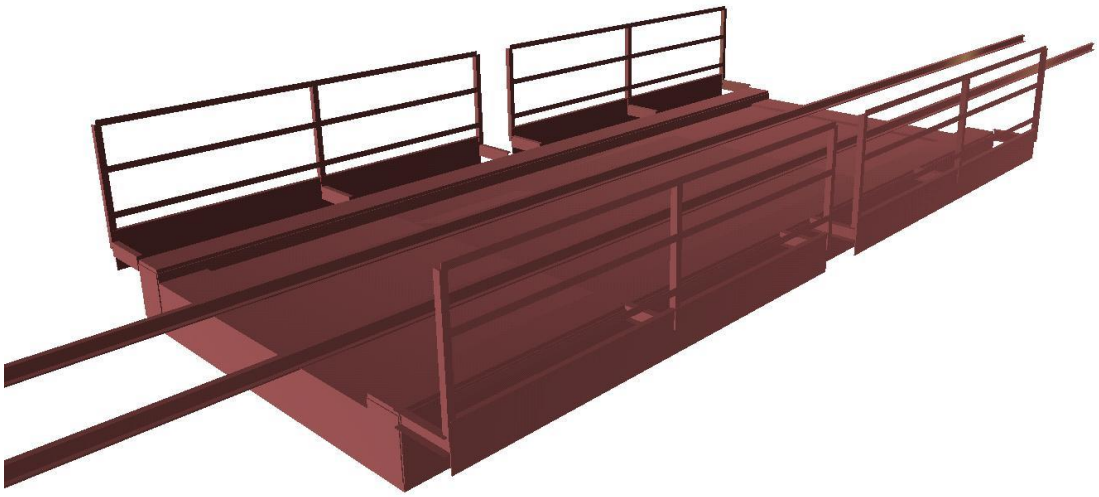

Figure 83: Simplified model for quick analysis

Mode	Frequency [Hz.]	Mode shape
1	9.93	First degree longitudinal bending
2	14.83	Torsional
3	20.23	Second degree longitudinal bending
4	24.03	First degree Transverse bending
5	29.82	Third degree longitudinal bending

Table 18: Summary of modes for the simplified model

5. Discussion and Conclusion

5.1. Comparison of experimental data with numerical results

Six different models in Abaqus and CSiBridge were used to determine the modal shapes and frequencies of the bridge in this thesis. A number of other models were made before arriving at these models. All the refinement and improvements were made with the intent of coming up with a model that best describes the actual bridge. This is proved by comparing the specific results from the experiment with the bridge properties obtained after analyzing the models. Table 19 presents the properties of each model in brief.

Mode	Models					
	CSI-BMO	**ABQ-B3D**	**ABQ-B&S3D**	**ABQ-WTR**	**ABQ-WTS**	**CSI-WTS**
Steel bridge						
Element type	Shell	Shell	Shell	Shell	Shell	Shell
Elastic Modulus	210GPa	210GPa	210GPa	210GPa	210GPa	210GPa
Ballast						
Element type	-	Solid 3D	Solid 3D	Solid 3D	Solid 3D	Solid 3D
Mass density	1850kg/m³	1850kg/m³	1850kg/m³	1850kg/m³	1850kg/m³	1850kg/m³
Elastic Modulus	-	80MPa	80MPa	80MPa	80MPa	80MPa
Sleepers						
Element type	-	-	Solid 3D	Solid 3D	Solid 3D	Beam
Mass density	2550kg/m³	2550kg/m³	2550kg/m³	2550kg/m³	2550kg/m³	2550kg/m³
Elastic Modulus	-	-	32GPa	32GPa	32GPa	32GPa
Rails						
Element type	-	-	-	Beam	Beam	Beam
Mass density	7850kg/m³	7850kg/m³	7850kg/m³	7850kg/m³	7850kg/m³	7850kg/m³
Connection						
Rail to sleeper (Inside the bridge)	-	-	-	Rigid	Springs	Rigid
Rail to sleeper (Outside the bridge)	-	-	-	Rigid	Springs	Springs

Table 19: Brief description of the models' parameters

The natural frequencies of the bridge structure without considering the stiffness of the ballast and the track are lower than those obtained from the experiment (see Table 20). The frequencies do not match in all modes. This discrepancy, as proved below, can only be explained by the additional stiffness of the ballast and the track.

The dynamic properties of the bridge became more and more close to those obtained from the tests up on including all the track elements and the ballast in to the model with proper

boundary conditions applied and interactions between the elements defined. A summary of the results is tabulated in Table 20 for comparison.

It can be seen from the table that the classical method of modelling (CSI-BMO) where only the mass of the track is included underestimates the stiffness of the bridge in four of the first five modes of oscillation. The second mode, which is torsional or twisting in nature, is the only mode that does not seem to be affected significantly by the stiffness.

In ABQ-B3D, improving the model by taking the mass and stiffness of the ballast alone in to account, resulted in a more or less the same result as the previous model. This could be attributed to the fact that a relatively small modulus of elasticity value adopted for the ballast.

Additional improvement of the model by including the sleepers, however, resulted in a significant change on the natural frequencies in the model ABQ-B&S3D. The increase in the stiffness of the system owing to the significant increase in the value of the elastic modulus (From 80MPa (ballast) to 36GPa(concrete)) in the regions of the sleepers manifested to have the upper hand in dictating the natural frequencies over the relatively smaller increase in mass density (1850kg/m^3 to 2550kg/m^3). It is to be noted here again that the frequency for the second mode (torsional mode) did not change much as compared to the others.

Further refinement of the model by including the rails (ABQ-WTR) was marked by yet another step/approach towards the test results. The connection between the sleepers and the rail is made using a tie constraint and can thus be considered rigid. The calculated frequencies and shapes are in line with the experimental results in almost all modes with the exception of mode 4. The vibration mode shape in mode 4 (see Figure 68) displays an erratic deformation as the bridge bends in the transverse direction. A possible cause to this is thought to be the rigid connection close to the edges of the sleepers. Despite this “abnormal” detail, the frequency and shape matches closely to the test results.

ABQ-WTS, the final model in Abaqus, is a modification of the previous model that involves the use of springs to depict the connection between the rail and the sleepers. Both the vertical and longitudinal stiffness are modelled. On a final note, the fourth mode shape from the test results are not in line with the majority of the analysis model results. This could be explained by the fact that a range of frequencies, probably of different shapes, were obtained at an uncertainty of ±1.1Hz. The FFT plot in Figure 35 shows four visible peaks in the frequency range 27Hz – 32Hz. These peaks each have different mode shapes and the calculated mode shapes are possible in the uncertainty range of 1.1Hz.

Mode	Numerical Models										Experiment		
	CSI-BMO		ABQ-B3D		ABQ-B&S3D		ABQ-WTR		ABQ-WTS				
	Freq [Hz.]	Shape	Freq [Hz.]	Shape	Freq [Hz.]	Shape	Freq [Hz.]	Shape	Freq [Hz.]	Shape	Freq [Hz.]		Shape
1	9.295	1° L B	9.23	1° L B	10.24	1° L B	10.663	1° L B	10.435	1° L B	10.4	± 0.3	1° L B
2	16.27	T	15.77	T	16.58	T	16.54	T	16.626	T	15.9	± 0.3	T
3	17.68	2° L B	18.73	2° L B	21.01	2° L B	22.7	2° L B	21.668	2° L B	22.5	± 0.3	2° L B
4	26.68	3° L B	25.95	3° L B	25.58	3° L B	26.48	1° T B	29.705	3° L B	27.8	± 1.1	1° T B‡
5	27.69	1° T B	26.46	1° T B	32.18	1° T B	31.49	3° L B	32.498	1° T B	31.5	± 0.3	1° T B/3° L B

Table 20: Summary of frequencies and modes of vibration from the numerical models

Legend:

1° LB = First degree longitudinal bending mode shape

T = Torsional mode shape

2°LB = Second degree longitudinal bending mode shape

1°TB = First degree transverse bending mode shape

3°LB = Third degree longitudinal bending mode shape

‡ Natural frequency decreased gradually from 28.9 Hz to 27.0 Hz during the dynamic load test. Therefore, the expanded measurement uncertainty at this frequency is higher than the remaining frequencies.

Mode	Test	CSI-BMO		ABQ-WTR		ABQ-WTS	
	Freq [Hz.]	Freq [Hz.]	Δ	Freq [Hz.]	Δ	Freq [Hz.]	Δ
1	10.4	9.295	-10.63%	10.663	2.53%	10.435	0.34%
2	15.9	16.27	2.33%	16.54	4.03%	16.626	4.57%
3	22.5	17.68	-21.42%	22.7	0.89%	21.668	-3.70%
4	27.8	26.68	-4.03%	26.48	-4.75%	29.705	6.85%
5	31.5	27.69	-12.10%	31.49	-0.03%	32.498	3.17%

Table 21: Comparison of FEM results with the experiment

It can be concluded from table 20 that the ballast and track stiffness/interaction has major influence on the bridge dynamics. The 1st mode which had a discrepancy of 10.63% when the interaction was not considered comes to 0.34% discrepancy after considering the interaction. Similarly for the 3rd mode, the discrepancy dropped from 21.42% to 3.7%. The same can be said about the 4th and 5th modes as well. What remained relatively constant despite the modelling of the ballast and track is the 2nd mode. This torsional/ twisting mode is unaffected by the stiffness change and is mainly dependent on the mass and support conditions. (See below).

5.2. Impact of the ballast properties on the dynamic behaviour of the bridge

The influence of the mass and stiffness properties of the ballast is studied in this section. For the purpose of this comparison, Model ABQ-WTS that has close agreement with the test results is chosen as a reference and a variation of the mass and stiffness properties have been considered to assess their effects. The mode shapes remained the same as the reference case up on running analysis, however, changes were observed on the natural frequencies to a varying degree. Details of the observations are presented below.

5.2.1. Influence of the ballast mass

The implications of the variation of the ballast mass were checked by considering three different sets of unit weight (mass density) for the material. The results are summarized in Table 22.

Mode	Frequency [Hz.]				
	ρ = 1850kg/m³	ρ = 1500kg/m³	Δ	ρ = 2100kg/m³	Δ
1	10.435	10.917	4.62%	10.128	-2.94%
2	16.626	17.201	3.46%	16.245	-2.29%
3	21.668	22.757	5.03%	20.979	-3.18%
4	29.705	31.193	5.01%	28.755	-3.20%
5	32.498	33.236	2.27%	32.005	-1.52%

Table 22: Influence of ballast mass on vibration frequencies

As expected, an increase in the mass results in a decrease in the natural frequency. An increase of the mass density by 300kg/m³ resulted in 2 – 3.2% decrease in the natural frequency for the first 3 modes. Inversely, decreasing the mass density of the ballast by 350kg/m³ lead to 3.5-5% higher first three frequencies.

5.2.2. Influence of the ballast stiffness

Three different ballast elastic modulus, thereby stiffness, values were evaluated. The modulus values ranged from 40MPa to 160MPa, which represent the quality of the ballast from extremely bad to good. Comparative analysis of the results is shown in Table 23.

Mode	Frequency [Hz.]				
	E = 80Mpa	E = 40Mpa	Δ	E = 160Mpa	Δ
1	10.435	10.046	-3.73%	10.863	4.10%
2	16.626	16.319	-1.85%	17.038	2.48%
3	21.668	20.251	-6.54%	23.711	9.43%
4	29.705	-	-	32.576	9.67%
5	32.498	-	-	36.369	11.91%

Table 23: Influence of ballast elastic modulus on vibration frequencies

Decreasing the stiffness of the ballast to a very low value of 40MPa (half the reference value), brought 3.73% drop in the fundamental frequency and up to 6.5% decrease in the higher frequencies. While increasing this value to 160MPa (Double the reference value) caused a 4.1% increase in the first mode and up to 11.91% increase in the higher modes. Here as well, it can be seen that the change in the ballast modulus had the least impact on the twisting mode frequency.

5.3. Influence of the support conditions

Thereafter, the actual bearing support conditions used in the mentioned model were changed to an all fixed support system first and later to a pinned support with the aim of quantifying the influence of such a change on the dynamic properties of the bridge. Significant increase as high as 12.3% is observed in the frequency of the 2nd mode. This mode is highly influenced by the support conditions. The fully fixed (including restrained rotational freedom), which has the furthest difference from the reference case, has the most changes. The latter case, where all are simply fixed against translations only, had relatively smaller contribution to the frequency change as this boundary condition is relatively closer to the one used in the reference model.

Mode	Frequency [Hz.]				
	Actual support conditions	All fully fixed	Δ	All fully pinned	Δ
1	10.435	11.353	8.80%	10.8	3.50%
2	16.626	18.681	12.36%	18.428	10.84%
3	21.668	22.441	3.57%	21.681	0.06%
4	29.705	30.904	4.04%	29.722	0.06%
5	32.498	34.124	5.00%	33.61	3.42%

Table 24: Influence of boundary condition on vibration frequencies

5.4. Conclusions

The following conclusions can be drawn from the analysis of the bridge in this thesis:

- Half-through steel bridges are good options for replacement of old railway bridges in situations where there is a limit on structural depth.
- The interaction of the ballast/track with the bridge structure has considerable influence on the dynamic properties of the short steel bridges.
- Neglecting the contribution of the ballast stiffness leads to lower natural frequencies that under-estimate the actual bridge stiffness.
- A fairly good result can be obtained by modeling the ballast as 3D solid element even in common structural analysis software such as CSiBridge.
- An approximate/simplified model of the ballast and track, where both are modeled as beam elements with appropriate eccentricities and boundary conditions applied, can be used for quick analysis with fair degree of accuracy, as was used by the original designer of the bridge.
- Using alternative safe lower bound damping values may be closer to the reality, as in this bridge, than using the damping values recommended in Eurocodes.
- The acceleration time history plot from the tests/reality appears to be better than that obtained from analysis. Accelerations obtained from CSiBridge analysis were higher than the measured ones. The damping from the locomotive wheel springs could probably had influence in this regard; but this needs further study.

5.5. Recommendations and further research

The tasks performed in this thesis have proven that there is a significant influence coming from both the mass and stiffness of the ballast and the track. However, modifying the Abaqus model using shell elements for the rails and running a dynamic analysis by applying moving load to see the time-history plot of accelerations would be interesting, though time consuming.

In addition, such a model could help elevate our understanding of the level of interaction between the track and the bridge when a horizontal force such as braking force is applied to the track. Also, investigating the interaction between the train and the track itself could shed some light on the discrepancy between the measured and calculated accelerations at mid-span.

6. Bibliography

[1] Steelconstruction.info, "www.steelconstruction.info/Half-through_bridges," [Online]. Available: www.steelconstruction.info/Half-through_bridges. [Accessed 2016].

[2] D. C. ILES, Design Guide for Steel Railway Bridges, Berkshire: The Steel Construction Institute, 2004.

[3] P. Gerard and H. Nigel, ICE manual of bridge engineering, 2nd ed., London: Institute of Civil Engineers, 2008.

[4] D. M. Steffens, Identification and Development of A Model of Railway Track Dynamic Behaviour, Master's Thesis: Queensland University of Technology, 2005.

[5] J. Fink and T. Mähr, Influence of ballast superstructure on the dynamics of slender steel railway bridges, Vienna, Austria, 2009.

[6] S.-I. Kim, "Experimental evaluations of track structure effects on dynamic properties of railway bridges," *Journal of Vibration and Control*, vol. 12, pp. 1817-1826, 2010.

[7] C. Rigueiro, C. Rebelo and L. S. d. Silva, "Influence of ballast models in the dynamic response of railway viaducts," *Journal of Sound and Vibration*, no. 329, pp. 3030-3040, 2010.

[8] H. Feng, 3D-models of Railway Track for Dynamic Analysis, Stockholm: Master's Thesis: Royal Institute of Technology, 2011.

[9] K. Liu, E. Reynders, G. D. Roeck and G. Lombaert, "Experimental and numerical analysis of a composite bridge for high-speed trains," *Journal of sound and vibration,* no. 320, pp. 201-220, 2009.

[10] L. Bornet, Influence of the ballast on the dynamic properties of a truss railway bridge, Stockholm, Sweden: Masters Thesis: Royal Institute of Technology (KTH), 2013.

[11] ČSN 736209: Zatěžovací zkoušky mostů (Loading tests of bridges), Praha: Český Normalizační Institut, 1996.

[12] EN 1990 – Eurocode : Basis of structural design Annex A2 : Application for bridges, European Committee for Standardization, 2005.

[13] M. Polák, "Statická a dynamická zatěžovací zkouška mostu so 03-20-02 na trati rokycany - mirošov," CVUT, Praha, 2016.

[14] C. A. Felippa, "Type of Finite Elements and Steps in FEA Process," in *Introduction to Finite Element Methods*, 2000.

[15] Dassault Systèmes' Simulia Corp., Getting Started with Abaqus 6.12 : Interactive Edition, 2012.

[16] "Element types in FEM," [Online]. Available: http://fea-cae-engineering.com/fea-cae-engineering/element_types.htm. [Accessed Dec. 2016].

[17] L. Fryba, Dynamics of Railway Bridges, London: Thomas Telford Ltd., 1996.

[18] Eurocode 1: Actions on structures - Part 2: Traffic loads on bridges, Brussels: European Committee For Standardization, 2002.

[19] UIC, UIC 774-3R: Track/bridge interaction - Recomendations for calculations, 2nd ed., 2001.

[20] P. Ryjáček, Zatížení ocelových mostů od termické interakce s bezstykovou kolejí, Praha, 2013.

[21] L. Björklund, Dynamic analysis of railway bridges subjected to high speed trains, Stockholm: Royal Institute of Technology, 2004.

[22] P. Ryjáček, "Technická zpráva - Revitalizace trati Rokycany - Nezvěstice SO 03-20-02 Rokycany - Mirošov, most v ev. km 9,296," Praha, 2014.

[23] Dassault Systèmes' Simulia Corp., Abaqus/CAE User's Manual, 2012.

[24] J. M. Proença, H. Casal and M. Neves, "Effect of the type of track on the dynamic behaviour of high speed railway brigdes," in *Computational Methods in Structural Dynamics and Earthquake Engineering*, Corfu, Greece, 2011.

[25] C. Rigueiro, C. Rebelo, L. S. d. Silva and M. Pircher, "Dynamic behaviour of twin

single-span ballasted railway viaducts — Field measurements and modal identification," *Engineering Structures,* no. 30, pp. 2460-2469, 2008.

[26] Computers & Structures, Inc, "CSI Analysis Reference Manual," Berkeley, California, USA, 2016.

[27] E. L. Wilson, "Three-Dimensional Static and Dynamic Analysis of Structures," Berkeley, California, USA, 2002.

7. Annex

7.1. MATLAB codes used

```
% Plotting the FFT of whole signals from each sensor for the locomotive
% passing at a selected speed
clear; clc;
load('DZS081-50.mat')
N=length(A32);  % Number of data record points
Fs=512;         % Frequency of sampling

fft_A21 = (abs(fft(A21))/N);
fft_A22 = (abs(fft(A22))/N);
fft_A23 = (abs(fft(A23))/N);
fft_A31 = (abs(fft(A31))/N);
fft_A32 = (abs(fft(A32))/N);
fft_A33 = (abs(fft(A33))/N);
fft_A41 = (abs(fft(A41))/N);
fft_A42 = (abs(fft(A42))/N);
fft_A43 = (abs(fft(A43))/N);
xfft=Fs*[0:N-1]/N;
figure;
plot(xfft(xfft<35),fft_A21 (xfft<35),'b');grid;
hold on;
plot(xfft(xfft<35),fft_A22 (xfft<35),'r');grid;
plot(xfft(xfft<35),fft_A23 (xfft<35),'b');grid;
plot(xfft(xfft<35),fft_A31 (xfft<35),'g');grid;
plot(xfft(xfft<35),fft_A32 (xfft<35),'y');grid;
plot(xfft(xfft<35),fft_A33 (xfft<35),'color',[0.4 0.6 0.7]);grid;
plot(xfft(xfft<35),fft_A41 (xfft<35),'c');grid;
plot(xfft(xfft<35),fft_A42 (xfft<35),'k');grid;
plot(xfft(xfft<35),fft_A43 (xfft<35),'b');grid;
hold off;
xlabel('Frequency (Hz)','FontSize', 10);
title('FFT plot for DSZ081-50','Fontname','Timesnewroman');

%%  ************************************************************
%% Plotting the filtered acceleration signal alongside the original signal

load('DZS081-50.mat');  % Calling/loading acceleration data stored in
MATLAB format

%% Plotting the Original/Unfiltered signal

lo=33;  % Lower limit / Start time magnify the results when ploting the
graph
hi=37;  % Higher limit to magnify the results when ploting the graph

figure;
subplot(3,3,1);
plot(Time((lo<Time)&(Time<hi)),A21((lo<Time)&(Time<hi)),'color',[1.0 0.6
0.0]);
grid;
xlabel('Time (s)','FontSize',10);
ylabel('Acceleration (m/s²)','FontSize',10);
title('A21 Original Signal','Fontname','Timesnewroman');
set(gca,'XTick',lo:0.5:hi, 'XMinorTick','on');
```

```
subplot(3,3,2);
plot(Time((lo<Time)&(Time<hi)),A22((lo<Time)&(Time<hi)),'m');
grid;
xlabel('Time (s)','FontSize',10);
ylabel('Acceleration (m/s²)','FontSize',10);
title('A22 Original Signal','Fontname','Timesnewroman');
set(gca,'XTick',lo:0.5:hi, 'XMinorTick','on');

subplot(3,3,3);
plot(Time((lo<Time)&(Time<hi)),A23((lo<Time)&(Time<hi)),'c');
grid;
xlabel('Time (s)','FontSize',10);
ylabel('Acceleration (m/s²)','FontSize',10);
title('A23 Original Signal','Fontname','Timesnewroman');
set(gca,'XTick',lo:0.5:hi, 'XMinorTick','on');

subplot(3,3,4);
plot(Time((lo<Time)&(Time<hi)),A31((lo<Time)&(Time<hi)),'r');
grid;
xlabel('Time (s)','FontSize',10);
ylabel('Acceleration (m/s²)','FontSize',10);
title('A31 Original Signal','Fontname','Timesnewroman');
set(gca,'XTick',lo:0.5:hi, 'XMinorTick','on');

subplot(3,3,5);
plot(Time((lo<Time)&(Time<hi)),A32((lo<Time)&(Time<hi)),'g');
grid;
xlabel('Time (s)','FontSize',10);
ylabel('Acceleration (m/s²)','FontSize',10);
title('A32 Original Signal','Fontname','Timesnewroman');
set(gca,'XTick',lo:0.5:hi, 'XMinorTick','on');

subplot(3,3,6);
plot(Time((lo<Time)&(Time<hi)),A33((lo<Time)&(Time<hi)),'b');
grid;
xlabel('Time (s)','FontSize',10);
ylabel('Acceleration (m/s²)','FontSize',10);
title('A33 Original Signal','Fontname','Timesnewroman');
set(gca,'XTick',lo:0.5:hi, 'XMinorTick','on');

subplot(3,3,7);
plot(Time((lo<Time)&(Time<hi)),A41((lo<Time)&(Time<hi)),'color',[0.8 0.4
0.7]);
grid;
xlabel('Time (s)','FontSize',10);
ylabel('Acceleration (m/s²)','FontSize',10);
title('A41 Original Signal','Fontname','Timesnewroman');
set(gca,'XTick',lo:0.5:hi, 'XMinorTick','on');

subplot(3,3,8);
plot(Time((lo<Time)&(Time<hi)),A42((lo<Time)&(Time<hi)),'k');
grid;
xlabel('Time (s)','FontSize',10);
ylabel('Acceleration (m/s²)','FontSize',10);
title('A42 Original Signal','Fontname','Timesnewroman');
set(gca,'XTick',lo:0.5:hi, 'XMinorTick','on');

subplot(3,3,9);
plot(Time((lo<Time)&(Time<hi)),A43((lo<Time)&(Time<hi)),'color',[0.4 0.6
0.7]);
```

```
grid;
xlabel('Time (s)','FontSize',10);
ylabel('Acceleration (m/s²)','FontSize',10);
title('A43 Original Signal','Fontname','Timesnewroman');
set(gca,'XTick',lo:0.5:hi, 'XMinorTick','on');

%% Filtering and storing the acceleration record for each measurement point

filter_order=3; % Order of the Butterworth bandpass filter
freq_inf=0.5;   % Minimum frequency of interest
freq_sup=30;    % Maximum frequency of interest

A21_filtered_signal=butter_filter (filter_order , freq_inf , freq_sup,A21);
A22_filtered_signal=butter_filter (filter_order , freq_inf , freq_sup,A22);
A23_filtered_signal=butter_filter (filter_order , freq_inf , freq_sup,A23);
A31_filtered_signal=butter_filter (filter_order , freq_inf , freq_sup,A31);
A32_filtered_signal=butter_filter (filter_order , freq_inf , freq_sup,A32);
A33_filtered_signal=butter_filter (filter_order , freq_inf , freq_sup,A33);
A41_filtered_signal=butter_filter (filter_order , freq_inf , freq_sup,A41);
A42_filtered_signal=butter_filter (filter_order , freq_inf , freq_sup,A42);
A43_filtered_signal=butter_filter (filter_order , freq_inf , freq_sup,A43);

%% Storing the extereme acceleration values for all measuring points
filtered_extremes=[min(A21_filtered_signal),max(A21_filtered_signal),min(A2
2_filtered_signal),max(A22_filtered_signal),min(A23_filtered_signal),max(A2
3_filtered_signal),min(A31_filtered_signal),max(A31_filtered_signal),min(A3
2_filtered_signal),max(A32_filtered_signal),min(A33_filtered_signal),max(A3
3_filtered_signal),min(A41_filtered_signal),max(A41_filtered_signal),min(A4
2_filtered_signal),max(A42_filtered_signal),min(A43_filtered_signal),max(A4
3_filtered_signal)];

%% Plotting the filtered signal

figure;
subplot(3,3,1);
plot(Time((lo<Time)&(Time<hi)),A21_filtered_signal((lo<Time)&(Time<hi)),'co
lor',[1.0 0.6 0.0]);
grid;
xlabel('Time (s)','FontSize',10);
ylabel('Acceleration (m/s²)','FontSize',10);
title('A21 Filtered Signal','Fontname','Timesnewroman');
set(gca,'XTick',lo:0.5:hi, 'XMinorTick','on');

subplot(3,3,2);
plot(Time((lo<Time)&(Time<hi)),A22_filtered_signal((lo<Time)&(Time<hi)),'m'
);
grid;
xlabel('Time (s)','FontSize',10);
ylabel('Acceleration (m/s²)','FontSize',10);
title('A22 Filtered Signal','Fontname','Timesnewroman');
set(gca,'XTick',lo:0.5:hi, 'XMinorTick','on');

subplot(3,3,3);
plot(Time((lo<Time)&(Time<hi)),A23_filtered_signal((lo<Time)&(Time<hi)),'c'
);
grid;
xlabel('Time (s)','FontSize',10);
ylabel('Acceleration (m/s²)','FontSize',10);
title('A23 Filtered Signal','Fontname','Timesnewroman');
set(gca,'XTick',lo:0.5:hi, 'XMinorTick','on');
```

```
subplot(3,3,4);
plot(Time((lo<Time)&(Time<hi)),A31_filtered_signal((lo<Time)&(Time<hi)),'r'
);
grid;
xlabel('Time (s)','FontSize',10);
ylabel('Acceleration (m/s²)','FontSize',10);
title('A31 Filtered Signal','Fontname','Timesnewroman');
set(gca,'XTick',lo:0.5:hi, 'XMinorTick','on');

subplot(3,3,5);
plot(Time((lo<Time)&(Time<hi)),A32_filtered_signal((lo<Time)&(Time<hi)),'g'
);
grid;
xlabel('Time (s)','FontSize',10);
ylabel('Acceleration (m/s²)','FontSize',10);
title('A32 Filtered Signal','Fontname','Timesnewroman');
set(gca,'XTick',lo:0.5:hi, 'XMinorTick','on');

subplot(3,3,6);
plot(Time((lo<Time)&(Time<hi)),A33_filtered_signal((lo<Time)&(Time<hi)),'b'
);
grid;
xlabel('Time (s)','FontSize',10);
ylabel('Acceleration (m/s²)','FontSize',10);
title('A33 Filtered Signal','Fontname','Timesnewroman');
set(gca,'XTick',lo:0.5:hi, 'XMinorTick','on');

subplot(3,3,7);
plot(Time((lo<Time)&(Time<hi)),A41_filtered_signal((lo<Time)&(Time<hi)),'co
lor',[0.8 0.4 0.7]);
grid;
xlabel('Time (s)','FontSize',10);
ylabel('Acceleration (m/s²)','FontSize',10);
title('A41 Filtered Signal','Fontname','Timesnewroman');
set(gca,'XTick',lo:0.5:hi, 'XMinorTick','on');

subplot(3,3,8);
plot(Time((lo<Time)&(Time<hi)),A42_filtered_signal((lo<Time)&(Time<hi)),'k'
);
grid;
xlabel('Time (s)','FontSize',10);
ylabel('Acceleration (m/s²)','FontSize',10);
title('A42 Filtered Signal','Fontname','Timesnewroman');
set(gca,'XTick',lo:0.5:hi, 'XMinorTick','on');

subplot(3,3,9);
plot(Time((lo<Time)&(Time<hi)),A43_filtered_signal((lo<Time)&(Time<hi)),'co
lor',[0.4 0.6 0.7]);
grid;
xlabel('Time (s)','FontSize',10);
ylabel('Acceleration (m/s²)','FontSize',10);
title('A43 Filtered Signal','Fontname','Timesnewroman');
set(gca,'XTick',lo:0.5:hi, 'XMinorTick','on');

% set(gca,'YTick',-1.0:0.1:1.0, 'YMinorTick','on')
```

```
% Frequency computation and shape identification

clear;
clc;
load('DZS081-50.mat');
selected_acceleration = A32;
Fs=512; % Sampling frequency
filter_order=3;
freq_inf=9.5;
freq_sup=10.5;
% Filtering the original acceleration for the frequency ranges chosen above
filtered_signal=butter_filter (filter_order , freq_inf , freq_sup,
selected_acceleration);

%% Plot the original and filtered signals
figure;
subplot(1,2,1);
plot(Time, selected_acceleration, 'g'); grid;
xlabel('Time (s)','FontSize', 11)
ylabel('Acceleration amplitude (m/s²)','FontSize',11)
title('Original Signal','Fontname','Timesnewroman');
subplot(1,2,2);
plot(Time, filtered_signal, 'm'); grid;
xlabel('Time (s)','FontSize', 11)
ylabel('Acceleration amplitude (m/s²)','FontSize',11)
title('Filtered Signal','Fontname','Timesnewroman');

%% Isolating part of the signal
start_window=12*Fs;
end_window=13*Fs;
[isolated_signal1,isolated_signal_freq,Eigen_Frequency]=isolate_signal
(start_window,end_window, filtered_signal,Time);

%% Comparing two signals to determine mode shapes
acceleration1=A32;
acceleration2=A42;
% acceleration3=A42;
Fs=512; % Sampling frequency
filter_order=3;
freq_inf=9.5;
freq_sup=10.5;
start_window=33*Fs;
end_window=40*Fs;
%% Mode shape
%% Phase acceleration comparison
% Signal 1
filtered_signal1=butter_filter (filter_order , freq_inf ,
freq_sup,acceleration1);
[isolated_signal1,isolated_signal1_freq]=isolate_signal
(start_window,end_window, filtered_signal1,Time);
% Signal 2
filtered_signal2=butter_filter (filter_order , freq_inf ,
freq_sup,acceleration2);
[isolated_signal2,isolated_signal2_freq]=isolate_signal
(start_window,end_window, filtered_signal2,Time);
% Signal 3
% filtered_signal3=butter_filter (filter_order , freq_inf ,
freq_sup,acceleration3);
% [isolated_signal3,isolated_signal3_freq]=isolate_signal
(start_window,end_window, filtered_signal3,Time);
```

```
% Plot the time signals on the same graph
figure; hold on
plot(Time,isolated_signal1, 'b');
plot(Time,isolated_signal2, 'c'); grid;
% plot(Time,isolated_signal3, 'g'); grid;
xlabel('Time (s)','FontSize', 11)
ylabel('Acceleration amplitude (m/s²)','FontSize',11)
title('Signals Comparison','Fontname','Timesnewroman');

%% ------------------------------------------------
%% Functions used
%% function code originally from [10]
%% modified a little to suit the current test type
%% ------------------------------------------------

%% Butterworth function:

function filtered_signal = butter_filter (filter_order , freq_inf ,
freq_sup, signal)
%%load('variables_global')
Fs=512; %%Sample frequency
[B,A]=butter(filter_order, [freq_inf freq_sup]/(0.5*Fs)); %%, 'bandpass');
filtered_signal = filter(B,A,signal);

% % Plot the filtered signal
% figure;
% plot(t, filtered_signal, 'g'); grid;
% xlabel('Time (s)','FontSize', 11)
% ylabel('Acceleration amplitude (m/s2)','FontSize',11)
% title('Filtered Signal');
end


% % Signal isolation function:

function [isolated_signal,isolated_signal_freq,peak_position] =
isolate_signal(start_window, end_window, signal,t)
%load('variables_global')
Fs=512;
N = end_window - start_window;
% zero padding
% Put 0 before the chosen window
for i = 1:start_window
signal(i) = 0;
end
% Put 0 after the chosen window
for i = end_window:length(signal)
signal(i) = 0;
end
% compute the Hamming window
win_hamming = zeros(length(signal),1);
win_hamming(start_window:end_window-1, 1) = hamming(end_window-
start_window);
% compute the isolated signal (signal * windows)
isolated_signal = signal.*win_hamming;

figure;
subplot(1,2,1);
```

```
plot(t(start_window:end_window),isolated_signal(start_window:end_window),
'b'); grid;
xlabel('Time (s)','FontSize', 11)
ylabel('Acceleration amplitude (m/s²)','FontSize',11)
title('Isolated filtered signal','Fontname','Timesnewroman');

% compute fft
isolated_signal_filtered = isolated_signal(start_window:end_window);
isolated_signal_freq = (abs(fft(isolated_signal_filtered))/N);

f=Fs*[0:N-1]/N;
% plot fft
% figure;
subplot(1,2,2);
plot(f(f<35), isolated_signal_freq (f<35), 'r'); grid;
xlabel('Frequency (Hz)','FontSize', 11)
title('FFT of isolated filtered signal','Fontname','Timesnewroman');

[peak_value, peak_position]=max((isolated_signal_freq));
% give the peak frequency value
peak_position = f(peak_position);
```